

Advanced Highly Permeable and Thermally Stable Polyamide Thin Film Composite and Thin Film Nanocomposite Membranes

by

Pooria Karami

A thesis submitted in partial fulfillment of the requirements for the degree of

Doctor of Philosophy

in

Chemical Engineering

Department of Chemical and Materials Engineering
University of Alberta

© Pooria Karami, 2022

Abstract

Treating contaminated hot streams is essential to reduce water cooling/re-heating needs and greenhouse gas emission in water reclamation processes, such as the Canadian in-situ oil-sand extraction processes that produce contaminated water at 80-90 °C. Membrane separation processes have become one of the fastest growing methods for the desalination and treatment of water because they cost less, are more compact, and produce higher quality water than conventional processes. At the heart of this processes is the membrane. Thin film composite (TFC) membranes are the most common choices due to their high water recovery and contaminant rejection rates. However, commercially available TFC membranes do not perform well above 45 °C. The objective of this PhD thesis is to make new classes of TFC polymeric membranes with high permeability and separation performance at high water temperatures.

First, a novel reverse osmosis (RO) TFC membrane with enhanced thermal stability was made to address the limitation of available commercial TFC membranes. The goal was to make a new polymer with a rigid network, and therefore higher temperature resistance, as the selective layer. To reach this goal, triaminopyrimidine (TAP, a multifunctional amine) was added to the usual combination of m-phenylenediamine (MPD) and trimesoyl chloride (TMC) to crosslink the polymeric structure. The TAP-modified membranes had higher permeabilities and consistent permeate fluxes for 9 hours at high temperatures.

These polymers were used to develop novel highly permeable and robust forward osmosis (FO) membranes. TAP-modified FO TFC membranes mediated with polydopamine (PDA)/graphene oxide (GO) interlayers were synthesized. The presence of an interlayer and a low reactive monomer (TAP) slowed down the interfacial polymerization, leading to forming a permeable, selective, and thermally stable polyamide layer.

I also added nanodiamond (ND) particles with high thermal resistance into the polyamide layer. The surface of the ND particles was modified with MPD to covalently bond them in the polymer matrix. Thin film nanocomposite (TFN) membranes prepared with ND particles

overcame the trade-off between water flux and NaCl rejection, and showed less flux decline at high temperature compared with a polyamide commercial membrane.

In the next phase of this development, amine-modified ND particles were added to the polyamide layer to change its surface chemistry. The ND particles reduced fouling of the TFC membranes with sodium alginate (SA) and bovine serum albumin (BSA) foulants by decreasing the electrostatic and hydrophobic interactions between foulants and the membrane surface, and by reducing the membrane roughness.

Finally, we provided guidelines to test TFC membrane at high temperatures. The performance of three commercial RO membranes were evaluated with a series of high-temperature filtrations including long-term operation, cyclic tests, controlled step-wise temperature increments, and permeability tests.

Keywords: Membrane separation; Reverse osmosis; Forward osmosis; Thin film composite, Thin film nanocomposite; Interfacial polymerization; Triaminopyrimidine; Nanodiamond, Thermal stability; Antifouling

Preface

This dissertation is the original work by Pooria Karami. The majority of the content in chapters 1, 2, 3, 4, and 5 were published/submitted in/to the following journals:

1. **P. Karami**, B. Khorshidi, M. McGregor, J.T. Peichel, J.B.P. Soares, M. Sadrzadeh, Thermally stable thin film composite polymeric membranes for water treatment: a review, *Journal of Cleaner Production* 250 (220) 119447.
2. **P. Karami**, B. Khorshidi, J.B.P. Soares, M. Sadrzadeh, Fabrication of highly permeable and thermally-stable reverse osmosis thin film composite polyamide membranes, *ACS Applied Materials and Interfaces* 12(2) (2020) 2916-2925.
3. **P. Karami**, Md.M.H. Mizan, B. Khorshidi, J.B.P. Soares, M. Sadrzadeh, Triammonopyrimidine modified forward osmosis polyamide membranes mediated with graphen oxide/polydopamine interlayer, Ready for submission.
4. **P. Karami**, B. Khorshidi, L. Shamaei, E. Beaulieu, J.B.P. Soares, M. Sadrzadeh, Nanodiamond-enabled thin-film nanocomposite polyamide membranes for high-temperature water treatment, *ACS Applied Materials and Interfaces* 12(47) (2020) 53274-53285.
5. **P. Karami**, S. Aghapour Aktij, B. Khorshidi, M. Dadashi Firouzjaei, A. Asad, M. Elliott, A. Rahimpour, J.B.P. Soares, M. Sadrzadeh, Nanodiamond-decorated thin film composite membranes with antifouling and antibacterial properties, *Desalination* 522 (2022) 115436.
6. **P. Karami**, S. Aghapour Aktij, M. Rastegar, B. Khorshidi, F. Mohammadtabar, J. Peichel, M. McGregor, T. Reinders, A. Rahimpour, J.B.P. Soares, M. Sadrzadeh, High-temperature cross-flow filtrations of commercial reverse osmosis membranes: guidelines for characterization, Submitted to *Canadian Journal of Chemical Engineering*.

DEDICATED TO MY PARENTS
NAHID AND MOHAMMADREZA
FOR YOUR ENDLESS LOVE
LOVE YOU!

Acknowledgement

First, I would like to express my sincere gratitude to my supervisors, Dr. Mohtada Sadrzadeh and Dr. João B.P. Soares for their continuous support throughout my PhD journey. I am extremely grateful of Dr. Sadrzadeh for offering me a PhD position in 2018. It was a great privilege and honor to work and study under his supervision. I am always thankful of Dr. Soares for accepting me in his group after completing one semester in mechanical engineering. He gave me this chance to not only work under his supervision in GAME, but also complete my doctoral education in chemical engineering. I could not imagine to have better supervisors and mentors in my PhD. My sincere thank goes to my committee member, Dr. Phillip Choi for his guidance and support.

My deepest gratitude is extended to Dr. Behnam Khorshidi for his kind help, support, and encouragement. I am truly honored to have this chance to work with you, Behnam. Most of what I learned in the field of membrane science was because of you. You have showed me what a good researcher and a good person should be.

I would like to thank my fellow labmates at the Advanced Water Research Laboratory (AWRL) in mechanical engineering department and the Group of Applied Macromolecular Engineering (GAME) in chemical and material engineering department. I appreciate all the support that I received from Dr. Ahmad Rahimpour, Sadegh Aghapour, Laleh Shamaei, Asad Asad, Mizanul Haque, Saeid Mehdiabadi, Madeline Tuai, Amirhossein Taghipour, Nazanin Chitgar, Amireza Sohrabi, Amin Karkooti, Amirul Islam, Masoud Rastegar, Farah Rahman Omi, Longxin Jiang, Farhad Ismail, Parmiss Mojir Shaibani, Sadaf Noamani, Kavya Suresh, Nandini Debnath, Ishita Biswas, Farshad Mohammadtabar, and Ali Mohammadtabar.

I also acknowledge the financial support (Alberta Innovates Graduate Student Scholarship, AIGSS) from Alberta Innovates of the Alberta government, Canada.

Last but not the least, I would like to thank my family: my parents Nahid and Mohammadreza, and my brother, Peyman, for supporting me throughout my life. You have always been there for me, and I feel secure knowing that I have you!

Table of Contents

Chapter 1 Introduction	1
1.1 Water demand and membrane technology	2
1.2 Synthesis of polymeric membranes	5
1.3 Critical need for thermally stable membranes for hot water treatment	6
1.4 Overview of thermal properties of polymers	8
1.4.1 Impact of temperature on polymer structure	8
1.4.2 Influential factors on thermal properties of polymer	9
1.5 Thermal characterization of polymers	11
1.6 Progress of development of thermally stable TFC membranes	13
1.6.1 Novel thermally stable membranes in commercial scale	13
1.6.2 Novel thermally stable membranes in lab-scale	15
(i) Modification of the active layer	15
(ii) Modification of the support layer	18
(iii) Incorporation of nanofillers into TFC structure	21
1.7 Research objectives	25
1.8 Thesis structure	26
Chapter 2 - Materials and Methods	28
2.1 Materials	37
2.2 Preparation of the TFC polyamide membranes	37
2.3 Characterization of fabricated membranes and nanoparticles	38
2.3.1 Chemical characterizations	38
2.3.2 Morphological analysis	39
2.3.3 Evaluation of the membrane surface wettability	39
2.3.4 Evaluation of transport properties and salt rejection in RO filtration	39
2.3.5 Evaluation of separation performance at high-temperature in RO filtration	40

2.3.6	Evaluation of transport properties of membranes in FO filtration	42
2.3.7	Evaluation of the fouling propensity of membranes in FO filtration	44
2.3.8	Evaluation of antibacterial properties of the membranes in FO filtration.....	44
Chapter 3 Triaminopyrimidine (TAP)-modified thin film composite membranes with high permeability and thermal stability		46
3.1	Fabrication of highly permeable and thermally-stable RO TFC polyamide membranes.....	47
3.1.1	Introduction	47
3.1.2	Experimental methods.....	49
3.1.3	Results and discussion	50
3.1.3.1	Permeation performance of TFC membranes	50
3.1.3.2	Chemical composition of the polyamide selective layer.....	52
3.1.3.3	Morphological analysis	55
3.2	TAP-modified FO TFC membranes mediated with PDA/GO interlayer.....	59
3.2.1	Introduction	59
3.2.2	Experimental methods.....	61
3.2.3	Results and discussion	62
3.2.3.1	Evaluation of morphology.....	62
3.2.3.2	Chemical characterization	65
3.2.3.3	Separation performance of synthesized membranes	66
3.3	Conclusion	68
Chapter 4 Exploiting unique features of nanodiamond (ND) particles for fabricating high-performance TFC and TFN membranes.....		70
4.1	Nanodiamond-enabled TFN polyamide membrane for high-temperature water treatment	71
4.1.1	Introduction	71
4.1.2	Experimental methods.....	73
4.1.3	Results and discussion	75
4.1.3.1	Characterization of pristine and functionalized ND particles	75
4.1.3.2	ATR-FTIR and XRD analysis of synthesized membranes	77

3.1.3.3	Morphology characterization	80
4.1.3.4	Separation Performance	82
4.2	Nanodiamond-Decorated TFC membranes with antifouling and antibacterial properties.....	85
4.2.1	Introduction.....	85
4.2.2	Experimental methods.....	88
4.2.3	Results and discussion	89
4.2.3.1	FTIR and TEM Analysis of ND Particles	89
4.2.3.2	FTIR and XPS results of fabricated TFC membranes.....	90
4.2.3.3	Morphological evaluation of the synthesized M.....	91
4.2.3.4	Transport performance of the membranes	93
4.2.3.5	Antifouling properties of ND-modified membranes.....	96
4.2.3.6	Stability of grafted ND particles	97
4.2.3.7	Antibacterial activity of the ND membranes	98
4.3	Conclusion	100
Chapter 5 High-temperature cross-flow filtrations of commercial reverse osmosis membranes: guidelines for characterization		102
5.1	Introduction.....	103
5.2	Results and discussion	105
5.2.1	High-temperature filtrations of flat-sheet membranes	105
5.2.1.1	Long-term performance of the membranes at high temperature.....	105
5.2.1.2	Cyclic tests	107
5.2.1.3	Stepwise temperature increment	108
5.2.1.4	Permeability measurement of membranes at different temperatures	109
5.2.2	The effect of temperature on the morphological characteristics of TFC membranes ...	109
5.2.3	The effect of temperature on the chemical composition of TFC membranes	111
5.3	Conclusion	112
Chapter 6 Conclusion and future work		114

6.1	Conclusion	115
6.2	Contributions to knowledge	117
6.3	Future work	118
6.4	List of contributions	121
6.4.1	Journal papers	121
6.4.2	Conference presentations	122
References		123
Appendix A.....		139
Appendix B.....		140

List of Tables

Table 1-1: Some of the commercially available spiral wound polymeric membrane elements for higher temperature water treatment.	14
Table 1-2: Summary of the studies reported on development of thermally stable TFC membranes by tuning the chemistry of the selective polyamide layer.....	17
Table 1-3: Chemical structure of the polymers commonly used for improving the thermal stability of the TFC membranes.....	20
Table 1-4: Effect of incorporating nanoparticles into TFN membranes on their thermal properties.	24
Table 3-1: Different monomer concentrations used to make the polyamide thin membranes. The polymerization time was 12 min and the membranes were cured at 60 °C for 4 min. M0 is the reference membrane, made without TAP.	50
Table 3-2: Binding energy and peak area of chemical bonds for C1s and N1s XPS spectra.	55
Table 3-3: Average and root mean square roughness of synthesized TFC membranes. The SAD values were calcucalted by $SAD = (Actual\ surface\ area / Projected\ surface\ area) \times 100$ using nanoscope image analysis software.	56
Table 4-1: Elemental composition and peak area percentage of C 1s and N 1s species	80
Table 4-2: Peak area percentages of deconvoluted carbon and nitrogen peaks.	91
Table 5-1: The roughness data including Ra: average roughness and Rq: root mean square roughness of AK, AG, and AD membranes.....	110

List of Figures

Figure 1-1: Various types of membrane separation processes for water treatment categorized based on driving force and schematic representation of the most widely used pressure-driven membranes including microfiltration, ultrafiltration, nanofiltration and reverse osmosis (RO), in which membrane pore size reduces from microfiltration to RO and the size of rejecting contaminants decrease proportionally.	4
Figure 1-2: (a) Schematic structure of thin film composite (TFC) membrane having two at least compositional layers: a selective thin layer over a porous support layer. Reprinted from [36]; (b) chemical structure of the reacting monomers and the polyamide film. Reproduced with permission of The American Association for the Advancement of Science [38]; (c) AFM surface topography. Reproduced with permission of Elsevier [39], (d) FESEM surface morphology Reproduced with permission of Elsevier [40], (e) FESEM cross-section structure Reproduced with permission of Elsevier [41]; and (f) TEM cross-section image Reproduced with permission of Elsevier [42] of a typical polyamide TFC membrane.	6
Figure 1-3: a) Industrial and municipal high-temperature wastewaters and b) schematic illustration of SAGD process which produces wastewater at 80-90 °C. Reproduced with permission of SpringerNature [50].	7
Figure 1-4: Influential factors on thermal behavior of polymers.	9
Figure 1-5: (a) Schematic view of DSC along with different thermal transition phases such as glass transition, crystallization, melting temperatures. Reproduced with permission of Wiley and Sons [83]; (b) Schematic illustration of TGA along with a sample curve of PES and PES/ITO nanocomposite membranes. Reproduced with permission of Elsevier [88]; (c) Schematic view of Nano-TA along with sample curves. Reproduced with permission of Elsevier [85,89]	13
Figure 1-6: (a) Schematic synthesis route of TiO ₂ NPs via biphasic solvothermal reaction and (b) fabrication of TFN membranes via adding TiO ₂ NPs during interfacial polymerization. Reprinted from [106].	23
Figure 2-1: Schematic of interfacial polymerization on PES support.	38
Figure 2-2: RO cross-flow filtration setup. The feed tank and all the pipes were insulated to minimize the heat loss during the high-temperature filtrations.	40
Figure 2-3: Schematic representation of FO cross-flow filtration setup in AL-DS and AL-FS configuration modes.	43
Figure 3-1: (a) Permeate: Schematic illustration of interfacial polymerization on top of a PES support. The microporous support was first impregnated with an aqueous amine solution (TAP and MPD) and then contacted with an organic TMC solution. The formation of the incipient polyamide layer on the PES substrate is followed by diffusion of the amine monomers through the polymer film into the organic phase to continue the polymerization. The reaction is finished when the amine monomers can no longer diffuse through the polyamide membrane.	49

Figure 3-2: (a) Permeate flux of TFC membranes over extended filtration test. Operating conditions: transmembrane pressure of 220 psi, concentrate flow rate of 3 LPM, feed temperature of 25-75 °C. The filtration tests started with 2000 ppm NaCl solution at room temperature (25 °C); after 30 min, the feed solution was increased to 75 °C and remained constant for 9 hours; (b) Permeate flux of commercial RO membranes over a long filtration test; (c) Permeability of TFC membranes at different temperatures, obtained by adjusting the transmembrane pressure with respect to the permeate flux of M0; (d) NaCl rejections of TFC membranes at different temperatures from 25 to 75 °C.....	51
Figure 3-3: FTIR spectra of the PES support and of the M0-M4 TFC membranes. In the first inset, the intensity ratios of three polyamide peaks to PES reference peak (at 1150 cm ⁻¹) provided the quantitative analysis of amide linkages formation.	53
Figure 3-4: XPS survey spectra, elemental composition, and high resolution C1s and N1s spectra for M0, M1, and M4 membranes.	54
Figure 3-5: FESEM micrographs of the top surface of PES support and TFC samples at two different magnifications. The amine concentration for all TFC membranes was set to 2 wt% with different concentrations of TAP and MPD monomers. Increasing the TAP concentration changed the top surface morphology. The PES support is shown as a non-coated membrane.....	56
Figure 3-6: 3D AFM images and cross-section TEM images of TFC samples. AFM images are shown for the scanning area of 10 µm × 10 µm and same z-axis aspect ratio for all the samples. TAP monomer contributed to the formation of smoother and thinner polyamide skin layer. In the TEM images, the PES support has occupied a higher portion of the images. The clear difference of contrast between PES and polyamide layers reveals the structure and the thickness of the selective layer. The detachment of polyamide layer from the PES support (TEM image of M1) is due to TEM sample preparation.....	57
Figure 3-7: Schematic repetition of hypothetical structures of polyamide film made with a combination of MPD and TAP with TMC monomer, showing the possible formation of the network and aggregate pores within the polyamide structure.	58
Figure 3-8: Schematic representation of coating the PES support layer with PDA and GO, and the chemical structure of the polyamide layer of the synthesized TFC membranes. The presence of an interlayer and a low reactivity monomer, TAP, reduced the diffusion rate of amine molecules during the interfacial polymerization, forming thinner polyamide layers. The TFC membrane modified with an interlayer is called iTFC in this thesis.	61
Figure 3-9: 3D AFM and top surface FESEM images of the synthesized polyamide membranes. Roughness data including R_a , R_q , and SAD were estimated using the Nanoscope software.	63
Figure 3-10: Cross-section TEM images of coated PES and polyamide TFC membranes modified with PDA/GO interlayers.	64

Figure 3-11: 3D AFM, top surface FESEM, and cross-section TEM images of TFC4 with and without PDA/GO interlayer. The TFC membrane modified with an interlayer is called iTFC in this thesis.	65
Figure 3-12: FTIR spectra of PES, PDA/GO-coated PES, and polyamide membranes with interlayers. The blue, grey, and green arrows show the characteristic peaks of PDA, GO, and polyamide, respectively.	66
Figure 3-13: Water flux and reverse salt flux in AL-FS and AL-DS of TFC0 and TAP-modified TFC membranes. All membranes had an interlayer.	67
Figure 3-14: (a) The water flux and (b) reverse salt flux of TFC0 and TFC3 membranes in the temperature range of 25-65 °C. The filtrations in AL-FS modes were conducted with two different methodologies: same initial flux and same draw solution concentration (DS: draw solution).	68
Figure 4-1: (a) Schematic illustration of the functionalization route of ND particles with MPD and (b) Schematic representation of TFN membrane fabrication. The TFN fabrication method is divided into two steps. First, functionalized ND particles were dispersed in a heptane solution containing ethyl acetate followed with the sonication of the suspension. TMC solution was added after the sonication to avoid disturbing the reaction between ND-MPD and TMC. In the second step, the prepared TMC solution was brought into contact with the MPD solution to form an ND/polyamide composite layer.	75
Figure 4-2: (a) TEM images of pristine ND particles dispersed in water. Single nanoparticles are distinguishable due to the fine dispersion of NDs. (b) XRD pattern of pristine ND showing two characteristic peaks of the diamond structure at 43.8° and 75.4°. (c) FTIR spectra of pristine and functionalized ND particles. (d) TG curves of pristine ND, functionalized NDs, and ND+MPD mixture. ND+MPD is a mixture made by simply blending MPD and ND. TGA results are presented from 100 °C since the mass loss at 0-100°C is attributed to the possible absorbed water on the ND particles.	76
Figure 4-3: (a) FTIR spectra of PES support, TFC-1, and TFN membranes. The area ratios of two highlighted peaks, a polyamide peak at 1660 cm ⁻¹ and a PES peak at 1150 cm ⁻¹ , were listed in a table. (b) XRD spectra of ND-MPD, TFC-1, and TFN membranes. Higher magnification of the XRD spectra in the range of 2θ=40-50° was presented in a separate panel to illustrate the ND characteristic peak for TFN400.	79
Figure 4-4: Deconvoluted C 1s and N 1s XPS spectra of TFC-1 and TFN membranes.	79
Figure 4-5: FESEM top surface images of PES and TFC/TFN membranes. For all polyamide membranes, it is evident that the surface of PES is covered with a continuous defect-free thin film of polyamide.	81
Figure 4-6: 2D and 3D AFM micrographs of synthesized TFC/TFN membranes and roughness data including average roughness (R _a) and root mean square roughness (R _q).	81
Figure 4-7: TEM cross-section images of TFC-1 and TFN membranes. The formation of more polyamide on top of the dense initial layer for TFN membranes is an indication of intensified MPD diffusion.	82
Figure 4-8: (a) Permeate flux of TFC-1, TFN membranes, and SUEZ AG. The filtration started with pure water, and 2000 ppm NaCl solution was added after 30 minutes. Afterward, the feed temperature was increased to 75 °C and kept	

constant for 9 hours. The transmembrane pressure and feed flow rate were set to 220 psi and 3 LPM during the filtration test. (b) NaCl rejection of the membranes at 25 °C and 75 °C. To obtain the salt rejection percentage at 75 °C, the sample was collected at the end of filtration, and the measurement of the conductivity was conducted the next day when the sample cooled down to room temperature. (c) Permeate flux ratio between 25 °C and 75 °C. The flux at 75 °C was the initial recorded data at high temperature (t=3 hours). The flux decline was calculated at 75 °C for 9 hours (t=3-12 hours).84

Figure 4-9: Schematic representation of interfacial polymerization, ND particle functionalization, and ND particle grafting over the polyamide surface. The ND particles were modified with EDA in order to provide a reactive surface with polyamide COCl groups. The surface of polyamide membrane was coated with ND particles through formation of amide linkages between ND-EDA particles and unreacted COCl groups.88

Figure 4-10: (a) FTIR spectra of pristine ND, carboxylated ND, and ND-EDA particles and (b) TEM image of nanoparticles. The spherical shape of ND particles represents both diamond core and graphitic shell structures.89

Figure 4-11: (a) FTIR spectra of PES and fabricated membranes, (b) schematic of TFC membranes before and after ND grafting, and (c) deconvoluted carbon and nitrogen XPS peaks of all synthesized membranes.90

Figure 4-12: (a) Top surface FESEM and (b) cross-section TEM images of PES, TFC-0, TFC-EtOH, and ND-modified membranes. The membranes modified with ND particles show the presence of nanoparticles on the top surface, which become more distinguishable at higher ND loadings. The polyamide layer in panel b₂-TFC-0 represents the internal void structure which is mostly covered in the TEM images of ND-modified TFC membranes.92

Figure 4-13: (a) 3D AFM images, R_a : average roughness, and R_q : root mean square roughness, (b) water contact angle of membranes. All the 3D AFM images are presented with a same z-axis aspect ratio to give a better visual comparison.93

Figure 4-14: (a) Water flux in AL-FS configuration, (b) Water flux in AL-DS configuration, (c) reverse salt flux, (d) specific salt flux, and (e) transport parameters for TFC-0, TFC-EtOH, and ND-modified membranes. All the forward osmosis filtrations in AL-FS and AL-DS configurations were performed with 1 M NaCl draw solution and deionized water as the feed solution. The reported water flux in panel a and b is the flux at the beginning of the filtrations. The reverse salt flux is also calculated by measuring the NaCl concentration in feed solution during 2 hours filtration. ...95

Figure 4-15: Water flux of synthesized membranes with (a) SA feed solution and (b) BSA feed solution, (c) formation of alginate gel on TFC-0 and TFC-1000 membranes after 180 minutes fouling experiment. The abrupt flux decline of TFC-0 in the initial 30 minutes of the filtration is an indication of alginate cake layer formation. Fouling experiments started with 18 ± 1 LMH water flux for all TFC membranes to exclude the effect of hydrodynamic flow condition on the fouling.97

Figure 4-16: The release rate of ND particles, evaluated by total organic carbon, for the fabricated membranes. The samples were collected each three days for the analysis. The vials of the samples were refilled with pure water every day to report the release data daily.98

Figure 4-17: The antibacterial assessment of the ND membranes. (a) schematic illustration of colony plating and confocal microscopy tests preparation steps, (b1-b6) colony plating test of the membranes. The Solution for these plates has been 10^{-6} diluted. (c1-c6) confocal microscopy test of the membranes (green and red areas represent the live and dead bacteria, respectively). The mortality rate is the ratio of the red area to the total red and green area calculated using ImageJ software, and (d1-d6) inhibition zone test of the membranes (black circles (d2-d6) are the membrane samples). Bacteria inhibition rates of the membranes in (e) colony plating and (f) confocal microscopy tests.	100
Figure 5-1: Commercial polyamide TFC membranes used in this study. SUEZ AG and SUEZ AK are standard and low-pressure brackish water RO membranes, respectively. SUEZ AD is designed for delivering high NaCl rejection at seawater operating conditions.	106
Figure 5-2: Water flux and NaCl rejection of the AK, AG, and AD membranes in a long-term (15 hours) filtration. The permeate samples at high temperature were collected and allowed to be cooled down to room temperature for conductivity measurement.	106
Figure 5-3: Water flux and salt rejections of cyclic operations of AK, AG, and AD membranes in three days. The flux decline of the membranes at 75 °C for each cycle was calculated and listed in a Table in the first panel. After finishing each cycle, the feed solution was cooled down slowly overnight.	108
Figure 5-4: (a) The trans-membrane pressure of the membranes at different operating temperatures. The water flux was set to 35 LHM, 72 LMH, and 112 LMH for AD, AG, and AK membranes, respectively, and (b) NaCl rejection of the membranes at different temperatures.	108
Figure 5-5: The water permeability of membranes at different temperatures. The permeability was reported by calculating the slope of flux/pressure curves.	109
Figure 5-6: Top surface FESEM and 3D topography AFM images of AK, AG, and AD membranes.	110
Figure 5-7: Cross-section TEM images of AG, AK, and AD membranes before and after high-temperature filtrations. The polyamide layer contrasts with PSf support by its spongy structure with internal voids.	111
Figure 5-8: FTIR spectra of AG, AK, and AD membranes before and after room and high-temperature filtrations.	112

Abbreviation

3APS	3-Aminophenyl sulfone
6FDA	4,4'-(Hexafluoroisopropylidene)diphthalic anhydride
AAD	Amic acid diamines
ACBK	Acid chrome blue K
AFM	Atomic force microscopy
AL-DS	Active layer facing the draw solution
AL-FS	Active layer facing the feed solution
AMPS	2-Acylamido 2-methyl propane sulfonic acid
ATR-FTIR	Attenuated total reflectance-Fourier transform infrared
BBL	Poly(bisbenzimidazo-ben-zophenanthrolines)
BSA	Bovine serum albumin
CBMA	1,3-Cyclohexanebis(methylamine)
CP	Concentration polarization
DAP	2,3-Diaminopyridine
DI	Deionized
DMA	Dynamic mechanical analysis
DMDA	1,2-Dimethylenediamine
DMTA	Dynamic mechanical thermal analysis
DSC	Differential scanning calorimetry
ECP	External concentration polarization
FESEM	Field emission scanning electron microscopy
FO	Forward osmosis
GO	Graphene oxide
HA	Humic acid
ICP	Internal concentration polarization
IP	Interfacial polymerization
LMH	$\text{L m}^{-2} \text{ hr}^{-1}$
MF	Microfiltration
MPD	M-phenylenediamine
NIPS	Nonsolvent induced phase separation

NMP	N-Methyl-2-Pyrrolidone
NP	Nanoparticles
PA	Polyamide
PAN	Polyacrylonitrile
PC	Polycarbonate
PES	Polyethersulfone
PDA	Polydopamine
PSF	Polysulfone
PVDF	Polyvinylidene fluoride
RO	Reverse osmosis
SA	Sodium Alginate
SDS	Sodium dodecyl sulfate
TEA	Triethylamine
TEM	Transmission electron microscopy
TFC	Thin film composite
TMC	Trimesoyl chloride
TMP	Transmembrane pressures
TOC	Total organic carbon
UF	Ultrafiltration
XPS	X-ray photoelectron spectroscopy

Nomenclature

A	Pure water permeability coefficient
A_m	Effective membrane surface area
B	Solute permeability coefficient
C_D	concentration of draw solution
C_f	Concentration of feed
C_p	Concentration of permeate
C_t	Concentration of solute at time t
D	Diffusion coefficient of salt in bulk solution
J_s	Reverse salt flux

J_w	Permeate water flux
k	Mass transfer coefficient
M_w	Molecular weight
R	Salt rejection
R_a	Average roughness
R_q	Root mean square roughness
S	Structural parameter
SAD	Surface area difference
V_t	Volume of solution at time t
ΔP	Hydraulic pressure difference applied across FO membranes
Δt	Time interval

Greek Letters

π_F	Osmotic pressure of feed solution
π_D	Osmotic pressure of draw solution
ρ	Water density

Chapter 1

Introduction

1.1 Water demand and membrane technology

The rapid growth of the world's population, industrial advancements, and global climate change have increased the demand for freshwater drastically [1,2]. According to the latest assessment of the World Economic Forum, the water crisis will be the foremost global risk to the environmental, cultural and economic development of several nations in the coming decade [3]. To relieve the pressure of imminent international water scarcity, global efforts have been accelerated to improve current water treatment processes and to develop novel energy- and cost-efficient technologies to sustainably produce clean water by wastewater reclamation and seawater desalination [4].

Technologies for wastewater treatment are classified into three main categories: (i) physical methods, such as adsorption, membrane filtration, media filtration (sand, gravel, walnut shell), evaporation, distillation, and air floatation, (ii) chemical methods, such as chemical oxidation (by ozone, chlorine, iodine, hydrogen peroxide, and permanganate) and electrochemical processes, and (iii) biological methods, such as anaerobic reactors, activated sludge, aerated lagoons, and wetlands [5–7]. Among these methods, adsorption (by activated carbon, zeolites, clays, resins, and synthetic polymers) [8–11], chemical oxidation [12–15], biological treatment [16–19], and membrane processes [20,21] are most broadly employed for the treatment of industrial and residential wastewater. Adsorption is used for the removal of a broad range of pollutants in wastewater, mainly organic matter, oil, and grease [22]. The low adsorption capacity of most available adsorbents and the environmental concerns and costs associated with the disposal and regeneration of used adsorbents are the main shortcomings of adsorption processes [6,22]. Pollutants in chemical oxidation process are decomposed through a series of radical reactions. Highly reactive radicals are produced by using chemicals like ozone, hydrogen peroxide (Fenton), chlorine, iodine, and permanganate. The production rate of radicals can be increased by UV light (photocatalytic oxidation) or ultrasound (sonochemical oxidation). The drawbacks of chemical oxidation processes are reduction of radical formation and the rate of oxidation reaction due to the high concentration of salt and radical scavengers, such as chloride and bicarbonate in some wastewaters. Moreover, oxidation processes are energy-intensive and the complete removal of pollutants may not be achieved, particularly for low concentration of contaminants, e.g., the removal of emerging pollutants such as pharmaceutical compounds and micro-plastics [6].

Biological methods are mostly effective for municipal wastewater treatment but their application for purifying more complex industrial effluents is somewhat restricted as microorganisms may not survive in the harsh conditions of such effluents [22].

Membrane separation processes have become one of the fastest emerging technologies for removing pollutants of different sizes from contaminated water due to their distinct advantages over traditional processes, primarily higher separation efficiency, stable product quality, lower operating expenses and smaller carbon footprint. [23]. Furthermore, compared to thermal water treatment methods such as evaporation and distillation, membrane technology offers lower energy consumption over long term separation process [24]. Nowadays, conventional water treatment methods are integrated with membrane filtration to achieve the synergistic advantages of both techniques [25–27].

A membrane is a thin layer of semi-permeable material that allows the passage of water molecules but excludes the transport of solutes when a driving force (such as pressure, concentration, temperature, and electric potential gradient) is applied across the membrane (**Figure 1-1**). The most commonly used membrane processes for wastewater treatment and desalination are pressure-driven microfiltration, ultrafiltration, nanofiltration, and reverse osmosis. **Figure 1-1** shows how these membranes can be used to filter solutes of different sizes. Microfiltration is used to remove solutes larger than 100 nm diameter, such as oil, grease and some bacteria. Ultrafiltration membranes reject solutes within 10-100 nm diameter range, such as some viruses and humic organic matter. Nanofiltration separates solutes in the range of 1 nm to 10 nm and is mainly used to remove divalent ions from water (water softening). RO membranes are considered dense (nonporous) membranes and can separate even very small monovalent ions.

Membrane materials are broadly classified as organic (mainly polymeric) and inorganic (mainly ceramic) materials. Currently, polymeric membranes dominate the water treatment and desalination industry, primarily due to their easy and low-cost processing, as well as their high flexibility for surface chemistry customization to tune separation and antifouling properties. Historically, however, the main disadvantage of polymeric membranes has been their inability to resist high temperatures. At high temperatures, the chain network of a polymeric membrane plasticizes and results in loss of flux. Further degradation allows undesirable contaminants to permeate through the membrane or leads to loss of rejection. Thermally tolerant polymeric

membranes can potentially improve heat integration in a plant that produces high-temperature wastewater, thereby reducing reheating requirements and greenhouse gas (GHG) emission.

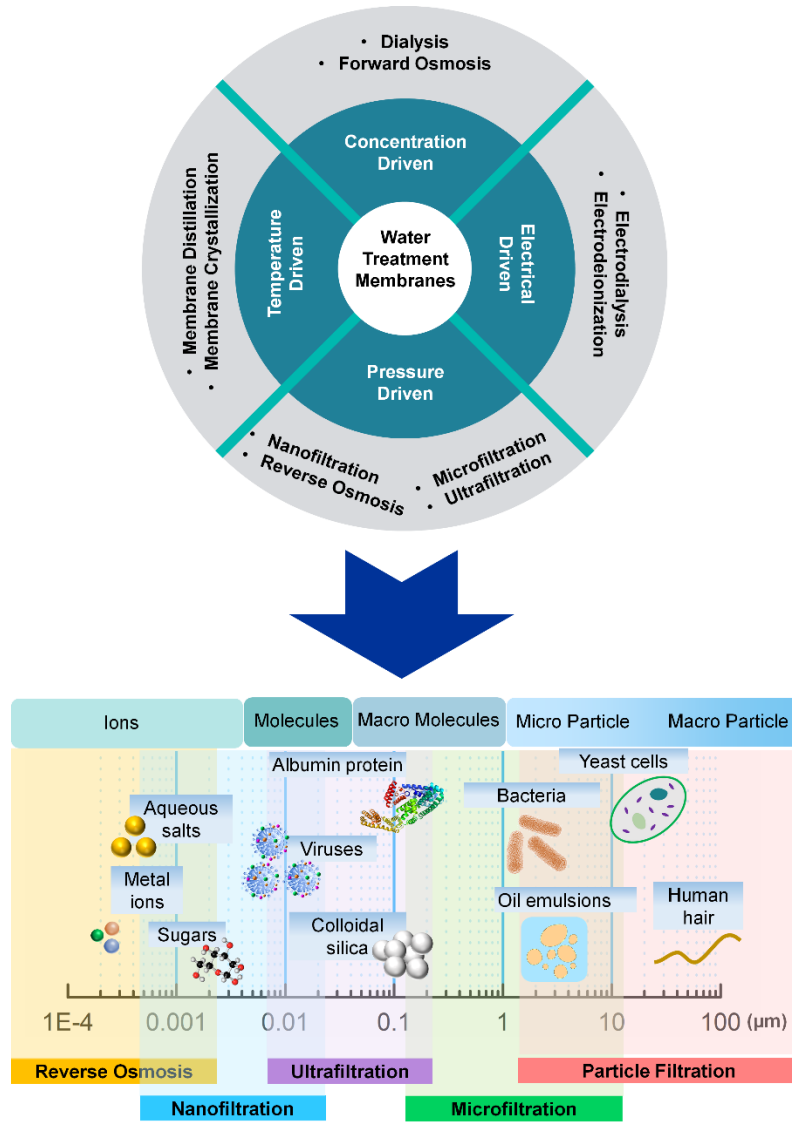


Figure 1-1: Various types of membrane separation processes for water treatment categorized based on driving force and schematic representation of the most widely used pressure-driven membranes including microfiltration, ultrafiltration, nanofiltration and reverse osmosis (RO), in which membrane pore size reduces from microfiltration to RO and the size of rejecting contaminants decrease proportionally.

Thin film composite (TFC) membranes currently represent the best platform for reverse osmosis (RO), nanofiltration (NF), and Forward osmosis (FO) water treatment processes owing to their outstanding separation performance [28].

1.2 Synthesis of polymeric membranes

Several methods are used to fabricate polymeric membranes. Membrane structure and polymer type are the main considerations when selecting a preparation technique. Phase inversion, interfacial polymerization, track-etching, electro-spinning, and stretching are the most common methods for the manufacture of polymeric membranes. The present study will focus on fabricating RO and forward osmosis TFC membranes by interfacial polymerization.

The emergence of TFC membranes was a significant development in the field of synthetic polymeric membranes [29,30]. The widespread success and uptake of TFC for RO and forward osmosis membranes for wastewater treatment and desalination is due to their unique multilayer structure. **Figure 1-2a** shows that a TFC membrane consists of a thin selective layer (100 nm to 200 nm) placed over an ultrafiltration or microfiltration substrate (50 μm to 100 μm). The support layer can also be reinforced with a non-woven polyester fabric [31,32]. The selective layer is often made of polyamide (PA) by interfacial polymerization of amine- and acyl-chloride monomers. **Figure 1-2b** illustrates the formation process of polyamide selective layer by interfacial polymerization. First, the diamine and acid chloride monomers are dissolved separately in two immiscible solvents, such as water and an organic solvent such as hexane [33]. The two monomer solutions are then brought into contact at the surface of the substrate where a polymerization reaction takes place at the interface between the water and organic solvent, and produces a thin polyamide film. The top surface and cross-section morphologies of a polyamide layer are shown in **Figure 1-2**. The AFM (**Figure 1-2c**) and FESEM images (**Figure 1-2d** and **1-2e**) show a ridge-and-valley structure on the top surface of the polyamide layer, which is a feature of the morphology of polyamide TFC membranes. This structure is formed by rapid diffusion of amine monomer into the organic solution during the interfacial polymerization. The TEM cross-section image (**Figure 1-2f**) depicts the typical internal structure of a polyamide selective layer of TFC membranes. The support layer of the TFC membranes is conventionally made from polyethersulfone (PES), polysulfone (PSf), and polyacrylonitrile (PAN), using phase inversion techniques. Non-solvent induced phase separation (NIPS) or immersion precipitation is the most versatile technique to make porous support layers. Briefly, this method includes dissolving the polymer into an appropriate solvent such as N-methyl-2-pyrrolidone (NMP) or dimethylacetamide (DMA), then casting the polymer solution on a non-woven fabric sheet, followed by immersion into a

coagulation water bath where the solvent and non-solvent (mainly water) exchange occurs, leaving a porous polymer film [34,35]. During the filtration process, the polyamide active layer plays the primary role in the separation of contaminants while the substrate provides mechanical support to the whole structure to withstand the high pressures of reverse osmosis and nanofiltration operations [36]. Because both the material selection and the preparation protocol for the active and support layers of the TFC membranes are flexible, these membranes are the most promising candidates for advanced water separation technologies [37].

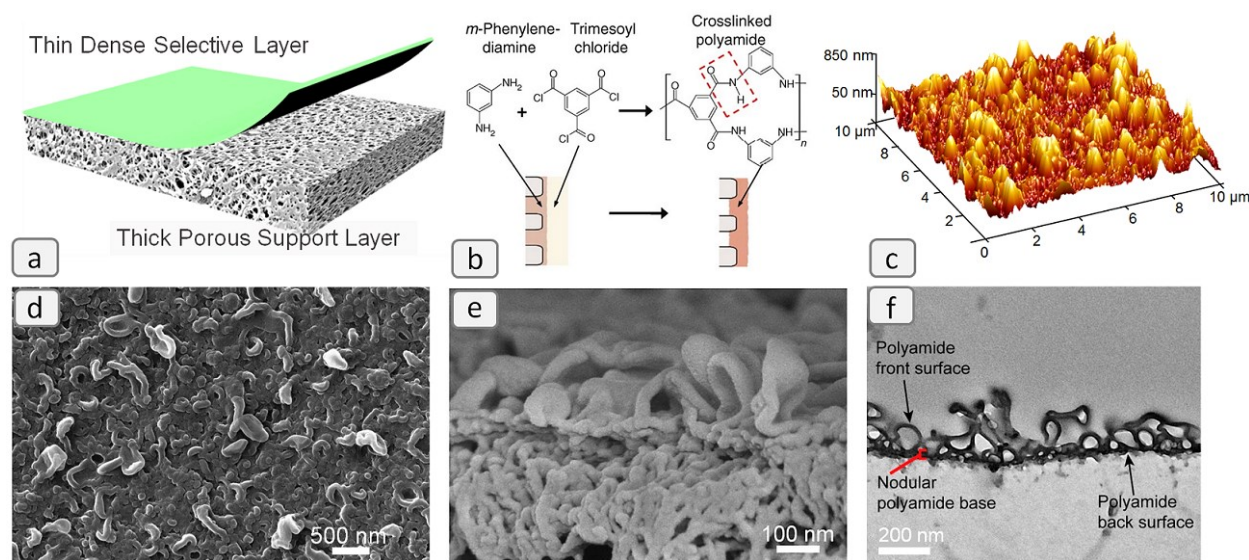


Figure 1-2: (a) Schematic structure of thin film composite (TFC) membrane having two at least compositional layers: a selective thin layer over a porous support layer. Reprinted from [36]; (b) chemical structure of the reacting monomers and the polyamide film. Reproduced with permission of The American Association for the Advancement of Science [38]; (c) AFM surface topography. Reproduced with permission of Elsevier [39], (d) FESEM surface morphology. Reproduced with permission of Elsevier [40], (e) FESEM cross-section structure. Reproduced with permission of Elsevier [41]; and (f) TEM cross-section image. Reproduced with permission of Elsevier [42] of a typical polyamide TFC membrane.

1.3 Critical need for thermally stable membranes for hot water treatment

In multiple industries, the contaminated process water must be treated at high temperatures for sustainable and energy-efficient water recycling. In food industries, as an example, process water needs to be treated at a temperature above 80 °C to mitigate the growth of microorganisms [43]. In the pulp and paper industry, a large-volume stream of recycled water at temperatures above 70 °C is generated from the integrated mill process [44,45]. Similarly, different operations in the textile industry, such as dyeing, consume a huge amount of water and produce high-temperature wastewater (90-95 °C) [46]. Hot condensates, that are needed to be treated and recycled, are

abundant in many industries including refinery operations, alcohol production, and production of rubber automotive tires. In heat-exchanger manufacturing, one of the cleaning methods is to use hot water to remove impurities such as grease and oil from heat-exchanger plates. To minimize the consumption of fresh water in the rinsing tanks, the recovery of hot contaminated water (at about 65 °C) is essential [47]. In steam assisted gravity drainage (SAGD) process, which is a thermally enhanced oil recovery method, high-pressure and high-temperature steam is injected underground to facilitate the extraction of the oil sands by lowering its viscosity. The de-oiled process water, which is typically at 80 °C to 90 °C, is treated and reused as the boiler feed water [48,49]. Different industrial and municipal high-temperature wastewaters along with the sketch of SAGD process are demonstrated in **Figure 1-3**.

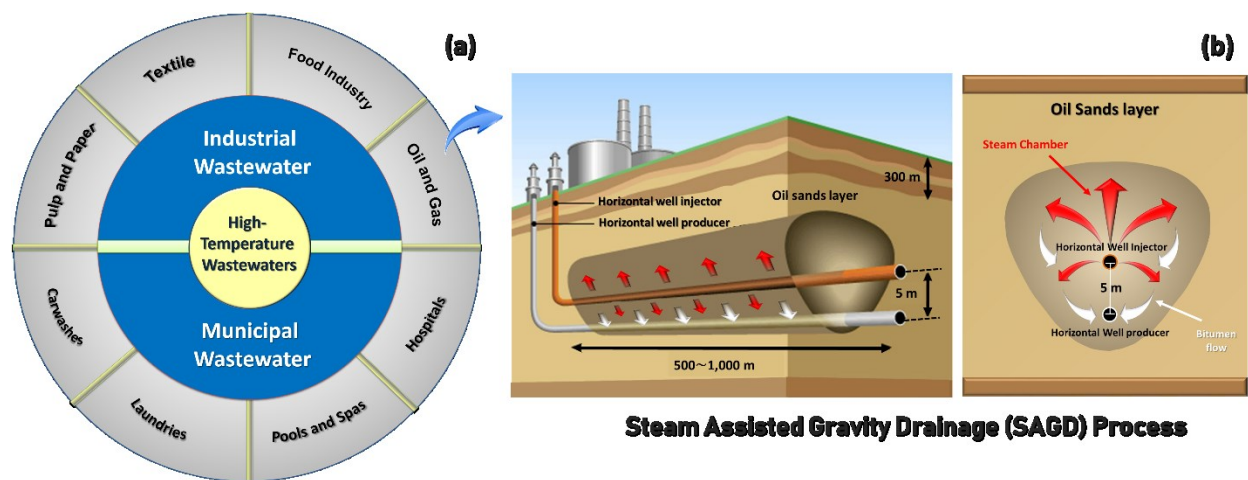


Figure 1-3: a) Industrial and municipal high-temperature wastewaters and b) schematic illustration of SAGD process which produces wastewater at 80-90 °C. Reproduced with permission of SpringerNature [50].

Separation processes based on polymeric based membrane have become common practice in many industrial sectors. However, the majority of these processes operate at temperatures below 45 °C and require cooling of the wastewater [51,52]. As a matter of fact, the process streams must be cooled solely to accommodate a membrane separation process, after which the processed fluid is heated back. This cooling followed by re-heating causes the waste of a considerable amount of energy. Given the growing concerns about water and energy consumption, thermally tolerant membranes can improve heat integration in many industrial applications, thereby reducing heating requirements and greenhouse gas production. Applying innovative membranes for the treatment of high temperature and chemically harsh wastewater opens up new paradigms for delivering high-quality water with low energy consumption [53].

1.4 Overview of thermal properties of polymers

1.4.1 Impact of temperature on polymer structure

Polymers undergo different phase transitions when they are heated or cooled, such as glass transition, melting, crystallization, and decomposition. Polymers can be divided into thermoplastics and thermosets based on their behavior when exposed to heat [54]. Thermoplastic polymers have high processability and are readily recycled through melting, shaping and cooling. Thermoplastics operate in a wide range of temperatures [55]. Thermoplastics are made mainly of linear polymer chains that interact with each other via non-covalent forces such as van der Waals interactions and hydrogen bonds. Such weak interactions allow the chains high mobility, the ability to undergo phase transitions, and be dissolved in solvents. In contrast, thermosets are materials in which the polymer chains are connected via covalent bonds (crosslinks). When heated, thermosets remain in the solid state until their polymer chains eventually decompose. The cross-linked network of thermosets hinders chain motion, leading only to decomposition at high temperatures.

The stages of a polymer's thermal transitions can be explained by considering the physicochemical changes in the polymer structure across temperature variations. The glass transition temperature (T_g) is the point at which the polymer changes from a glass-like state into a rubbery form. Below this temperature, there is no significant dimensional variation in the polymer network. The melting point (T_m) is the temperature at which the polymer crystallites melt, and the polymer becomes an isotropic liquid. While T_g is attributed to amorphous polymers or the amorphous phase of semi-crystalline polymers, T_m is mainly associated with the crystalline phase of polymers [56]. The glass transition temperature is always lower than melting temperature and has a direct relationship with the degree of crystallinity of polymer [56,57].

Polymers can also undergo chemical changes and decompose at high temperatures. The mechanisms of thermal degradation of polymers can be classified as random scission, depolymerization, and elimination of side groups [58]. Thermal decomposition of polymers occurs in different stages due to the different thermal resistance of their chemical groups. For the majority of polymers, the thermal stability of polymers is quantified by their first and second decomposition temperatures, as well as their decomposition temperature range. It is worth noting that thermal decomposition and thermal degradation of polymers do not stand for the same phenomenon. Thermal decomposition is an extensive change in the chemical structure of the polymer under

heating, while thermal degradation is attributed to the loss of the polymer's properties, such as physical or mechanical properties [59].

1.4.2 Influential factors on thermal properties of polymer

The phase transition stages of polymers depend on the polymer's intrinsic properties, including crystallinity, chain rigidity, backbone structure, crosslinking, steric hindrance effects and inter- and intra-chain interactions. **Figure 1-4** schematically illustrates the factors that influence the thermal behavior of polymeric films. Based on degree of crystallization, polymers can be classified as amorphous or semi-crystalline polymers [24,60].

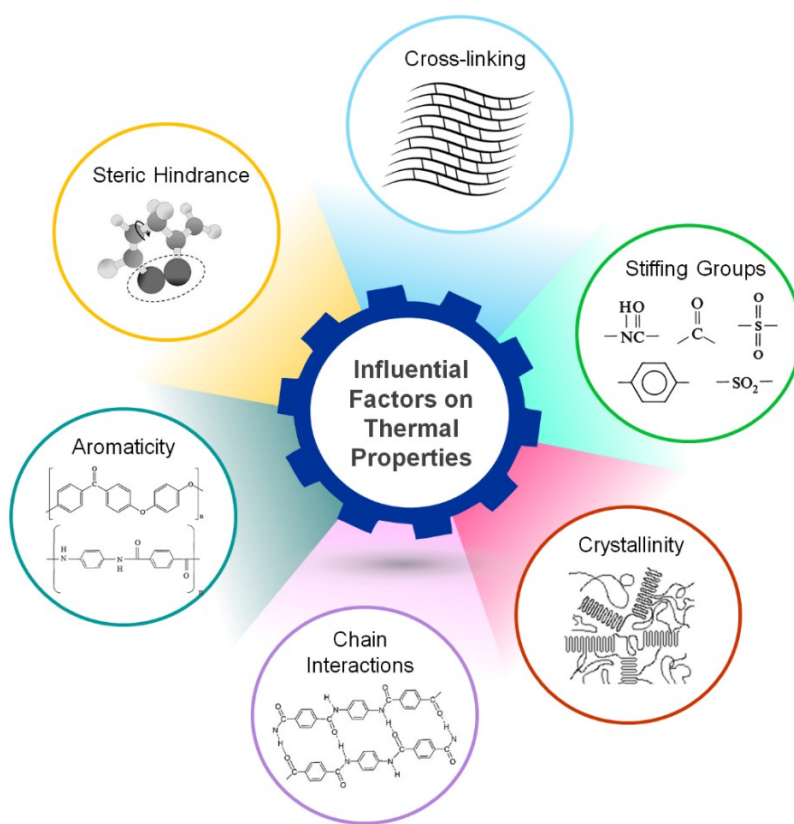


Figure 1-4: Influential factors on thermal behavior of polymers.

Amorphous polymer chains form disordered conformations, while semi-crystalline polymers consist of both ordered (crystalline lamella) and amorphous structures. The tendency of the polymers to form crystalline or amorphous phases is influenced by the regularity of the polymer chains and the strength of their intermolecular interactions [56,61]. In general, semi-crystalline

polymers have phase transition at higher temperatures than amorphous polymers. The glass transition temperature (T_g) can be considered as a property of the amorphous phase, while the melting temperature (T_m) is associated with the crystalline structure. In the glassy state, where the temperature is below T_g , atomic motion in the amorphous phase are limited, but they are even more restricted in the crystalline phase, where atoms can only vibrate around their equilibrium average positions. Above T_g , however, the higher thermal energy induces segmental motions of atoms in the amorphous phase, while atoms in the crystalline phase still retain their ordered structure (Beck et al., 1984; Kumar and Gupta, 2018; Walczak, 2012). Therefore, higher thermal energy is required for inducing segmental motion and phase transition (to rubbery state) in semi-crystalline polymers compared to amorphous polymers. [62–64].

The thermal phase transitions also vary with the rigidity of the polymer network. Chain rigidity or stiffness is caused by the restriction of segmental motion and rotation of polymer chains in the presence of stiffening groups. Primarily, the chemical bond energies of the polymer chains govern the thermal resistance of the polymers [65]. For instance, polytetrafluoroethylene ($-\text{CF}_2-\text{CF}_2-$)_n is more thermally-stable than polyethylene ($-\text{CH}_2-\text{CH}_2-$)_n due to the stronger C-F bonds compared to C-H bonds (C-F and C-H are 487 and 418 kJ mol⁻¹, respectively) [59,66]. Several linkages with high bond cleavage (scission) such as amides, sulfones, and ketones improve the rigidity of the polymer network. The presence of aromatic compounds, such as phenyl groups, also hinders polymer chain motion via resonance stabilization or electron delocalization effects, leading to an increase in the glass transition and melting temperatures [38,58,65]. Conversely, the presence of flexible groups like alkyls, ethers, and C-C or C-O bonds, lowers the temperature of phase transition [67,68]. For instance, due to the presence of abundant C-H groups in their structures, fully aliphatic polymers exhibit lower glass transition temperatures compared to aromatic polymers [65,69]. As another example, the thermal phase transition temperature of PEEK ($T_g = 151\text{ }^\circ\text{C}$ and $T_m = 338\text{ }^\circ\text{C}$) can be enhanced by eliminating one ether group to form polyether ketone (PEK) ($T_g = 160\text{ }^\circ\text{C}$ and $T_m = 372\text{ }^\circ\text{C}$) [70–72]. The mobility of a polymer chain is not only restricted by its single chain structure; rather, in a polymeric system, it is also influenced by adjacent chains [73,74].

One of the most common interactions that affect the thermal behavior of the polymers is the tendency to form hydrogen bonds. The density of the hydrogen bonds can result in a variation of

the glass transition temperatures of the linear polymer chains. As an example, the difference between the glass transition temperature of polyethylene and polyamide is mainly attributed to the high tendency for hydrogen bond formation in the latter [75,76]. The well-known heat resistant polyamide fiber, Kevlar, has high crystallinity due to the presence of polar amide groups in an aromatic backbone structure, leading to the formation of an ordered hydrogen-bonded network [77]. The conjunction of space-filling groups, especially as side groups in the polymer backbone, may induce steric hindrance and thus lower the segmental motion in the polymer network. Halogen-containing polymers demonstrate a higher glass transition temperature, owing to the size of the halogen atoms [78]. Similarly, phenyl side groups in polystyrene (PS) hinder the flexibility of the chains, which partly explains its higher glass transition temperature ($\sim 100\text{ }^{\circ}\text{C}$), as compared to low-density polyethylene (LDPE) ($-75\text{ }^{\circ}\text{C}$) with the similar backbone structure [56,79].

1.5 Thermal characterization of polymers

The thermal properties of the polymers can be evaluated using multiple characterization techniques such as differential scanning calorimetry (DSC), thermogravimetric analysis (TGA), dynamic mechanical analysis (DMA), and dynamic mechanical thermal analysis (DMTA). These techniques are commonly performed to evaluate the chemical structure, thermal transitions, viscoelastic behavior, thermal decomposition, and thermal conductivity of polymers.

Figure 1-5 shows the schematic of a DSC cell and characteristic phase transition curves, including glass transition, crystallization, melting, and decomposition. DSC analyzes the heat flow of a sample during heating, cooling, or at constant temperature, compared to a reference sample. By gently heating the sample, it undergoes first and second order transitions. First-order transitions, such as melting and crystallization, involve changes in both heat capacity and enthalpy (latent heat). Second order transitions such as glass transition, on the other hand, involve changes in heat capacity but not in latent heat. At the glass transition temperature, the DSC thermogram baseline shifts before and after the transition, revealing the difference between the heat capacity of the glassy and rubbery regions. Furthermore, the melting point is determined by an endothermic peak in a heating thermogram of DSC, showing the required latent heat for the polymers crystallites to melt [80].

DMA or DMTA is a technique for investigating the viscoelastic behavior and phase transition temperature of polymers. These techniques measure the glass transition temperature using the

differences in the rheological characteristics and the heat capacity over a range of temperatures. The storage modulus (E') and the loss modulus (E'') are measured, and $\tan \delta$ is calculated as $\tan \delta = E''/E'$. The glass transition temperature is defined as the maximum value of the $\tan \delta$ curve, indicating a sharp decrease of E' as the polymer transitions from a glassy to a rubbery state [81,82].

Figure 1-5b illustrates a TGA cell which is commonly used to measure the thermal decomposition temperatures of polymers. Using this technique, the weight loss of the sample is measured continuously as a function of temperature. A typical TGA curve illustrates distinct weight loss regions at different temperatures, which can be attributed to adsorbed moisture (below 100 °C), residual substances such as solvents, chain scission, and cleavage of polymer covalent bonds [83,84].

Phase transition temperatures of polymers can also be evaluated using nanoscale thermal characterization techniques [78,79]. Nano-TA, presented schematically in **Figure 1-5c**, is an atomic force microscopy (AFM)-based thermal analysis, developed by Anasys Instruments Corporation to measure the melting and glass transition temperatures of single or multilayer polymeric samples. [80,81]. This technique utilizes a modified AFM cantilever with a heater-equipped tip. Over a fixed point on the samples, the deflection of the AFM probe is continuously monitored while the tip temperature elevates steadily with time. The softening temperatures (T_g for amorphous polymers or T_m for semicrystalline polymers) are recorded when a significant variation in tip bending is captured due to penetration of the tip into the sample [85,86].

In the case of polymeric membranes, it is very informative to evaluate the thermal stability of the membrane using direct performance tests (water flux and salt rejection measurements) at varying temperatures. When the solution temperature rises, the water viscosity decreases and thus the membrane water flux increases, which is quite favorable. However, polymeric membrane materials plasticize at high temperatures which, significantly reduces their performance regarding the rejection of contaminants [51]. Consequently, for high solution temperature applications, it is essential to maintain salt separation performance and the chemical and mechanical structure of the polymeric membrane at reasonable levels. As a matter of fact, the best method to evaluate the thermal stability of the polymeric membranes is monitoring the permeation, solute rejection, and mechanical robustness of the membrane at various operating conditions, such as cyclic heating and cooling and long-term exposure to the high-temperature solution [51,87].

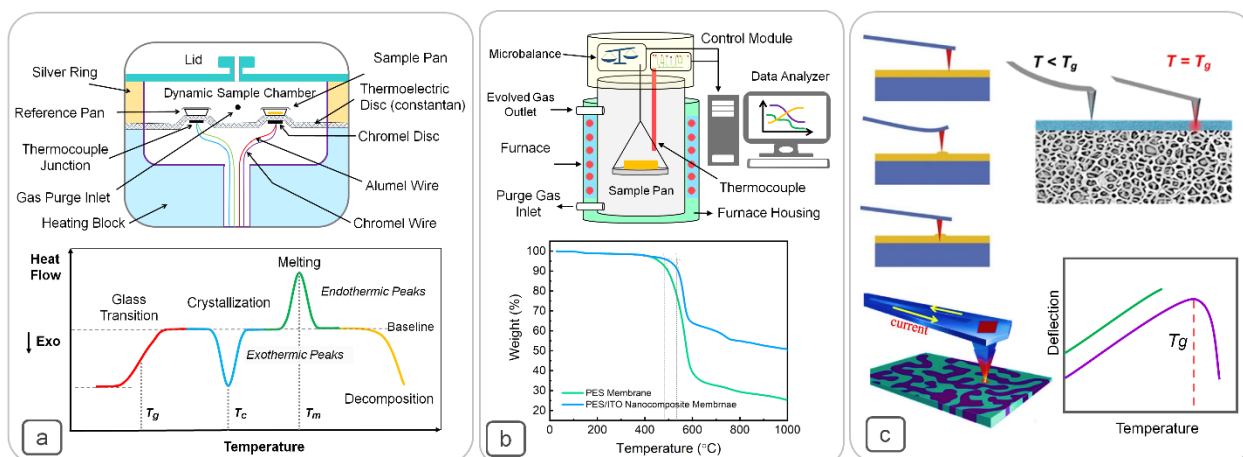


Figure 1-5: (a) Schematic view of DSC along with different thermal transition phases such as glass transition, crystallization, melting temperatures. Reproduced with permission of Wiley and Sons [83]; (b) Schematic illustration of TGA along with a sample curve of PES and PES/ITO nanocomposite membranes. Reproduced with permission of Elsevier [88]; (c) Schematic view of Nano-TA along with sample curves. Reproduced with permission of Elsevier [85,89]

1.6 Progress of development of thermally stable TFC membranes

1.6.1 Novel thermally stable membranes in commercial scale

The majority of commercially available RO and nanofiltration TFC membranes are recommended to be used at feed temperatures below 45 °C. In recent years, a few thermally stable membrane modules have emerged in the market to address the need for hot water purification. The main developments have focused on the design of spiral elements, rather than on the polymeric membrane material itself. For instance, XUS120308 and XUS120304 are thermally robust RO elements that are specifically designed by DuPont™ to operate at feed temperatures up to 80 °C. These elements also feature a machined polypropylene rigid outer shell (called DOW HYPER SHELL™ technology) which is necessary for sanitary food application and use DOW FILMTEC™ SW30 polyamide TFC membranes to provide high salt rejection performance when operated at higher temperatures. Duratherm™ HWS series is another line of commercially available, high-temperature elements developed by SUEZ Water Technologies & Solutions (previously known as GE Osmonics and Desal or DSI) which contain RO, NF and UF flat sheet membranes. These elements can be hot water sanitized up to 90°C and operated continuously up to 50 °C. For applications between 50 and 70 °C, the manufacturer's data sheet provides helpful guidance on performance impacts such as salt (NaCl) rejection loss of about 3% for filtration at 70 °C. Similarly, the Hydranautics Nitto group fabricates the HYDRApro® 500 series membranes

for higher temperature industrial process applications and also includes a curve that lowers the maximum operating pressure as the feed water temperature increases. **Table 1-1** lists some of the thermally stable polymeric membranes made with new elements or designed to operate at high water temperatures.

Table 1-1: Some of the commercially available spiral wound polymeric membrane elements for higher temperature water treatment.

Brand	Model	Type	Max. operating pressure (psi)	Max. operating temperature (°C)
Microdyn Nadir (TRISEP®)	TurboClean High-Temperature RO 8040	ACM Fully aromatic PA advanced composite membrane	300	70
DuPont Water Solutions (FILMTEC™)	XUS120308 and XUS120304 RO	PA TFC based RO sheets with machined polypropylene shell	435	80
Nitto Group Company (Hydranautics)	HYDRApro® 500 Series	PA composite	300	90
SUEZ Water Technologies & Solutions (Osmonics, Desal)	Duratherm™ HWS Series	Durasan™ cage outer wrap, polysulfone ATD, and central tube	200	70

Microdyn Nadir/Trisep TurboClean High Temp RO 8040 advanced composite membranes (ACM) consists of a fully aromatic polyamide top layer that provides 99% salt rejection at temperatures as high as 70 °C. The XUS120308 and XUS120304 RO modules of DuPont Water Solutions is equipped with FILMTEC™ SW30 polyamide membranes. The special element and membrane design are claimed to provide continuous operating up to 80 °C with 99.4% salt rejection. However, the maximum operating temperature of FILMTEC™ SW30 is 45 °C. HYDRApro® 500 is a low-fouling spiral wound module made by Nitto Group Company/Hydranautics, which houses polyamide composite membranes. These membranes are specially designed to treat a variety of challenging industrial water streams, including high fouling, high temperature (up to 70 °C), or chemically aggressive wastewaters with the average salt rejection of 99.5%. The Duratherm™ HWS series of SUEZ Water Technologies & Solutions (Osmonics, Desal) includes ultrafiltration, nanofiltration and reverse osmosis membrane elements specifically designed to sanitize hot water at feed stream temperatures up to 70 °C. Duratherm™ HWS RO thin film membranes provide salt rejections higher than 99%.

1.6.2 Novel thermally stable membranes in lab-scale

The recent efforts to improve the thermal stability of TFC membranes have focused on limiting the segmental motions of both the top active layer and the bottom support layer. At elevated solution temperatures, the polymer chain network becomes more flexible, which results in a significant loss of separation performance. The proposed methodologies to restrict membrane pore expansion can be categorized as (i) modification of the chemical structure of the active layer, (ii) tuning of the chemical structure of the porous sublayer, or (iii) incorporation of nanofillers into both active and support layers.

(i) Modification of the active layer

Table 1-2 contrasts the performance of thermal resistant TFC membranes with modified active and support layers. Many studies listed in this table investigated the effect of membrane synthesis parameters, such as type and concentration of monomers, reaction time, and curing time/temperature needed to make thin films with denser, more rigid, and more cross-linked structures. Dodda and Kullova [90] investigated the effect of reaction conditions including monomer type and concentration, reaction time, curing time and temperature on the permeability and physicochemical properties of TFC membranes. Different amine monomers diethylenetriamine, 1,3-cyclohexanebis(methylamine) (CBMA), 2,3-diaminopyridine (DAP), m-phenylenediamine (MPD), piperazine (PIP) or a mixture of MPD and PIP/DAP – were reacted with trimesoyl chloride (TMC) over a reinforced PES microporous support to form polyamide films with different chemical structures. The permeation properties and the phase transition temperatures of the prepared polyamide films varied significantly with the chemical composition and concentration of the reacting monomers. Increasing TMC concentration from 0.01 wt.% to 0.2 wt.% in organic solution caused the T_g of the resulting poly(CBMA-TMC) membranes to rise from 198 °C to 212 °C. A similar increase in T_g was reported for polyamide films made using higher concentrations of amine monomers at a fixed TMC concentration. The higher T_g was attributed to the higher molecular weight of the polyamide films made at higher monomer concentrations.

Dodda et al. [91] investigated the effect of the monomer structural chemistry on the permeation and thermal stability of polyamide TFC membranes. The membranes were prepared by interfacial polymerization between amic acid diamines (AADs) and trimesoyl chloride (TMC). The AADs were synthesized by reacting trimellitic anhydride chloride (TMAc) with five different diamines,

including 1,3-cyclohexanebis(methylamine) (CDA), 4,4'-diaminophenylmethane (MDA), 4,4'-oxydianiline (ODA), 3-aminophenyl sulfone (3APS), and m-phenylenediamine (MPD). Since the synthesized amine monomers had different chemical and structural compositions, they formed nanofiltration and reverse osmosis membranes with a range of permeation performance. The glass transition temperature of the prepared membranes was found to strongly depend on the concentration and chemical structure of the reactants. Moreover, the polyamide films that had contained aromatic groups exhibited higher T_g due to their stiffer chain networks compared to polyamide membranes with aliphatic groups. The highest T_g was reported as 240 °C for poly(TMAc-MPD-TMC) TFC membranes.

Aromatic and semi-aromatic polyamides have more thermal resilience than those with aliphatic structures, owing to their aromatic rings such as phenyls, benzenes, and furans [92,93]. Han [94] reacted amine and acyl chloride monomers with aromatic and triazine rings to improve the thermal resistance of polyamide TFC membranes. The polyamide films were prepared by the interfacial polymerization of 2,4,6-triamino-1,3,5-triazine (known as melamine) and TMC over polyetherimide (PEI) ultrafiltration substrates. The poly(melamine-TMC) membranes had higher thermal and chlorine resistance than poly(PIP-TMC) membranes. When the operational feed temperature increased from 18 °C to 95 °C, the water flux of the poly(melamine-TMC) TFC membranes increased from 32 LMH (Liters per square Meter per Hour) to 138 LMH, without a significant variation in solute rejection (78% for Na₂SO₄).

Wei et al. [87] studied the impact of the chemical structure of amine reactants on the thermal stability of polyamide TFC membranes. Diamines inducing m-phenylenediamine (MPD), piperazine (PIP), and 1,2-dimethylenediamine (DMDA) were reacted with trimesoyl chloride (TMC) over a poly(phthalazinone ether sulfone ketone) (PPESK) substrate to study the effect of the MPD aromatic rings, PIP alicyclic rings, and DMDA aliphatic linear structure on the thermal stability of the synthesized membranes. The salt rejection rates showed that the fabricated polyamide films with fully aromatic (poly(MPD-TMC)) structures exhibited the best thermal resistance and the least sensitivity to solution temperature, followed by alicyclic aromatic (poly(PIP-TMC)), and finally aliphatic aromatic (poly(DMDA-TMC)) membranes. Such a high thermal tolerance was attributed to the higher rigidity of the aromatic diamine constituents.

Table 1-2: Summary of the studies reported on development of thermally stable TFC membranes by tuning the chemistry of the selective polyamide layer.

Constituent Monomers	Substrate Material	Operating Pressure (MPa)	Operating Temperature (°C)	Flux Enhancement (LMH)	Solute Rejection (%)	Solute	Ref.
PIP-TMC	PPEA	1	25-80	87 to 264	12.2-6.9 99.3-99.7	NaCl ACBK	[95]
PIP-TMC	PPBES	1	18-85	61 to 290	92-88.5	Na ₂ SO ₄	[96]
PIP-TMC	PPENK	1	20-80	50 to 197	95.1-95.1	Na ₂ SO ₄	[97]
PIP-TMC (reinforced by GO)	PES	0.6	30-80	20 to 35	97-97	Na ₂ SO ₄	[98]
Melamine-TMC	PEI	1	18-95	32 to 138	78-78	Na ₂ SO ₄	[94]
MPD-TMC	PPESK	1.2	20-90	10 to 30	97.6-97.3	Na ₂ SO ₄	[87]
DMDA-TMC				8 to 24	88.4-76	Na ₂ SO ₄	
PIP-TMC				24 to 58	96.8-93.2	Na ₂ SO ₄	
MDP-TMC	PI	2.76	20-95	31 to 165	98-98	NaCl	[43]
PIP-TMC	PSf	0.8	30-80	55 to 105	96.5-91	Na ₂ SO ₄	[99]
	PES			55 to 84	91-93	Na ₂ SO ₄	
	PEI			70 to 120	94.5-98	Na ₂ SO ₄	

Several studies have reported the promising thermal resistance of sulfonated polymer films as an active layer for TFC membranes. Guan et al. [100] developed new composite nanofiltration membranes by coating a sulfonated copoly (phthalazinone biphenyl ether sulfone) (SPPBES) as a selective layer on PPESK ultrafiltration substrate. The permeation performance of the SPPBES films was optimized by evaluating the impact of SPPBES concentration, the degree of sulfonation, the concentration of the crosslinking agent, and the temperature and duration of thermal post-treatment. The results revealed that the SPPBES-PPESK nanofiltration membrane provided three times higher permeation flux (32 to 95 LMH) with 2% loss in Na₂SO₄ rejection (~ 90%) when the feed temperature was elevated from 20 °C to 90 °C. The low salt rejection sensitivity of the prepared TFC membranes to feed temperature was attributed to the high rigidity of the cross-linked SPPBES active layer, which is composed of fully aromatic structure.

Han et al. [101] developed thermally resistant hollow fiber nanofiltration TFC membranes by coating sulfonated poly(phthalazinone ether sulfone) (SPPEs) as the selective layer over a

poly(phthalazinone ether sulfone) (PPES) substrate. PPES was selected as a thermally stable substrate due to its high glass transition temperature of 305 °C. Several synthesis conditions were investigated to optimize the performance of the SPPEs films. Enhancement of water flux from 8.7 LMH to 58 LMH, with a slight decline in Na₂SO₄ rejection (from 93.6% to 92.5%), was reported when the feed temperature raised from 20 °C to 90 °C. In most cases, Na₂SO₄ was selected as the solute to investigate the membrane performance at higher temperatures, but the fabrication of RO membranes with a reasonable NaCl rejection at high temperature remains a challenging issue.

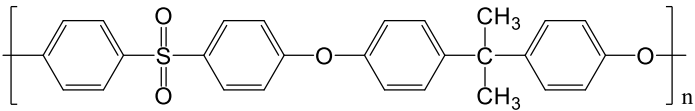
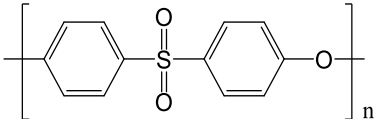
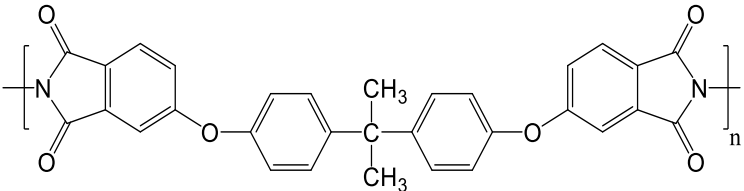
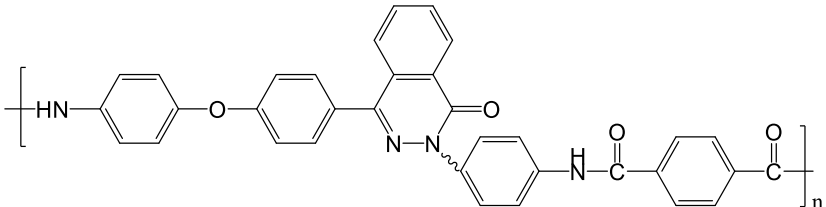
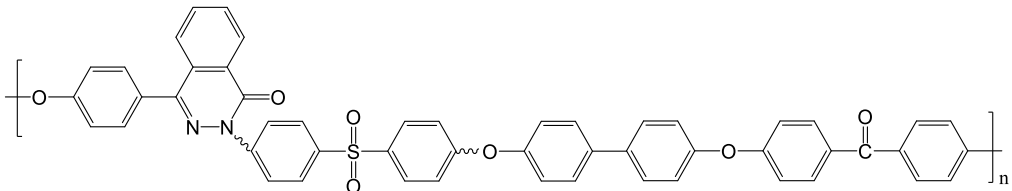
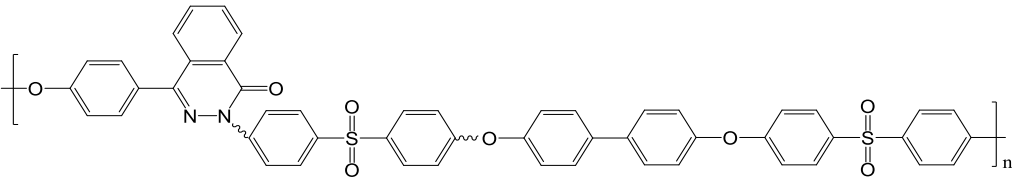
(ii) Modification of the support layer

The support layer of the TFC membrane significantly affects the thermal stability of the TFC membrane. Since the active layer and the substrate are firmly attached, any stress on the substrate would be reflected in the active layer. Hence, the expansion of the support layer pores at high temperatures can severely stretch the active layer and create pathways (defects) for the penetration of solutes.

Wei et al. [87] studied the impact of the support layer on the thermal stability of polyamide TFC membranes. Novel poly(phthalazinone ether sulfone ketone) (PPESK) porous membranes were compared with polysulfone (PSf) as a substrate for TFC membranes made by interfacial polymerization between *m*-phenylenediamine (MPD) and trimesoyl chloride (TMC). The polyamide/PPESK TFC membranes were more thermal resistant, with stable salt rejection, than polyamide/PSf TFC membranes. The observed performance was attributed to the superior physical properties and higher T_g (284°C) of PPESK as compared to the PSf substrate. Wu et al. [95] investigated the effect of synthesis parameters and operational conditions on the permeation performance of the nanofiltration polyamide TFC membranes prepared using piperazine (PIP) and TMC over a thermally-stable poly(phthalazinone ether amide) (PPEA) ultrafiltration substrate. The concentration of reacting monomers, as well as the immersion time in aqueous and organic solutions, were studied. The flux of the optimized poly(PIP-TMC)-PPEA nanofiltration membranes increased steadily from 87 LMH to 265 LMH when the operation temperature increased from 25 °C to 80 °C. When tested with a dye-salt mixed solution, the prepared polyamide membranes provided a similar rejection rate (above 99%) for acid chrome blue K (ACBK) dyes at low and high temperatures. However, a decline of about 5% (from 12.2% to 6.9%) was observed for NaCl rejection. Bo and Economy [43] developed thermally-stable TFC RO membranes by

synthesizing novel asymmetric poly(pyromellitic dianhydride-co-4,4'-oxydianiline) polyimide (PMDA/ODA polyimide) substrate. The polyamide active layer was prepared by interfacial polymerization using MPD and TMC. Imide bonds are stable groups at high temperatures. The PMDA/ODA polyimide has a glass transition temperature of approximately 400 °C. The permeation flux of NaCl solution increased from 31 LMH to about 164 LMH with a steady salt rejection (98%) rate when the feed temperature was elevated from 25 °C to 95 °C. The consistent separation performance of the TFC membranes was attributed to the high mechanical stability of the polyimide support layer that prevented pore expansion in the active layer. Han et al. [96] developed copoly (phthalazinone ether sulfone) (PPBES) as a substrate for poly(PIP-TMC) nanofiltration composite membranes. Due to the presence of heterocyclic groups in the backbone of PPBES, this polymer has a high glass transition temperature of about 289 °C. Increasing the feed water temperatures from 18 °C to 85 °C enhanced the permeate flux from 61 to 290 LMH with a slight decline in Na₂SO₄ rejection from 92.0 to 88.5%. Furthermore, over a 72-hour permeation test, the PPBES-based composite membrane exhibited a robust performance while the PSf-based membranes could not survive the high-temperature operation. Hu et al. [97] fabricated novel thermally resistant nanofiltration poly(PIP-TMC) TFC membranes using poly(phthalazine ether nitrile ketone) (PPENK) as a substrate. The PPENK ultrafiltration substrate was selected because of its high glass transition (277 °C) owing to its aromatic, heterocyclic, and twisted non-coplanar structure. The effect of interfacial polymerization parameters, such as the concentration of PIP and TMC monomers concentration, reaction time, and the type of organic solvents, were also investigated. The synthesized polyamide-PPENK membranes exhibited about four times higher water flux with almost stable salt rejection (about 95% for Na₂SO₄) at 80 °C compared to 20 °C. The invariant separation performance of the prepared membranes was attributed to the high hydrophilicity of PPENK support due to the presence of polar cyano (nitrile) groups, as well as the improved binding between the polyamide active layer and the PPENK substrates. Misdan et al. [99] investigated the effect of the substrate structure on the performance of the composite nanofiltration membranes at different operating temperatures. Polysulfone (PSf), polyethersulfone (PES) and Polyetherimide (PEI) were used as microporous supports for the poly(PIP-amide) active layer.

Table 1-3: Chemical structure of the polymers commonly used for improving the thermal stability of the TFC membranes

Name	Structure
Polysulfone (PSf)	
Polyethersulfone (PES)	
Polyetherimide (PEI)	
Poly(Phthalazinone Ether Amide) (PPEA)	
Poly(Phthalazinone Ether Sulfone Ketone) (PPESK)	
Copoly (Phthalazinone Biphenyl Ether Sulfone) (PPBES)	

The thermal resistance of the TFC membranes was found to be influenced by the physicochemical properties of both support and the polyamide active layer. X-ray photoelectron spectroscopy (XPS) results revealed that the polyamide-PSf membranes had a higher degree of cross-linking than PEI- and PES-based polyamide TFC membranes with more linear structures. The PEI-based TFC membranes provided superior water flux at elevated temperatures compared to PES- and PSf-based TFC membranes due to having fewer cross-linked polyamide in the active

layer. Contrary to polyamide/PES and polyamide/PSf membranes, which showed lower salt (Na_2SO_4) rejection, the salt removal efficiency of the polyamide/PEI membranes improved as the feed solution increased to 80 °C. The low thermal resistance of the polyamide/PSf membranes was attributed to the lower T_g of the PSf substrate, which enlarged the void size of the polyamide active layer. **Table 1-3** presents the chemical structure of the support layers used for fabrication of thermally stable TFC membranes.

(iii) Incorporation of nanofillers into TFC structure

Incorporating multifunctional inorganic nanofillers into the structure of the TFC membranes to synthesize thin-film nanocomposite (TFN) membranes have shown promising potential to improve the thermal and mechanical characteristics. **Table 1-4** summarizes the recent developments of TFN membranes which achieve higher thermal resistance by adding nanofillers to either the selective layer or the substrate. To ensure the nanoparticle are well dispersed in, and compatible with, the host polymer, different surface modifications technique are employed to tune the surface chemistry of nanoparticles. Since amines and acyl chlorides are the two most common monomers used in interfacial polymerization, surface modification strategies such as acid functionalization (Rakhshan and Pakizeh, 2015), amination [102,104], and chlorination [98] have been used.

Rajaeian et al. [102] developed TFN nanofiltration membranes by incorporating aminosilanized TiO_2 nanoparticles (NPs) into polyamide active layer. Based on thermogravimetric analysis (TGA) data, lower weight loss was recorded compared with base TFC membrane and the synthesized TFN by unmodified TiO_2 nanoparticles, showing the strong interactions between modified TiO_2 nanoparticles and polyamide chains. Fathizadeh et al. [105] reported that the addition of NaX nano-zeolites into the polyamide layer improved the glass transition temperature of the resulting TFN membranes by about 17% compared to unmodified polyamide TFC membranes. No permeation performance at elevated temperatures was reported.

The major challenge in fabricating a defect-free nanocomposite membrane has been preventing the aggregation of the dispersed nanomaterials during the interfacial polymerization. Therefore, the preparation of well-dispersed nanofillers suspension in either aqueous or organic monomer solution is of high importance for the development of a robust TFN membrane. This is accomplished primarily by using surface modifying agents, e.g., surfactants, and attaching proper

functional groups to the nanomaterials, which can contribute to the interfacial polymerization, e.g., COCl. Rakhshan and Pakizeh [103] prepared nanocomposite polyamide membranes using oleic acid-modified silica nanoparticles. The TFN polyamide membranes were fabricated by dispersing surface modified silica nanoparticles in TMC-organic solution prior to the interfacial polymerization. It was reported that the functionalization of silica nanoparticles with oleic acid shifted the initial decomposition temperature of the polyamide layer from 452 °C for neat polyamide to 490 °C for SiO₂/polyamide. The intensified interactions between the polyamide network and silica nanoparticles improved the thermal properties of the prepared TFN membranes. Khorshidi et al. [106] developed thermally-stable RO membranes by incorporating TiO₂ nanoparticles into the polyamide active layer. In order to lower the aggregation of the nanoparticles, the TiO₂ nanoparticles were synthesized and surface modified by oleic acid using biphasic solvothermal reaction.

Figure 1-6 demonstrates the synthesis of the surface functionalized TiO₂ as well as the sequential steps of TFN fabrication through interfacial polymerization. The real-time interfacial polymerization and entrapment of monodispersed nano-sized TiO₂ nanoparticles (~10 nm) within the polyamide matrix improved the onset of intense thermal degradation about 20 °C compared to the pristine TFC membrane. Furthermore, the TFN membrane with an optimum concentration of the TiO₂ nanoparticles (0.0124 wt.% in heptane) exhibited higher water flux and more stable performance compared to unmodified TFC polyamide membrane over a 6 h filtration test at 65 °C.

By grafting magnesium silicate (MgSiO₃) nanoparticles on polyamide surface using 2-acylamido 2-methyl propane sulfonic acid (AMPS) monomers, Kotp et al. [107] also improved the thermal properties of TFC membranes. Due to the stronger chemical bonds of polyamide network with the modified nanoparticles and the sulfonic group, the incorporation of MgSiO₃ nanoparticles shifted the initial thermal decomposition temperatures about 50 °C [107].

Wen et al. [98] developed TFN nanofiltration membranes by incorporating acyl chloride graphene oxide (GO) nanofillers into the polyamide layer. The TFN polyamide/GO-COCl membranes provided superior water flux and salt rejection compared to the TFC polyamide membranes. In addition, increasing the feed temperature from 30 °C to 80 °C, improved the water

flux of the TFN polyamide/GO-COCl membranes about 75% with no sacrifice in salt rejection percentage.

Li et al. [108] demonstrated that the incorporation of carboxylated graphene oxide (cGO) nanoparticles into the structure of poly(PIP-amide) nanofiltration membranes enhanced the permeation flux at high temperature without a notable loss of salt rejection. Wu et al. [109] showed that with the incorporation of the multi-walled nanotube (MWNT) into the polyamide active layer, the temperature associated with the highest decomposition rate increased from 197 °C to 209 °C.

Ormanci-Akar et al. (Ormanci-Acar et al., 2018) made TFN membranes by incorporating halloysite nanotubes (HNTs) into the polyamide layer and tested all the samples at three different temperatures (15 °C, 25 °C, and 40 °C). The TFN sample made by adding 0.04 w/v% of HNT into the organic solution led to higher fluxes and almost the same rejection of setazol reactive dye solution compared with the pristine membrane at different operating temperatures, indicating the thermal stability of new membranes.

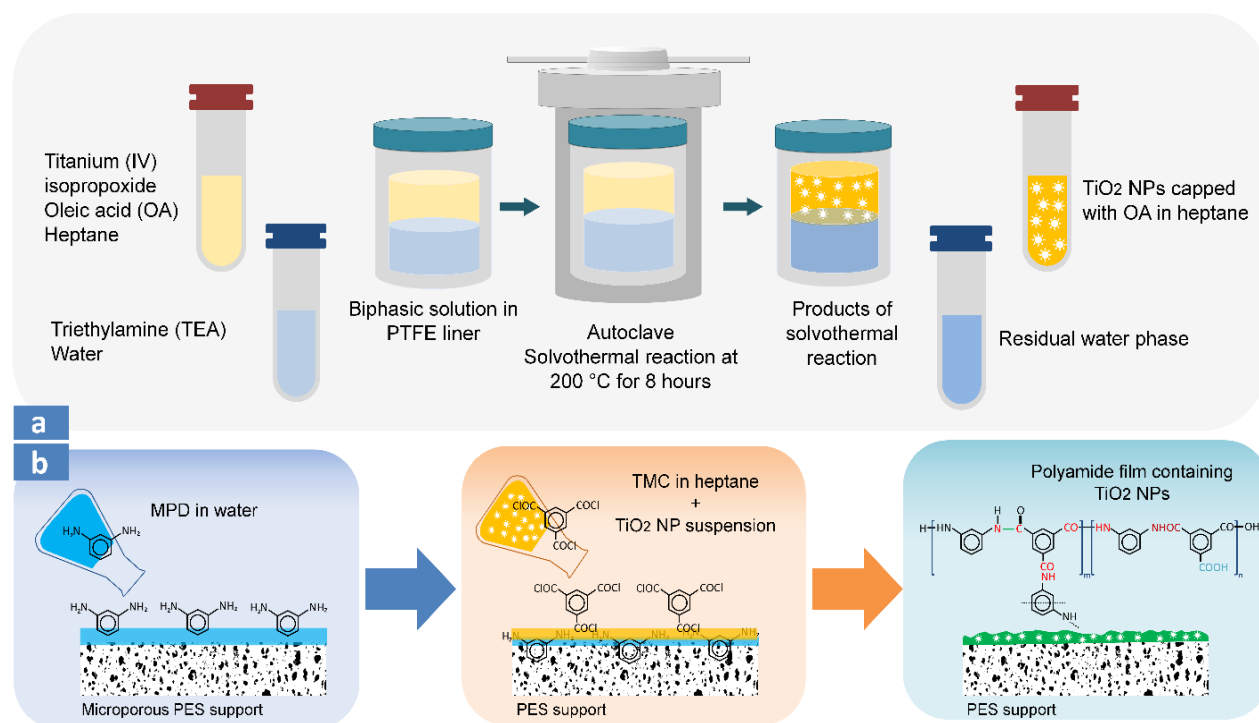


Figure 1-6: (a) Schematic synthesis route of TiO₂ NPs via biphasic solvothermal reaction and (b) fabrication of TFN membranes via adding TiO₂ NPs during interfacial polymerization. Reprinted from [106].

Table 1-4: Effect of incorporating nanoparticles into TFN membranes on their thermal properties.

Selective layer / Substrate layer	Incorporated layer	Type of nanoparticle	Nanoparticle concentration [*]	Nanoparticle functionalization	Improvement of thermal properties	Ref.
PA/PES	Selective	TiO ₂	0.005 wt% (in aqueous solution)	Aminosilanization	Lower weight loss compared with neat TFC and TFC with pure nanoparticles after TGA	[102]
PA/PES	Selective	TiO ₂	0.0245 wt% (in organic solution)	Acid functionalization (biphasic solvothermal method)	Improvement of onset of intense degradation temperature (20 °C) (based on TGA)	[106]
PA/PSf	Selective	SiO ₂	3.3 wt/v% (in organic solution)	Acid functionalization	(1) Improvement of initial decomposition temperature (8 %) (2) higher residual mass compared with neat TFC (5.7%) after TGA	[103]
PA/PEI	Substrate	SiO ₂	5 wt% (in substrate layer)	Aminosilanization	(1) Improvement of first (12.19 °C) and second (18.95 °C) decomposition temperatures of substrate layer, (2) higher residual mass compared with neat TFC (15.6%) after TGA	[104]
PA/PSf	Selective	MgSiO ₃	0.1% of monomer concentration	-	Improvement of the initial decomposition temperature (~80 °C) compared to base TFC membrane (based on TGA)	[107]
PA/PES	Selective	GO	0.002 wt/v% (in organic solution)	Acyl chlorination	Water flux increased by ~0.76 with consistent rejection in the temperature range of 30-80 °C	[98]
PEST/PSf	Selective	MWNT	0.05 wt/v% (in aqueous solution)	Carboxylation	Improvement of temperature at highest decomposition rate (12 °C) compared with base TFC membrane (based on TGA)	[109]
PA/PES	Selective	NaX nano-zeolite	0.2 wt/v% (in organic solution)	-	(1) Improvement of T _g (36 °C), and (2) wider initial decomposition temperature range as compared with base TFC	[105]
PA/PSf	Selective	HNT	0.04 wt/v% (in organic solution)	-	Water flux increased without considerable loss on rejection for the temperature range of 15-40 °C	[110]

* Highest thermal properties were achieved at this concentration

1.7 Research objectives

The objective of this thesis was to develop a strategy, based on systematic design and materials selection, to make and characterize highly permeable and thermally resistant thin film composite (TFC) membranes. This goal was met through several steps: tuning the chemistry of the polyamide layer using novel multifunctional monomers, incorporating functionalized nanoparticles with high thermal resistance in the polyamide layer, and modifying the current fabrication method of TFCs using additives and a new substrate. These steps were needed to overcome the existing limitations in the synthesis of high-performance selective layers.

To achieve this goal, the research adopted the following approach:

1. *Fabrication of robust and permeable membranes by tuning the chemistry of the selective layer using a new multifunctional monomer:* The first phase of this research used new amine and acid chloride monomers to make new polyamide selective layers in TFC membranes. Monomer reactivities, chemical structure stability, and membrane structure requirements were the factors that were considered. A major advantage of interfacial polymerization is the flexibility for material selection and fabrication parameters, but the synthesis of a uniform and integrally-skinned film is a serious challenge. This becomes even more challenging when we realize that, for the last two decades, no other polymer selective layer for reverse osmosis (RO) membranes has been developed with better properties than those of polyamides. The introduction of a new monomer, triaminopyrimidine (TAP), into the traditional polyamide structure was considered to synthesize copolymers that allowed for synergistic interactions among the different monomers. Changing monomer concentrations and introducing additives were of prime importance to attain much higher separation performances in terms of flux and rejection as well as thermal stability, compared with available commercial membranes.
2. *Exploiting hydrophilic and high thermal properties of nanofillers to modify bulk and surface properties of the selective layer of polyamide membranes:* Introducing surface-functionalized nanomaterials in the host polyamide membrane matrix to modify its thermal stability and surface properties is a well-known and promising approach. One of the critical challenges is to finely disperse and avoid self-agglomeration of the nanoparticles due to van der Waals interactions. Indeed, the nanoparticles concentration should be optimized to

make defect-free membranes and with high flux. While nanoparticles have been incorporated into polymer membranes to make them thermal-stable, they also restrict polymer segmental motions and decrease the structural free volume of the membrane, which lowers their permeability. Therefore, we needed to find ways to make novel polymeric membranes that had high perm-selectivity as well as high resistivity at high temperatures.

3. *Providing guidelines for filtration methodologies in high-temperature RO processes:* Developing high temperature RO membranes is a new field of study. There are no standards for testing the membranes at high temperatures, unlike antifouling experiments, chlorine resistance filtrations, and antibacterial evaluation. It is very important to introduce guidelines for high temperature testing because they will motivate more contributions in this field and establish standard experimental methods.

1.8 Thesis structure

The current thesis is prepared in a paper-based format. Chapters 2, 3, 4, and 5 were based on the published or submitted papers.

Chapter 2 describes materials and characterization techniques used in Chapter 3, 4, and 5, particularly the fabrication of polyamide TFC membranes, which is as the heart of all experimental methodologies for making membranes in this thesis. Further experimental method details for each project are presented in later chapters.

Chapter 3 explains the use of a new triamine monomer, TAP, to control the cross-linking degree of the polyamide structure of TFC membranes. Two types of TAP-modified membranes, one for RO and one for forward osmosis (FO) process, with different fabrication routes are described in this chapter. The effect of TAP on the thermal stability, water permeability is also explained.

Chapter 4 reports the results of bulk and surface modification of the polyamide layer of thin film nanocomposite (TFN) and TFC membranes with amine-functionalized nanodiamond (ND) particles. The effect of diamond nanoparticles on the performance of polyamide membranes at elevated temperatures was investigated. In the second part of this chapter, the ability of ND particles to make an antifouling layer on the polyamide surface was explored. Our results highlight the importance of controlling the structure of polyamide films on the separation

performance of TFC membranes. The first part of this chapter focused on RO filtration since the performance of the membrane at high temperature/pressure was the main interest of study. In the second part, the surface properties of the membranes was modified. Therefore, the antifouling properties of the membranes were explored using forward osmosis filtrations (no applied pressure).

Chapter 5 introduced high temperature filtration methodologies for three commercial membranes. The effect of temperature on the morphological and chemical structure of TFC membranes was also investigated.

Finally, Chapter 6 summarizes the main outcomes of the research presented in this dissertation. We also gave a perspective for future research directions of in the field of high-performance thermally stable TFC membranes.

Chapter 2

Materials and Methods*

* This chapter is organized based on reference [150,153,166].

2.1 Materials

Commercial flat sheet polyethersulfone (PES) membranes with the average pore size of 30 nm and 200 nm were purchased from Sterlitech Co. (WA, USA), and used as the substrates for the synthesis of TFC membranes. SUEZ AG, SUEZ AK, and SUEZ AD as flat-sheet commercial polyamide TFC membranes were supplied by SUEZ Water Technologies & Solutions (MN, USA).

MPD ($\geq 99\%$), TMC (98%), and TAP (97%) were received from Sigma-Aldrich, and used as reacting monomers for the synthesis of polyamide TFC membranes. n-Heptane ($\geq 99\%$) was purchased from Fisher Scientific. Sodium dodecyl sulfate (SDS) and triethylamine (TEA) were purchased from Fisher Scientific, and used as additives in aqueous-amine solution. Ethyl acetate as the co-solvent in the organic TMC solution was received from Fisher Scientific.

Detonation nanodiamond (ND) was purchased from US Research Nanomaterials Inc. (Houston, TX, USA) with an average particle size of 3-10 nm, specific surface area of 272.6289 m²/g, purity of $>98.3\%$, and density of 3.05-3.30 g/cm³. ND particles were used for fabrication of TFN membranes as well as surface modification of TFC membranes. Ethylenediamine (EDA), Thionyl chloride ($\geq 99\%$), anhydrous tetrahydrofuran ($\geq 99.9\%$), and dimethylformamide were all obtained from Sigma-Aldrich, and used for the surface functionalization of ND particles. All chemicals were used as received, without further purification.

For the fouling experiments, sodium alginate (SA, 12-80 kDa, St. Louis, MO) and bovine serum albumin (BSA) were obtained from Sigma-Aldrich and ChemCruz, respectively, and used as the organic foulants. Calcium chloride (CaCl₂) was obtained from Fisher Scientific to be added to the foulant solution as a chain cross-linker.

2.2 Preparation of the TFC polyamide membranes

The polyamide TFC membranes were prepared by interfacial polymerization of the selective layer on top of a microporous PES support. As shown in **Figure 2-1**, the polymerization took place at the interface of two immiscible aqueous and organic solvents containing amine monomer(s) and acid chloride monomer. In the first step, the PES support was impregnated with aqueous solutions containing amine monomer(s), sodium dodecyl sulfate (SDS) and triethylamine (TEA) for 9 min. TEA acts as the catalyst and shifts the polymerization equilibrium reaction towards the synthesis of polyamide by consuming the by-product, HCl.

SDS surfactant was used to improve the affinity between the two solutions at the interface and to accelerate the reaction in the organic phase. After removing the excess amines by rolling the support, the TMC solution was poured onto the impregnated support for the synthesis of polyamide layer. The produced membranes were dried in air followed by curing at 60 °C for 4 min. All the specimens were then rinsed with deionized water to eliminate any remaining monomer solution, and stored in a deionized water bath before characterization.

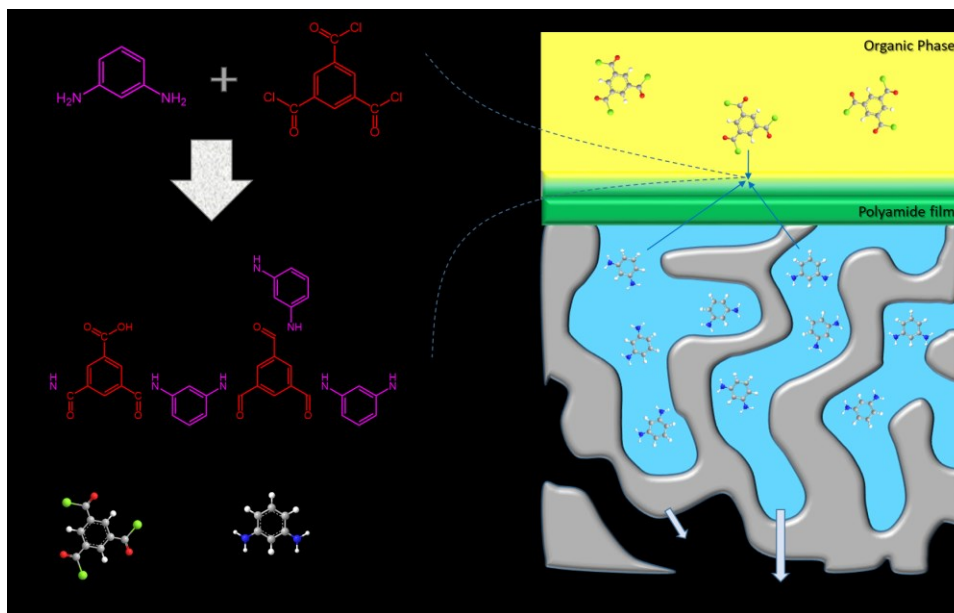


Figure 2-1: Schematic of interfacial polymerization on PES support.

2.3 Characterization of fabricated membranes and nanoparticles

2.3.1 Chemical characterizations

Attenuated total reflectance-Fourier transform infrared (ATR-FTIR) and X-ray photoelectron spectroscopy (XPS) were used to determine the chemical composition of the polyamide layer. The FTIR adsorption spectra were recorded using an Agilent Technologies, Cary 600 series FTIR spectrometer operated at room temperature over the range of 400-4000 cm^{-1} , at 4 cm^{-1} resolution and 30 scans. Chemical bonds and elemental composition (O, C, and N) of the polyamide layer were also analyzed with Kratos AXIS ULTRA XPS equipped with a monochromatic Al $K\alpha$ X-ray source. The information was collected from 1-10 nm thickness of the surface layer in the range of 0-1100 eV with high-resolution scans of 0.1 eV.

Thermogravimetric analysis (TGA) and ATR-FTIR were conducted to determine the surface characteristics of as-received and functionalized ND particles. The thermal stability of ND particles was evaluated using TGA-Q500 (TA instrument, USA). TG curves were recorded over the temperature range of 25-800 °C with a heating rate of 10 °C/min under a nitrogen atmosphere. To study the crystallinity of ND particles and the membranes, the X-ray diffraction (XRD) spectra were recorded by a Rigaku XRD Ultima IV machine with the rate of 2 degrees/min.

2.3.2 Morphological analysis

The surface image of the PES support, TFC, and TFN membranes were observed with field-emission scanning electron microscopy (FESEM, Zeiss Sigma 300 VP) and transmission electron microscopy (TEM, Philips/FEI Morgagni 268, The Netherlands). The surface topography of the membranes was evaluated using atomic force microscopy (AFM, Bruker Dimension Icon, USA) in tapping mode in air. The roughness data including average roughness (Ra) and root-mean-square roughness (Rq) were also estimated using Nanoscope software.

2.3.3 Evaluation of the membrane surface wettability

Contact angle measurement using Krüss DSA 100 instrument (Krüss GmbH, Germany) was performed to study the surface hydrophilicity of the membranes. The static contact angle was reported at the first moment of placing a sessile droplet of water on the membrane surface

2.3.4 Evaluation of transport properties and salt rejection in RO filtration

The separation performance of the membranes was evaluated using a cross-flow filtration setup (Sterlitech Corp., USA). **Figure 2-2** illustrates a schematic of a laboratory RO cross-flow filtration setup. The transmembrane pressure (TMP) and feed flow rate were set based on each experiment. The feed temperature was controlled using a circulating water bath (Isotemp3013, Fisher Scientific). All components of the filtration setup, including the feed tank, connecting tubes, and fittings, were insulated to minimize the heat loss during the filtration at high temperatures. To evaluate the NaCl rejection, the conductivities of the feed and permeate solution were measured using a conductivity meter (Accumet AR50, Fisher Scientific). Then, the conductivity data was

converted to NaCl concentration using a calibration curve. The permeate flux (J_W) and NaCl rejection (R) were calculated as follows:

$$J_W = \frac{\Delta m}{\rho \cdot A \cdot \Delta t} \quad (2-1)$$

$$R (\%) = \left(\frac{C_F - C_P}{C_F} \right) \times 100 \quad (2-2)$$

where Δm is the mass difference of the collected permeate, ρ is the permeate density, A is the effective surface area of membrane ($20.6 \times 10^{-4} \text{ m}^2$), Δt is the time interval, and C_F and C_P are the salt concentration in feed and permeate solution, respectively, which were measured using a conductivity meter (Accumet AR50, Fisher Scientific).

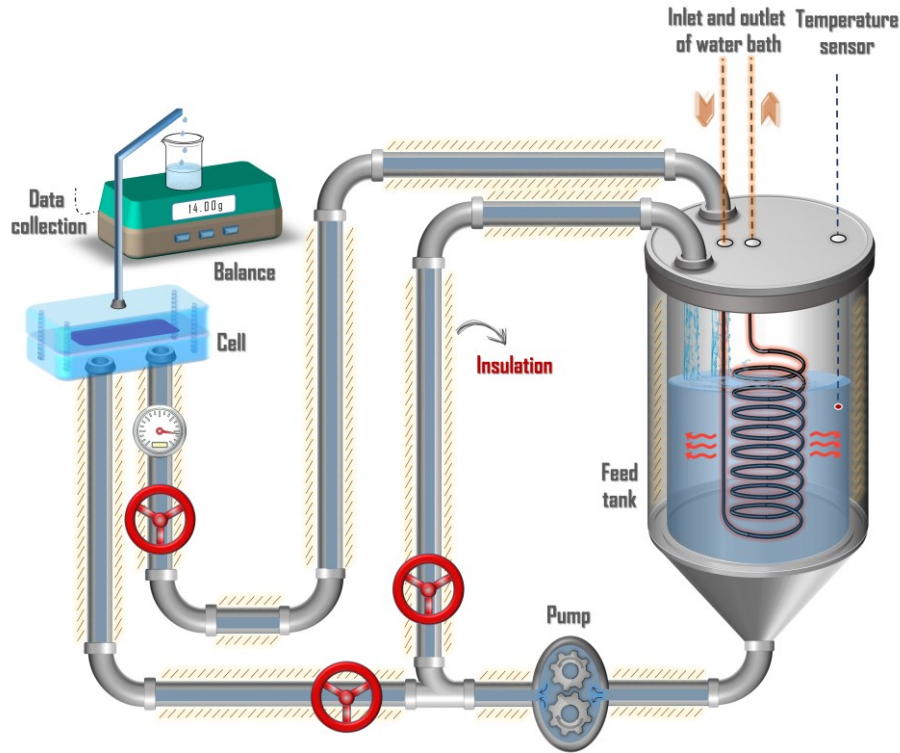


Figure 2-2: RO cross-flow filtration setup. The feed tank and all the pipes were insulated to minimize the heat loss during the high-temperature filtrations.

2.3.5 Evaluation of separation performance at high-temperature in RO filtration

High-temperature cross-flow filtration tests were conducted at different modes in order to study the behavior of commercial RO membranes when they are exposed to high temperatures: (i)

long-term high-temperature filtrations, (ii) cyclic tests, (iii) stepwise temperature increment by adjusting pressure, and (iv) permeability measurement at different operating temperatures.

(i) Long-term high-temperature filtrations

High-temperature long-term operations were conducted with two different methodology.

1. The filtration started with pure water at room temperature for 30 minutes. Then, a 2000 ppm NaCl solution was added to the feed tank. The feed temperature was steadily increased to 75 °C. The filtration at 75 °C continued for 9-15 hours to evaluate the stability of the membranes. The water level in the feed tank and water circulator was constantly monitored to eliminate possible high-temperature evaporation. The transmembrane pressure and concentrate flow rate were set to 90/220 psi and 3 L/min, respectively, during the filtration.

2. The filtration started at 25 °C for 30 minutes and then the feed temperature ramped with 10 °C intervals to 75 °C. The transmembrane pressure was set to 220 psi for the reference sample (low permeable membrane). However, the transmembrane pressures for the other membranes were adjusted at each temperature to deliver the same initial permeate flux measure for the reference membrane. At each temperature increment, the flux and the salt rejection were recorded.

(ii) Cyclic tests

We conducted cyclic experiments to simulate the real industrial high-temperature applications that involve on/off operations. The filtration started with pure water at 25 °C and a 2000 ppm NaCl solution was added after 30 minutes. The operation temperature was increased continuously from 25 to 75 °C and kept constant for 4 hours. Then, the operating temperature was decreased to 25 °C. The next day, the feed solution was heated again to 75 °C, and the filtration continued for 4 hours at elevated temperatures. The same cycle was repeated for the third day. The trans-membrane pressure was set to 90 psi in all cycles.

(iii) Stepwise temperature increment by adjusting the pressure

To exclusively study the effect of the temperature on the performance of the membranes, we employed this technique to minimize the impact of operating pressure on the membrane performance at elevated temperatures. The transmembrane pressure was adjusted at each level of temperature to deliver the same water flux. Filtration started with pure water at 25 °C for 30

minutes. Then, a 2000 ppm NaCl solution was added to the feed tank. The feed temperature was ramped up with 10 °C intervals to 75 °C. At each temperature level, the pressure was adjusted (decreased) to have the same permeate flux.

(iv) Permeability measurement at different operating temperature

The pure water filtration was conducted at different temperatures (25, 35, 45, 55, 65, and 75 °C), and the permeability of the membranes was calculated. The permeate flux at four operating pressures was measured at each temperature level. The slope of water flux vs. operating pressure gives the permeability of the membranes. For each temperature, a new membrane coupon was used.

2.3.6 Evaluation of transport properties of membranes in FO filtration

The transport performance of the membranes were measured by a cross-flow forward osmosis filtration setup (effective membrane area 20.6 cm²). The flow rate of the solutions on the two sides of the membrane was 0.5 L/min. Deionized water was used as the feed solution. Different concentrations of NaCl solution (0.5, 1, 1.5, and 2 M) were used as the draw solution. The membranes were tested in two different configurations: active layer facing feed solution (AL-FS) and active layer facing draw solution (AL-DS). All the experimental parameters are the same for both AL-FS and AL-DS configurations. The permeate water flux, J_w , was calculated with the equation below [111]

$$J_w = -\frac{\Delta m}{A_m \rho \Delta t} \quad (2-3)$$

where Δm is the mass variation (loss) of the feed solution, A_m is the effective membrane surface area, ρ is the water density, and Δt is the time interval.

Using the equation below, the reverse salt flux, J_s , was calculated [112]

$$J_s = \frac{\Delta(C_t V_t) \cdot M_w}{A_m \cdot \Delta t} \quad (2-4)$$

where C_t is the salt concentration at time t , V_t is the feed solution volume at time t , and M_w is the molar mass of water. Finally, C_t was calculated using a concentration/conductivity calibration curve.

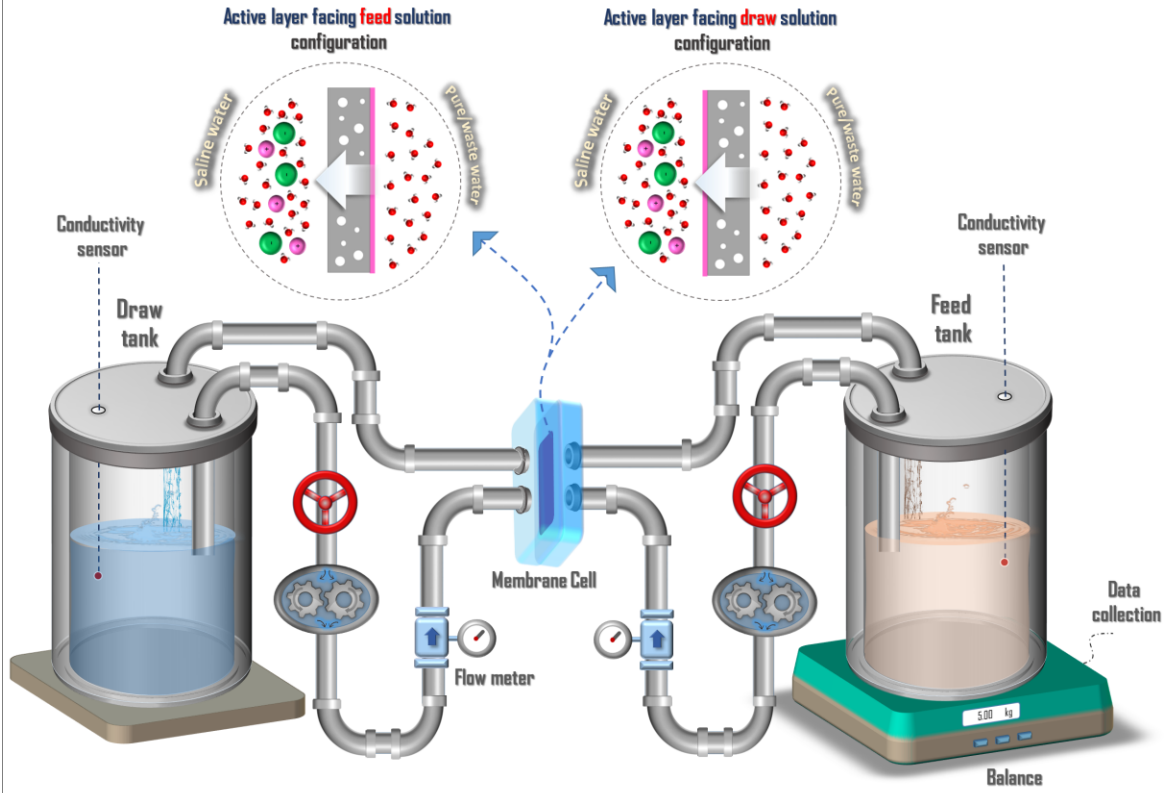


Figure 2-3: Schematic representation of FO cross-flow filtration setup in AL-DS and AL-FS configuration modes.

The transport parameters of the membranes: pure water permeability (A), solute permeability (B), and structural parameter (S), were determined with a methodology proposed by Tiraferri et al. [113]. This method is a single forward osmosis experiment with four steps. In each step, the water flux and reverse salt passage were measured at a certain NaCl draw solution concentration. The following equations provide the water flux, J_w , and reverse salt flux, J_s , based on membrane properties and hydrodynamic conditions of the filtration system:

$$J_w = A \left\{ \frac{\pi_D \exp\left(-\frac{J_w S}{D}\right) - \pi_F \exp\left(\frac{J_w}{k}\right)}{1 + \frac{B}{J_w} \left[\exp\left(\frac{J_w}{k}\right) - \exp\left(-\frac{J_w S}{D}\right) \right]} \right\} \quad (2-5)$$

$$J_s = B \left\{ \frac{c_D \exp\left(-\frac{J_w S}{D}\right) - c_F \exp\left(\frac{J_w}{k}\right)}{1 + \frac{B}{J_w} \left[\exp\left(\frac{J_w}{k}\right) - \exp\left(-\frac{J_w S}{D}\right) \right]} \right\} \quad (2-6)$$

where π is the osmotic pressure, c is the salt concentration, D is the diffusion coefficient of salt in the bulk solution, k is the mass transfer coefficient of salt, and the subscripts D and F denote

the draw and feed solutions, respectively. The adjustable parameters A , B , and S were estimated by nonlinear least squares regression using the measured water and reverse salt fluxes of each stage.

2.3.7 Evaluation of the fouling propensity of membranes in FO filtration

Sodium alginate (SA), a polysaccharide, and bovine serum albumin (BSA), a protein, were used as model organic foulants for the fouling experiments [6,7]. Foulant solutions contained 250 mg/L of the foulants and 0.5 mM CaCl₂ in DI water. Before adding the foulants, the initial permeate flux was set to 18 ± 1 LMH by adjusting the draw solution concentration. The fouling experiments were run for 180 minutes at room temperature while the water flux was monitored continuously. A baseline experiment was performed using the feed solution without foulant (DI water) to exclusively study the effect of foulants on the flux decline during filtration.

2.3.8 Evaluation of antibacterial properties of the membranes in FO filtration

Escherichia coli (*E. coli*) was used to study the antibacterial properties of the membranes. Colony plating, confocal microscopy, and inhibition zone tests were carried out. For all tests, the bacterial culture grew overnight in tryptic soy broth until reaching the stationary phase of the bacteria growth rate. This gave an approximate 10^9 colony forming unit (CFU)/ml bacteria solution. For colony counting and confocal microscopy tests, the bacteria cultures were diluted to achieve 10^8 CFU/ml concentration. Membrane samples were cut in 16 mm diameter discs and placed at the bottom of well plates with the active side at the top. A volume of 2 ml of bacteria culture was poured on the membrane discs and incubated for 3 hours at room temperature in the dark. After 3 hours, the suspension at the top of the membranes was pelletized, resuspended, and taken for colony plating and confocal microscopy tests. BBL™ MacConkey agar was used to prepare the agar solution for plating. All plates were incubated overnight at 37 °C. SYTO® 9 and propidium iodide (PI) were injected into the samples to stain the bacteria cells for confocal microscopy 15 minutes prior to imaging. The cell in images of the confocal microscopy test were quantified by ImageJ software's analyze particle tool.

Disc inhibition zone tests show the antibacterial mechanisms of the membranes. BBL™ MacConkey agar was also used to prepare the plates. The bacterial culture was diluted to 10^6

CFU/mL and spread with a cotton swab on the surface of the agar. 20 mm membrane discs placed upside down on the agar. All the plates were incubated at 37 °C for 12 hours to observe how the colonies grew around the membranes.

Chapter 3

Triaminopyrimidine (TAP)-modified thin film composite membranes with high permeability and thermal stability[†]

[†] The first part of this chapter was prepared based on reference [166].

3.1 Fabrication of highly permeable and thermally-stable RO TFC polyamide membranes

3.1.1 Introduction

Separation processes that rely on polymer-based membranes have become common practice in many industrial applications. The main drawback of the current polymer membranes, however, is their low tolerance to high temperatures, which restricts their application in high-temperature water treatment processes [44–48]. From the viewpoint of cost and energy savings, it is essential to operate membrane processes at the same (high) temperature of the process water. If the temperature of the process water needs to be lowered to adjust it to the performance requirements of a membrane that is not thermal stable, the costs associated with cooling the water stream to a lower temperature, subjecting it to the membrane separation process, and finally heating it up back to its original temperature will increase not only the operation costs and energy consumption, but also contribute to the emission of greenhouse gases. In some applications, such as steam-assisted gravity drainage (SAGD) for oil recovery in Alberta, Canada, the hot process streams need to be cooled solely to accommodate the membrane separation process, after which the processed fluid must be heated back. This cooling followed by reheating wastes a considerable amount of energy [49,114]. Developing thermally-stable polymer membranes, therefore, is essential to open up new fields of applications for membrane technology.

Thin film composite (TFC) membranes are the most widely used membranes for RO and nanofiltration in water treatment processes. TFC membranes are made of an ultrathin cross-linked polyamide layer made on top of a microporous support via interfacial polymerization between two monomers, typically m-phenylenediamine (MPD) and trimesoyl chloride (TMC), which are polymerized at the interface of two immiscible solvents to form the selective polyamide layer [31,115]. Since the invention of TFC membranes, much research and development have been undertaken to improve the physicochemical properties of the polyamide layer. Although notable advances in the development of chlorine-resistant [116,117], hydrophilic [118,119][39], and fouling-resistant [120,121] TFC membranes have been made, less progress has been achieved in the fabrication of thermally-stable TFC membranes. Several parameters, including type and concentration of monomers, as well as fabrication methods were investigated to tweak the structural characteristics of the selective layer, such as aromaticity and cross-linking degree. Wu

et al. [87] showed that the thermal stability of TFC membranes with fully aromatic selective layers was substantially higher than that of the aliphatic-aromatic structures. The salt rejection of TFC membranes with fully aromatic selective layers was almost constant (0.5% reduction) in the range of 20-90 °C, while the rejection decreased about ~11% for TFC membranes with aromatic-aliphatic selective layers.

The need for synthesizing highly cross-linked membranes has motivated some researchers to explore new monomers, such as 1,3,5-triazine-2,4,6-triamine (melamine), due to its multifunctionality and the thermal resistance of triazine rings [94,122–124]. Han [94] used melamine for the first time to make poly(melamine-TMC) nanofiltration TFC membranes. By raising the operating temperature from 18 to 95 °C, a noticeable increase in Na₂SO₄ solution flux (almost 3 times) was achieved with no reduction in salt rejection, indicating the thermal stability of poly(melamine-TMC) TFC membranes. However, the solute rejection of poly(melamine-TMC) TFC was still considerably lower (78%) than those for common types of nanofiltration membranes such as poly(piperazine-TMC) (97%) at room temperature. The low reactivity of melamine [94] and its low solubility in water (0.32 wt% at room temperature) [122,125] has hindered the use of melamine for the fabrication of thermally-stable TFC membranes with high solute rejection. Our search in the literature and experimental studies on a large library of monomers have indicated that using any amine and acid chloride monomer, other than MPD and TMC, has always created challenges regarding the production of an integrated thin polyamide selective layer for RO TFC membranes with reasonable separation performances.

In this study, we developed a new generation of thermally stable TFC membranes with a novel combination of a tri-functional monomer, triaminopyrimidine (TAP), with the highly reactive MPD in aqueous solution. Our strategy was based on enhancing the cross-linking of the polyamide layer using TAP, while simultaneously improving the integrity of the polymer network with the conventional MPD-TMC reaction. To this end, different concentrations of TAP were added to a diluted aqueous amine solution containing MPD. Interfacial polymerization between both amine monomers and TMC was conducted to form a polyamide layer with novel chemistry on top of the porous substrate. The permeability and separation properties at high temperature (75 °C) and long-term performance (9 hours at 75 °C) of the novel membranes demonstrated their thermal stability.

3.1.2 Experimental methods

TFC membranes were made over the PES support through a step-growth interfacial polymerization between an aqueous solution containing TAP and MPD, and organic solution containing TAP. In the first step, the desired concentration of amine (MPD and TAP) and acid chloride (TMC) monomers were dissolved in water and n-heptane, respectively. Then, the PES support was impregnated with the amine solution containing sodium dodecyl sulfate (0.2 wt.%) and triethylamine (1 wt.%) for 9 minutes. After removing the excess amines by rolling the support, the TMC solution (0.2 wt.%) was poured over the impregnated support and allowed to react for 12 minutes. The resulting membranes were dried in an oven at 60 °C for 4 minutes. All the membranes were then rinsed with deionized water to eliminate residual reactants and stored in a deionized water bath before characterization (**Figure 3-1**).

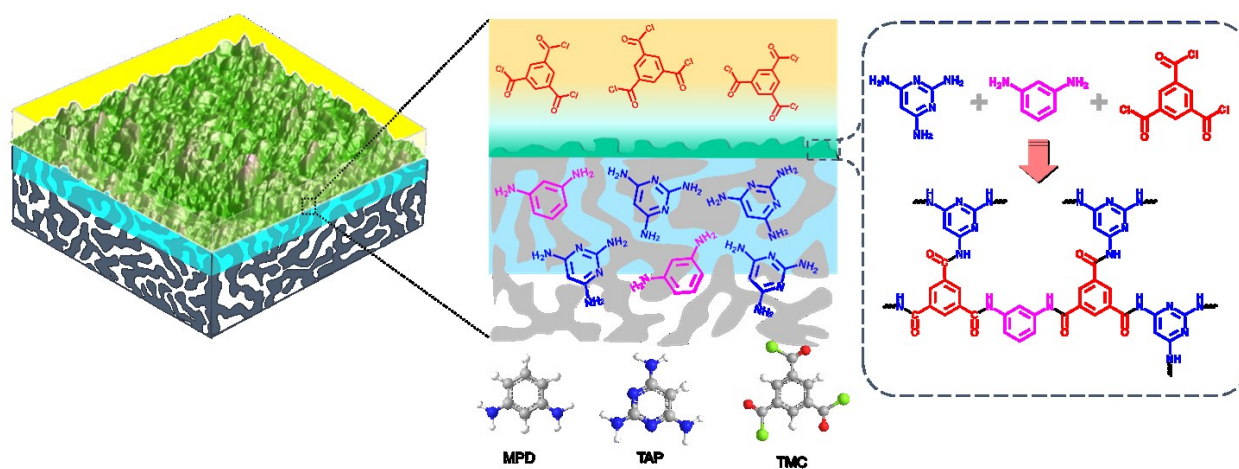


Figure 3-1: (a) Permeate: Schematic illustration of interfacial polymerization on top of a PES support. The microporous support was first impregnated with an aqueous amine solution (TAP and MPD) and then contacted with an organic TMC solution. The formation of the incipient polyamide layer on the PES substrate is followed by diffusion of the amine monomers through the polymer film into the organic phase to continue the polymerization. The reaction is finished when the amine monomers can no longer diffuse through the polyamide membrane.

Table 3-1 presents the list of produced TFC membranes with their corresponding reactant concentrations. The total concentration of amine monomers was set to 2 wt % for all samples. After a series of screening experiments, it is found that the TFC membranes with TAP concentration more than 1.8 wt % cannot be considered to work as RO membranes since they had less than 30% NaCl rejection. By lowering the concentration of TAP to 1.4 wt %, the permselectivity of the membranes was similar to that of TAP-free membrane (M0), showing the

dominating effect of MPD. Therefore, four membranes with TAP concentration varying from 1.5 to 1.8 wt % were synthesized. M0 was considered as a control membrane (TAP-free).

Table 3-1: Different monomer concentrations used to make the polyamide thin membranes. The polymerization time was 12 min and the membranes were cured at 60 °C for 4 min. M0 is the reference membrane, made without TAP.

Sample	TAP (wt %)	MPD (wt %)	TMC (wt %)
M0	0	2	0.2
M1	1.5	0.5	0.2
M2	1.6	0.4	0.2
M3	1.7	0.3	0.2
M4	1.8	0.2	0.2

3.1.3 Results and discussion

3.1.3.1 Permeation performance of TFC membranes

Figure 3-2a shows the permeate flux of the prepared TFC membranes evaluated by filtration test method 1 (see section 2.3.5: Long-term high-temperature filtrations). At room temperature, the control TAP-free membrane (M0) provided the lowest permeate flux of 15.2 LMH. The permeate flux becomes higher as the concentration of TAP in the membrane increases. The permeate flux rate almost doubled for M4 (43 LMH) as compared to M1 (22 LMH). A similar trend in permeate flux was observed when the feed solution temperature ramped up to 75 °C. While the flux of M0 reached 50.0 LMH at 75 °C, water flux through M4 increased more than three times to 130 LMH. It is worth noting that the permeation fluxes of the prepared TFC membranes remained stable at 75 °C, proving that the polyamide selective layer and the PES sublayer did not degrade at high temperatures. For comparison, the permeation performances of three commercial RO membranes (BW30, SUEZ AG, X201) were evaluated by filtration test method 1 and presented in **Figure 3-2b**. A sharp decrease of permeate flux was observed for all three commercial membranes in 6 hours of filtration at 75 °C. The X201 membrane, however, reached a relatively constant flux after 6 hours. The permeate flux also varied less drastically for BW30 and SUEZ membranes in the last 3 hours of filtration. In contrast, the permeate fluxes through membranes M0 to M4 was practically constant up to 9 hours of operation. One may infer from this observation that their long-term operation would also continue to be stable, but additional longer experiments are required to confirm this supposition.

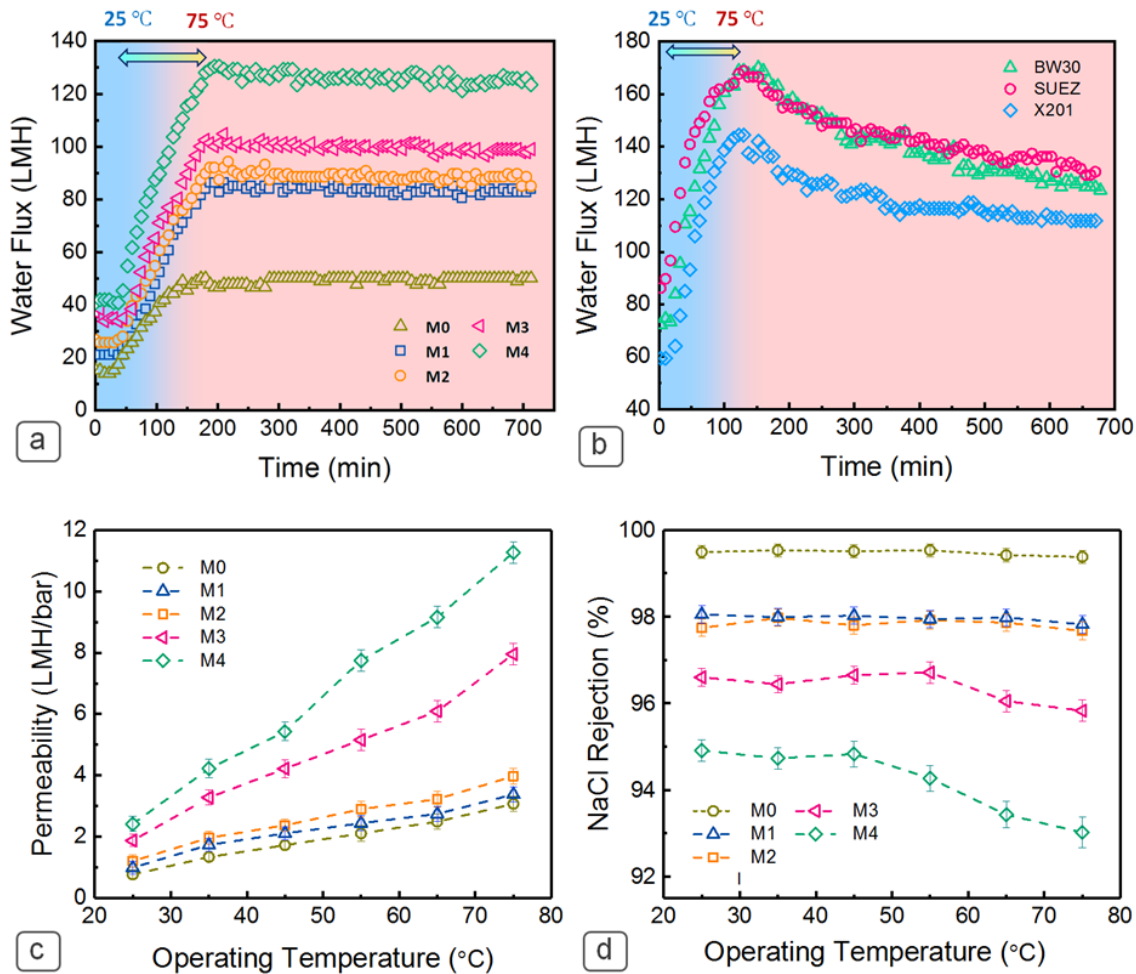


Figure 3-2: (a) Permeate flux of TFC membranes over extended filtration test. Operating conditions: transmembrane pressure of 220 psi, concentrate flow rate of 3 LPM, feed temperature of 25-75 °C. The filtration tests started with 2000 ppm NaCl solution at room temperature (25 °C); after 30 min, the feed solution was increased to 75 °C and remained constant for 9 hours; (b) Permeate flux of commercial RO membranes over a long filtration test; (c) Permeability of TFC membranes at different temperatures, obtained by adjusting the transmembrane pressure with respect to the permeate flux of M0; (d) NaCl rejections of TFC membranes at different temperatures from 25 to 75 °C.

Figure 3-2c compares the permeability of the TFC membranes at different temperatures using filtration test method 2 (see section 2.3.5: Long-term high-temperature filtrations). In order to minimize the impact of the transmembrane pressure on salt rejection, the operating pressures of M1 to M4 membranes was adjusted at each temperature interval so that these membranes produced the same permeate flux as M0. The hydraulic permeability of the membranes was then calculated by normalizing the permeate flux by the transmembrane pressure. **Figure 2-3c** shows that the TAP-containing membranes had higher permeability than the TAP-free membrane for all temperatures. For instance, at 25 °C the permeability of the TFC membranes increased about three times, from

0.77 LMH/bar to 2.41 LMH/bar for the M0 and M4 membranes, respectively. The permeability of the membranes grew even more at higher temperatures. For instance, a permeability difference of about 10 LMH/bar was recorded between M0 and M4 membranes at 75 °C. **Figure 3-2d** compares the salt rejections of the prepared TFC membranes at different temperatures. Among the membranes, M0 showed the highest salt rejection of 99.5%, while M4 could remove only 94.9% of the dissolved sodium chloride in the feed solution. Increasing the temperature up to 75 °C, the TAP-free M0, as well as M1 and M2 membranes provided steady salt rejections, but the performances of M3 and M4 deteriorated: the salt rejection of M3 was constant up to 55 °C (96.8%), then decreased slightly (about 0.8%) when the solution temperature reached 75 °C; a more noticeable variation was observed for M4, for which the salt rejection was constant up to 45 °C and then dropped by 1.9% at 75 °C.

3.1.3.2 Chemical composition of the polyamide selective layer

Figure 3-3 illustrates the ATR-FTIR spectra of the PES support and the synthesized TFC polyamide membranes. The IR spectra capture the characteristic peaks of both polyamide and PES layers due to the low thickness of the selective layer and the high penetration depth of the IR beam. The three characteristic peaks at 1540 cm⁻¹ (N-H in-plane bending of amide II and C-N stretching), 1610 cm⁻¹ (C=C aromatic ring stretching) and 1660 cm⁻¹ (C=O stretching of amide I) indicate the successful formation of the polyamide selective layer [106,126,127]. The intense peaks at 1150 cm⁻¹ (symmetric SO₂ stretching vibration), 1240 cm⁻¹ (asymmetric stretching of C-O-C), 1410 cm⁻¹ (C=C aromatic ring stretching), and 1485 cm⁻¹ and 1580 cm⁻¹ (aromatic in-plane ring stretching vibration) correspond to the PES support [128]. The variation of the polyamide peak intensities allows for the qualitative comparison of the amount (per unit volume) of the amide linkage formed on the PES substrate. For all amide characteristic peaks at 1540, 1610, and 1660 cm⁻¹, M4 and M0 showed the highest and lowest intensities, respectively. This observation suggests that polyamide films with a higher concentration of amide linkage were formed in TAP-modified membranes as compared to TAP-free control membrane. Furthermore, the intensity of the characteristic peak at 1150 cm⁻¹ (-S=O stretching vibration) can be considered as a qualitative measure of the polyamide membrane thickness. Since this peak is only present in the PES substrate, the higher its intensity, the thinner the polyamide upper layer. As shown in **Figure 3-3** (inset 1), the comparison of the intensity ratio (I_{PA}/I_{PES}) at 1150 cm⁻¹ provides the lowest value for M4 membranes, suggesting

thinner PA films with more amide linkages for TAP-modified membranes than for TAP-free membranes.

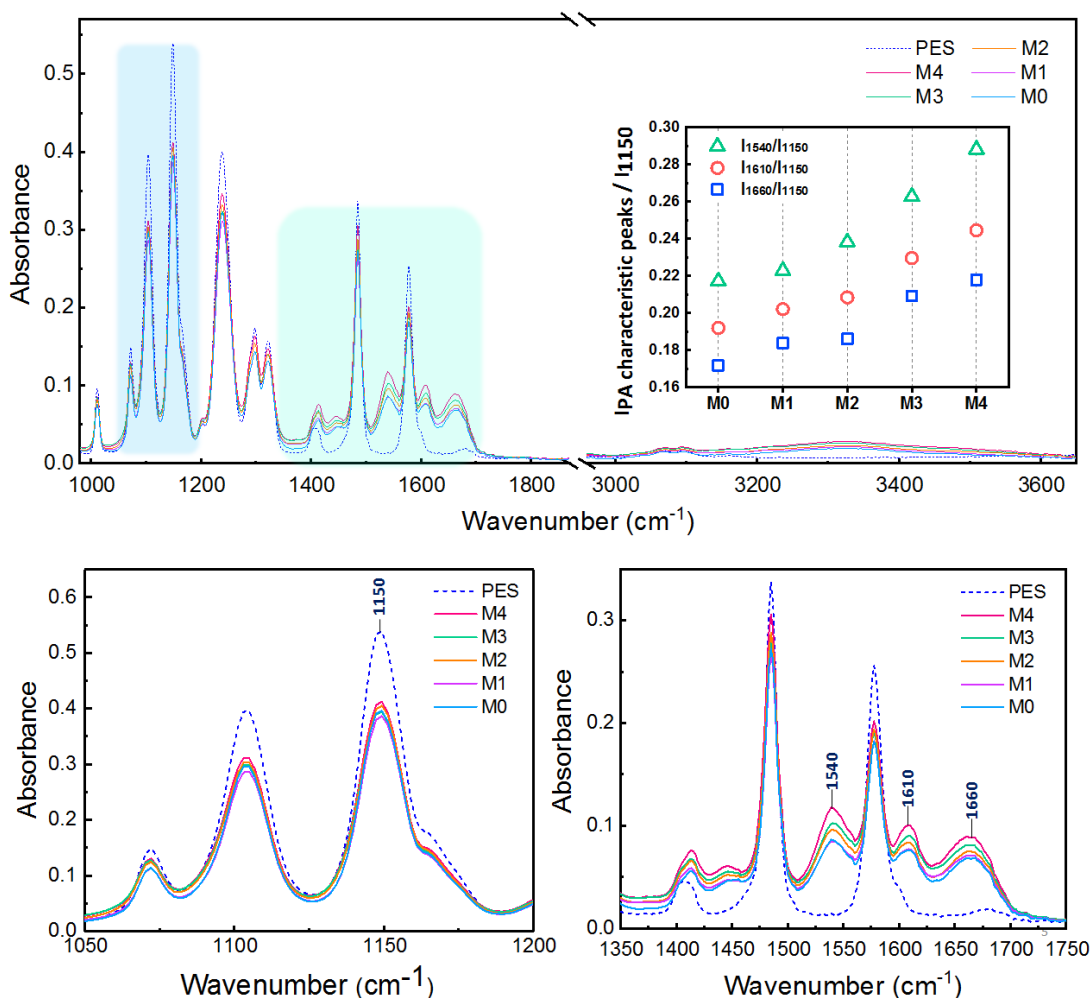


Figure 3-3: FTIR spectra of the PES support and of the M0-M4 TFC membranes. In the first inset, the intensity ratios of three polyamide peaks to PES reference peak (at 1150 cm⁻¹) provided the quantitative analysis of amide linkage formation.

Figure 3-4 displays the XPS survey and high-resolution carbon (C 1s) and nitrogen (N 1s) peaks for M0 (no TAP), M1 (lowest TAP fraction) and M4 (highest TAP fraction) membranes. Since the average XPS scanning depth is 5-10 nm [129], it only measures the elemental composition and chemical bonding of the polyamide top layer. The survey spectra detect the presence of carbon (285 eV), nitrogen (400.5 eV), and oxygen (532 eV). High-resolution C1s spectrum is deconvoluted to O-C=O at 288.5 eV (carbon attached to carboxyl group), N-C=O at 288.4 eV (amide linkage), -CN- at 286.2 (carbon attached to amide linkage or unreacted amines

and carbon attached to aromatic nitrogen in TAP), C-COOH and C-CONH at 285.7 eV (carbon attached to carboxyl group and amine linkage, respectively), and C-H and C-C at 285 eV (carbon bonds in the aromatic rings) [130]. The high-resolution N1s spectrum is deconvoluted to -NH-CO- (amide linkage) at 400.5 eV and R-NH₂ (unreacted amine) at 398.5 eV [130].

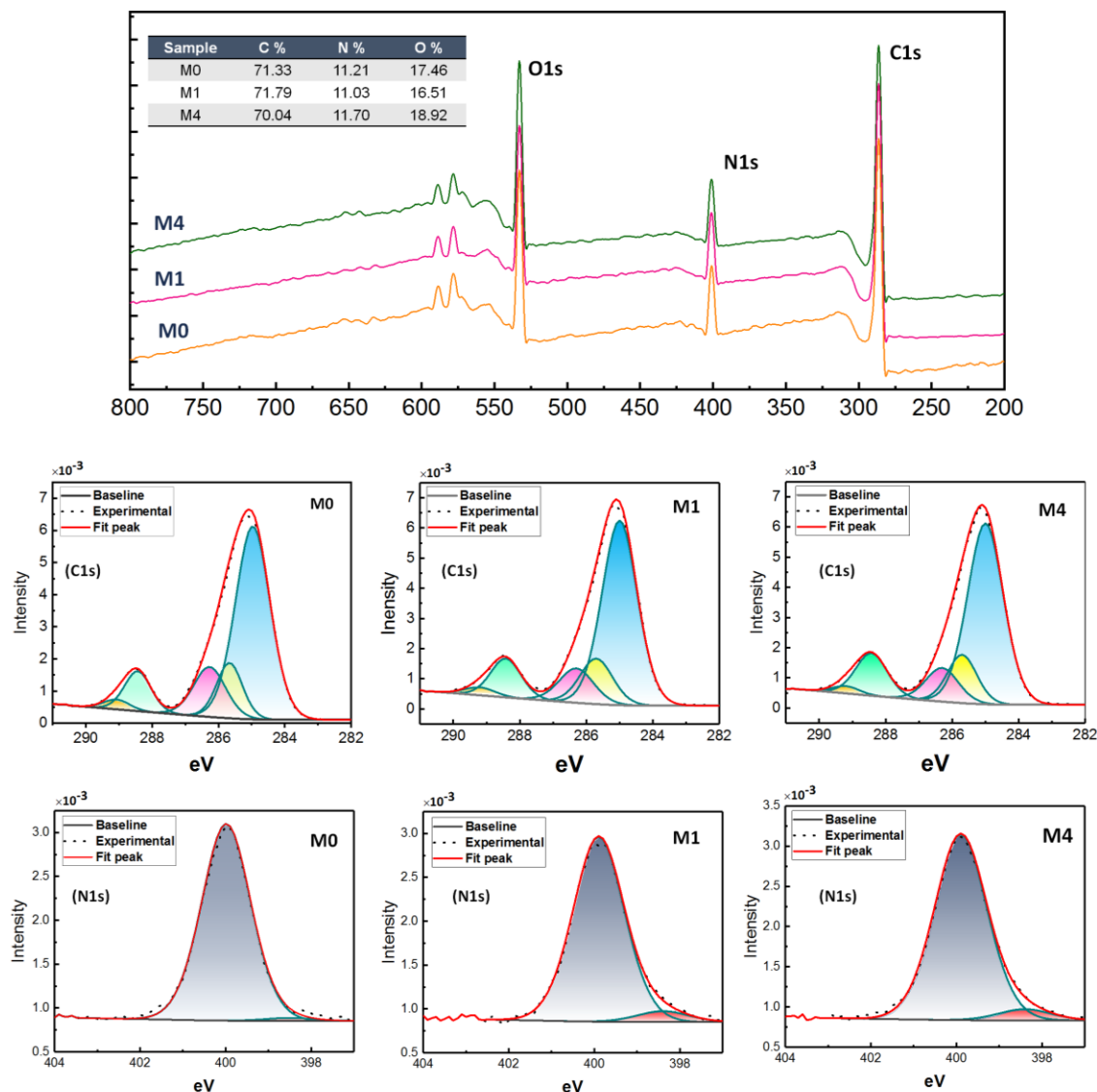


Figure 3-4: XPS survey spectra, elemental composition, and high resolution C1s and N1s spectra for M0, M1, and M4 membranes.

Table 3-2 presents the components of the deconvoluted C1s and N1s XPS spectra. It is worth comparing the ratio of amide bonds to the carboxylic group using the O-C=O/N-C=O in C1s spectrum. The larger values of this ratio indicate the formation of more amide linkage and less

hydrolysis of acyl chloride groups during the polymerization reaction. The TAP-modified membranes had more amide linkage and fewer pendant carboxylic functional groups, suggesting the formation of a more cross-linked structure with an increase in TAP concentration. Furthermore, the TAP-modified membranes contained higher unreacted amine functional groups based on the R-NH₂/–CON–/ ratio in **Table 3-2**, which implies a higher number of reacting amine moieties than the acyl chloride functional groups.

Table 3-2: Binding energy and peak area of chemical bonds for C1s and N1s XPS spectra.

Sample	C 1s species (%)						N 1s species (%)		
	C-H, C-C	C-COO, C-CON	-CN-	N-C=O	O- C=O	$\frac{N-C=O}{O-C=O}$	R-NH ₂	N-C=O	$\frac{R-NH_2}{N-C=O}$
M0	60.80	12.89	14.52	9.51	2.27	4.18	1.52	98.48	0.015
M1	61.36	14.03	11.20	11.17	2.24	4.99	5.57	94.43	0.059
M4	61.54	10.44	13.48	12.73	1.84	6.88	5.71	94.29	0.06

3.1.3.3 Morphological analysis

The morphology of the polyamide layer was investigated using FESEM, AFM, and TEM. **Figure 3-5** shows the FESEM micrographs of the top surface of TFC membranes and of the PES support. In all TFC membranes, a continuous polyamide film with typical ridge-and-valley structure covered the surface of the substrate. Contrary to the TAP-free M0 membrane, the surface topology of the membranes prepared with higher concentrations of TAP tended to be flatter, with more leaf-like features. This observation was also confirmed by AFM images, where smoother features were observed at the surface of TAP-modified membranes.

Table 3-3 presents the average roughness (R_a), root mean square roughness (R_q), and surface area difference (SAD) of the M0, M1, and M4 membranes [131]. Among the membranes, M4, which was prepared with the highest TAP concentration, had the lowest average roughness (59.2 ± 2.0), and root mean square roughness (69.1 ± 1.8). Variation in surface roughness among these membranes may be attributed to different diffusion rates of the MPD and TAP monomers to the reaction zone, which is governed by the size and concentration of the monomers [132,133]. We may speculate that the formation of rough ridges and valleys at the surface of M0 may be ascribed to fast diffusion of MPD from the aqueous phase to the organic phase, where polymerization takes place. In contrast, the smoother surface of the TAP-modified membranes may be the result of higher degrees of cross-linking caused by addition of TAP, as well as to the lower diffusion rates

of the TAP molecules (as compared to MPD) and lower MPD concentration in the aqueous solution of the TAP-modified membranes.

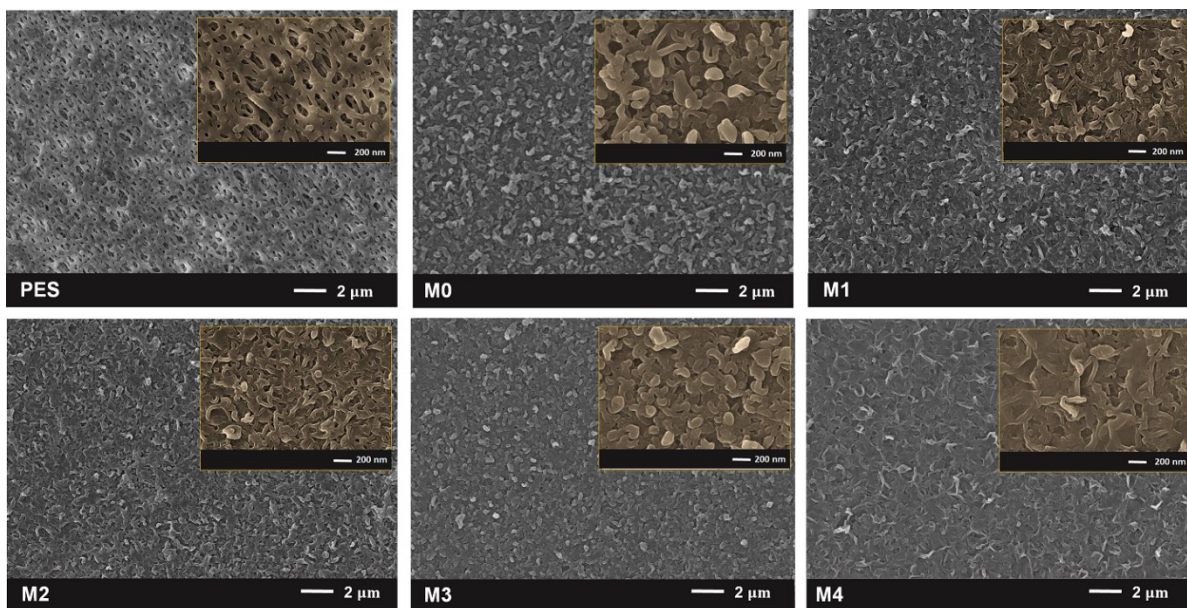


Figure 3-5: FESEM micrographs of the top surface of PES support and TFC samples at two different magnifications. The amine concentration for all TFC membranes was set to 2 wt% with different concentrations of TAP and MPD monomers. Increasing the TAP concentration changed the top surface morphology. The PES support is shown as a non-coated membrane.

Table 3-3: Average and root mean square roughness of synthesized TFC membranes. The SAD values were calculated by $SAD = (Actual\ surface\ area / Projected\ surface\ area) \times 100$ using nanoscope image analysis software.

Sample	Roughness		
	R_a (nm)	R_q (nm)	SAD (%)
M0	76.0 ± 1.1	100.2 ± 1.7	59.5 ± 3.6
M1	64.2 ± 1.6	84.4 ± 0.6	42.0 ± 0.6
M4	59.2 ± 2.0	69.1 ± 1.8	18.6 ± 0.9

Figure 3-6 compares the TEM cross-section images of the M0, M1, and M4 membranes. The thickness of the polyamide layers decreased in the order $M0 > M1 > M4$. The thickness of the selective layer of TFC membranes is not uniform because different amine monomers have distinct diffusion rates and the distribution of internal voids in the polyamide structure is not uniform. In addition, amine monomers have different diffusion rates in the organic solution based on their local concentration, as well as the porosity of PES support. The M0 membrane is thicker than those of the TAP-modified TCF membranes (M1-M4). The effect of TAP on the formation of a thinner selective layer was schematically presented in Figure A1 in the Appendix A. The thickness of TFC

membranes may be significantly influenced by mass transfer resistances during interfacial polymerization. A dense incipient polyamide layer hinders monomer diffusion from the aqueous phase to the reaction zone in the organic phase, and thus limits the growth of the polyamide film. Consequently, the lower thickness of the TAP-modified membranes compared to the TAP-free membranes may be attributed to a lower diffusion rate of TAP molecules (as compared to that of MPD molecules) through the already-formed polyamide film into the reaction zone. The lower reactivity of TAP might also form a polyamide layer with undesired nanoscale defects, which may explain the lower salt selectivity of TAP-modified membranes and lower salt rejection of M4 (with highest TAP concentration) with increasing the temperature.

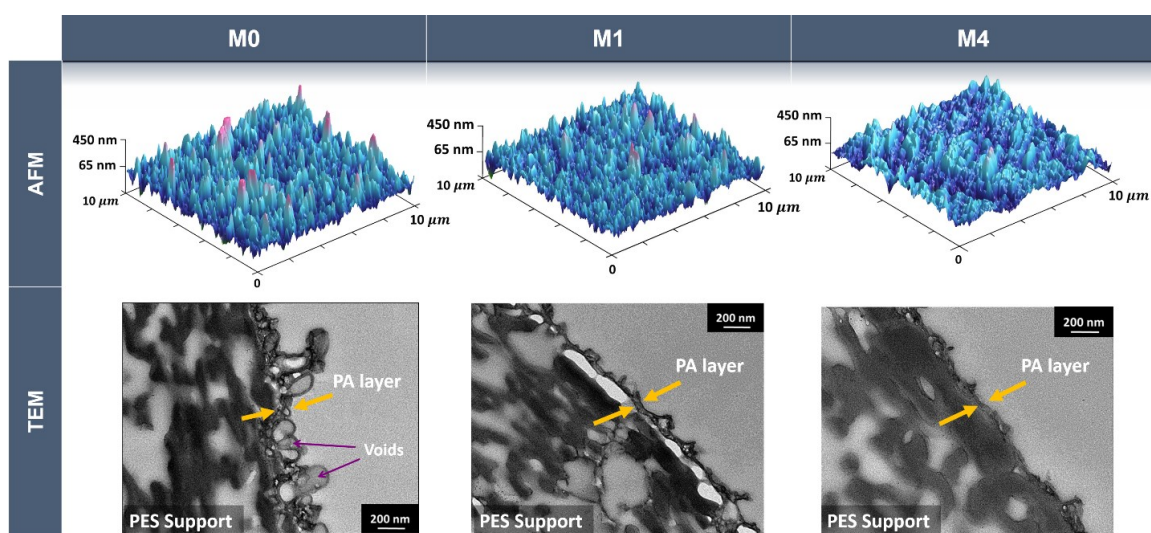


Figure 3-6: 3D AFM images and cross-section TEM images of TFC samples. AFM images are shown for the scanning area of $10\ \mu\text{m} \times 10\ \mu\text{m}$ and same z-axis aspect ratio for all the samples. TAP monomer contributed to the formation of smoother and thinner polyamide skin layer. In the TEM images, the PES support has occupied a higher portion of the images. The clear difference of contrast between PES and polyamide layers reveals the structure and the thickness of the selective layer. The detachment of polyamide layer from the PES support (TEM image of M1) is due to TEM sample preparation.

It is also worth discussing the formation of empty micro-scale voids within the polyamide layer. While the TEM images shows multiple voids in the polyamide layer of M0, fewer and smaller voids were also formed in the M1 and M4 membranes. These voids are reported to be created by the release of gas bubbles during the exothermic interfacial polymerization reaction [134]. Ukrainsky and Ramon [135] showed that during interfacial polymerization reaction, the temperature may increase up to $85\ ^\circ\text{C}$, which is higher than the boiling point of the conventionally used organic solvents such as hexane, and heptane. The presence of more voids in M0 than M1 and M4 might be attributed to the higher polymerization rate of MPD with TMC than of TAP with

TMC. Since polymerization reactions are exothermic, higher polymerization rates release more heat and cause a higher increase in the medium temperature, leading to the formation of more gas bubbles at the interface. AFM/TEM images and roughness data of M2 and M3 are also presented in Figure A2 and Table A1, respectively, in the **Appendix A**.

It is worth mentioning that the micro voids in the TEM cross-sectional images of the polyamide layer of the M0 membrane are not defects, as this membrane provided the highest salt rejection percentage. In contrast, it has been reported that molecular-size free volumes within the polyamide matrix are the actual regulator of the separation properties of the polyamide selective layer [136]. These voids can be classified according to their sizes as network pores (2-5 Å) or aggregate pores (5-10 Å) [136]. The size and distribution of these nano-voids depend on the chemical composition of the reacting solutions used to make the polyamide membranes. It has also been reported that an increase in the cross-linking density of the polyamide film results in the formation of more aggregate pores than of network pores [136,137]. Considering the higher water permeation and lower salt rejection of the TAP-modified membranes, this may suggest that adding TAP to the polymerization recipe leads to the synthesis of polyamide structures with more aggregate pores than network pores. **Figure 3-7** compares hypothetical structures for TAP-free and TAP modified membranes, where larger aggregate voids are created by the copolymerization of the TAP/MPD mixture with TMC. More detailed characterization analyses at nano-scale resolution need to be carried out to draw solid conclusions about the impact of amine monomers on the complex molecular-scale voids within the polyamide layer.

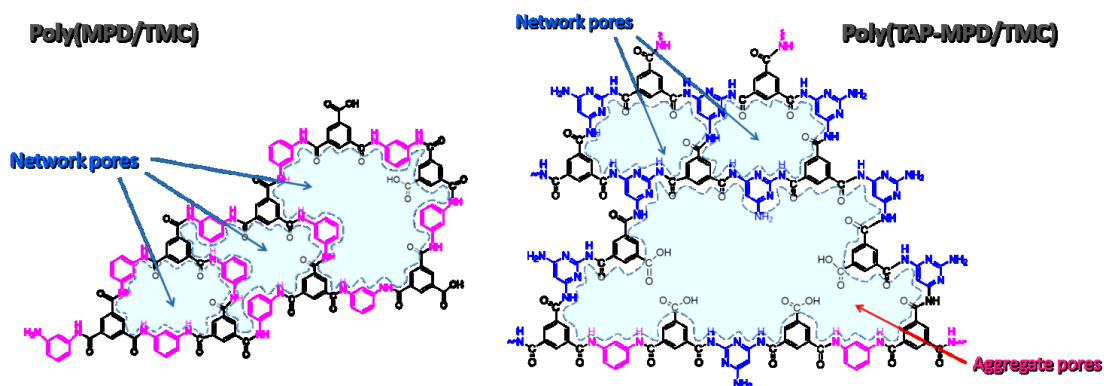


Figure 3-7: Schematic repetition of hypothetical structures of polyamide film made with a combination of MPD and TAP with TMC monomer, showing the possible formation of the network and aggregate pores within the polyamide structure.

3.2 TAP-modified FO TFC membranes mediated with PDA/GO interlayer

3.2.1 Introduction

Forward osmosis over semi-permeable membranes is a method to treat saline water and wastewater. In this process, the osmotic pressure induces a net flow of water through the membrane from the feed solution (lower solute concentration) to the draw solution (higher solute concentration) [138]. When FO membranes were first introduced around 2000, they were expected to be an alternative to traditional pressure-driven filtrations such as RO, which consumes energy due to the applied hydraulic pressure. Despite a concerted effort in the field of osmotic membrane fabrication, only a few companies offer commercial FO membranes in 2022. Suwaileh et al. [139] listed important industrial players in the market of FO membranes.

Developing high-performance FO membranes and designing a feasible FO process is challenging because their product needs an additional step before it can be used as fresh water. The draw solution regeneration step can be significantly energy-intensive. More importantly, it is hard to design novel membranes that meet the requirements of FO processes. TFC membranes are most popular for FO applications due to their unique combination of high permeability and solute selectivity. A TFC membrane is a multilayer structure made of a porous substrate and an ultrathin active layer. The active layer is synthesized by interfacial polymerization between an acid chloride monomer such as TMC and an amine monomer such as MPD at the interface of two immiscible solvents. The first attempts to develop FO processes used TFC membranes, but polyamide RO membranes had low water permeability in FO applications. An ideal FO membrane consists of a high-flux substrate with an ultrathin active layer having high water flux and salt selectivity. Furthermore, the active layer of FO TFC membranes is expected to be chemically resistant and have antifouling properties [140–142].

Significant research efforts have been made to improve the permeability of FO TFC membranes while maintaining the solute selectivity. Generally, investigations in this field can be divided into two categories: 1) developing a thin porous support layer that facilitates the flux of water molecules in the porous structure of the TFC membrane; and 2) synthesizing ultrathin polyamide layers with high water permeability and solute impermeability.

Khorshidi et al. [36,140] introduced an innovative adjustment of interfacial polymerization to fabricate highly permeable FO TFC membranes. They found that reducing the temperature of the organic solution (down to -20 °C) decreased the thickness of the polyamide layer and, therefore, considerably improved the water permeability of the membranes. The water flux increased from 17.6 LMH for the membrane made at room temperature to 38.5 LMH for the membrane made at -20 °C.

Constructing an interlayer between the porous support and the polyamide layer is a popular approach to fabricate high-performance TFC membranes because it allows for the precise control of interfacial polymerization. Dai et al. [143] studied different mechanisms for how the interlayer affects the polyamide structure: 1) controlled amine diffusion, 2) increased amine storage at the interface, 3) regulated nuclei formation, 4) reduced heat and nanobubble production, and 5) prevented intrusion of polyamide into the substrate. Among these mechanisms, controlled amine diffusion seems to dominate the formation of thinner and smoother polyamide layers [130,144,145].

Han et al. [146] showed that constructing a PDA interlayer over a polysulfone support simultaneously increased the water permeability and salt rejection of polyamide FO TFC membranes. The smaller surface pore size and narrower pore size distribution of the PDA interlayer compared with the polysulfone support reduced the diffusion rate of amine molecules, and decreased the thickness of the polyamide layer from 380 nm for the TFC made with a pristine polysulfone support to 150 nm for the TFC made with a PDA-coated support. In our previous work [147], we showed how using a combination of TAP and MPD as the amine monomers regulated the interfacial polymerization and reduced the rate of diffusion of amine molecules to the organic solvent interface. The triamine TAP monomer also increased the cross-linking density of the polyamide layer. The TAP-modified TFC membranes were thin, highly permeable, and thermally stable.

In this work, we combined two approaches to reduce the thickness of the polyamide layer of FO TFC membranes. We showed how the synergetic effects of an interlayer and a low reactivity monomer could reduce the rate of diffusion of amine molecules during the polymerization. We proposed a method to develop novel polyamide FO TFC membranes mediated with polydopamine/graphene oxide (PDA/GO) interlayers. First, the PES porous support was coated

with a layer of PDA/GO through polymerization of DA monomers in the presence of GO particles. Then, a polyamide layer was synthesized over the PDA/GO coated layer through interfacial polymerization of TAP, MPD, and TMC monomers. The FO performance of synthesized membranes was investigated at room and high temperatures.

3.2.2 Experimental methods

Figure 3-8 shows how to make PDA/GO coated PES supports and TAP-modified polyamides. The PDA/GO coating started with the oxidative self-polymerization of DA molecules over the PES support (average pore size of 200 nm). A 2000 ppm DA aqueous solution of pH = 8.5 (adjusted with a tris-buffer solution) was stirred for 8 hours. Then, the solution was replaced with 4000 ppm of GO aqueous solution and stirred for 8 hours. The PDA/GO coated PES support was cured in an oven for 30 minutes at 60 °C. Finally, the coated PES membrane was washed with pure water to remove unreacted DA molecules and residual GO particles. After the preparation of the PDA/GO-coated PES support, we synthesized the TAP-modified polyamide layer through interfacial polymerization. The details of the polyamide synthesis were presented in our previous work [147]. **Table 3-4** lists conditions for the synthesis of the polyamide TFC membranes. We made the TFC membranes by varying the concentration of TAP, and keeping constant the concentrations of MPD and TMC.

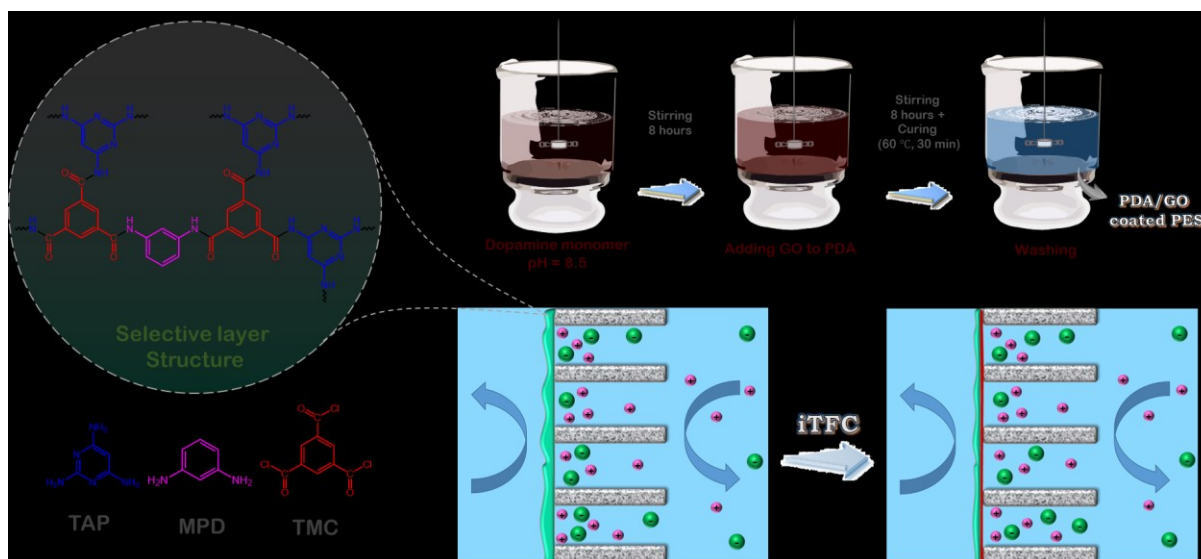


Figure 3-8: Schematic representation of coating the PES support layer with PDA and GO, and the chemical structure of the polyamide layer of the synthesized TFC membranes. The presence of an interlayer and a low reactivity monomer, TAP, reduced the diffusion rate of amine molecules during the interfacial polymerization, forming thinner polyamide layers. The TFC membrane modified with an interlayer is called iTFC in this thesis.

Table 3-4: Synthesis conditions for polyamide TFC membranes modified with PDA/GO interlayer. The composition of the interlayer is the same for all fabricated membranes.

Sample	TAP (wt %)	MPD (wt %)	TMC (wt %)
TFC0	0	0.4	0.4
TFC1	1.4	0.4	0.4
TFC2	1.6	0.4	0.4
TFC3	1.8	0.4	0.4
TFC4	2	0.4	0.4

3.2.3 Results and discussion

3.2.3.1 Evaluation of morphology

Figure 3-9 compares the 3D AFM and FESEM images of the top surfaces of the polyamide membranes. Membrane roughness was quantified with average roughness (R_a), root mean square roughness (R_q), and surface area difference (SAD). All membranes were modified with a PDA/GO interlayer. The FESEM image of the coated PES showed that a continuous PDA/GO layer was formed on the surface pores of the support. TFC0, made without TAP, however, had a typical ridge-and-valley morphology, indicating that the polyamide layer had been formed. The surfaces of the TAP-modified membranes (TFC1-4) had smaller features and flatter morphologies than the control membrane (TFC0). The roughness of the polyamide membranes decreased when the concentration of TAP increased; TFC0 (no TAP) and TFC4 (2 wt% TAP) had the highest and lowest average and root mean square roughness, respectively. The average and root mean square roughness for the coated PES and TFC4 were almost the same, while SAD was higher for TFC4. A higher SAD value explains how interfacial polymerization increases the available surface area of the membranes in a similar projected area.

TAP reacts more slowly than MPD. Therefore, increasing the concentration of TAP in the amine monomer solution slowed down the polymerization. Furthermore, the larger TAP molecules diffuse more slowly through the freshly formed polyamide layer (incipient layer) than the smaller MPD molecules. It can be assumed that the less reactive TAP monomer molecules make the polyamide layer smoother with lesser pronounced ridge-and-valley structure.

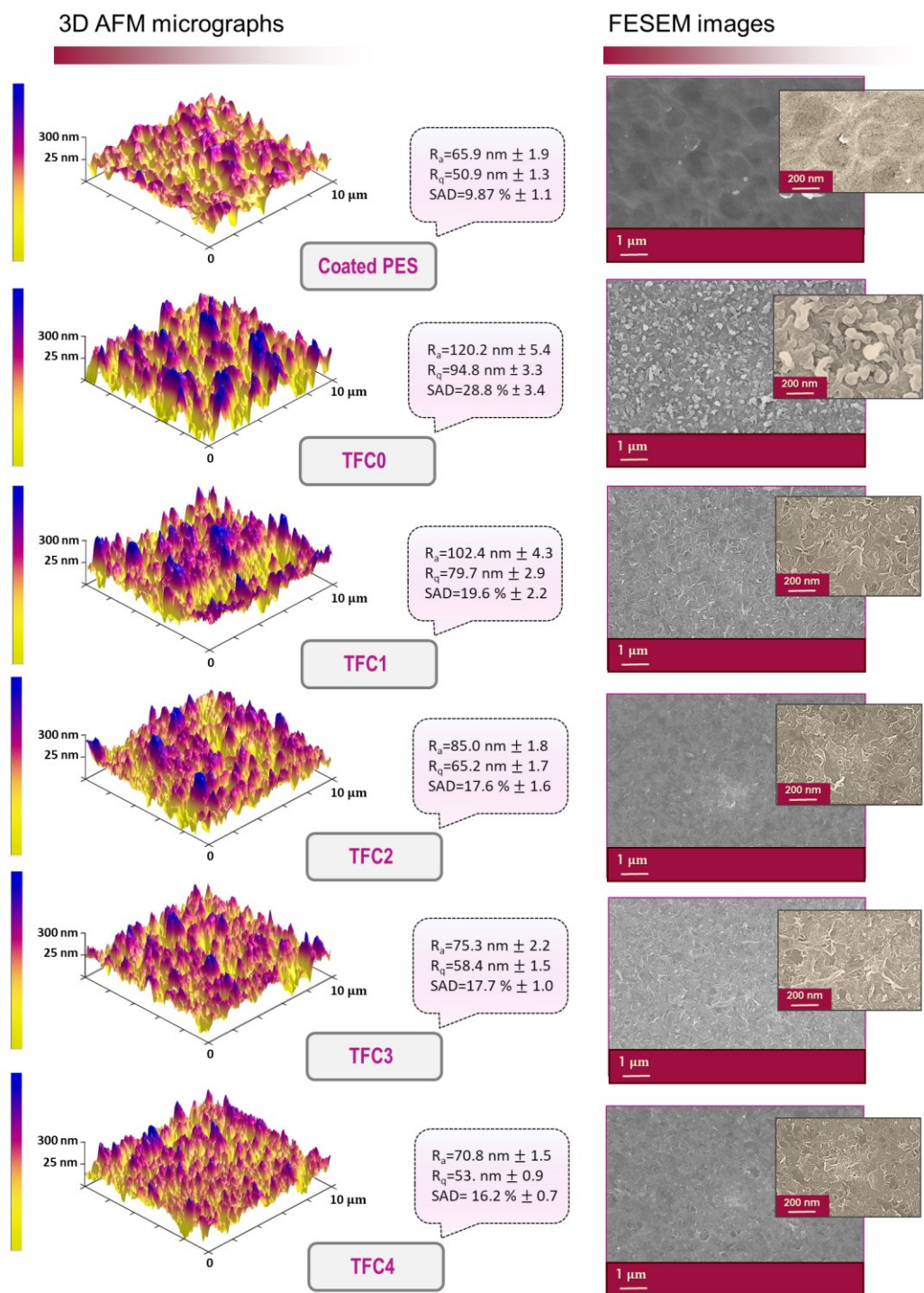


Figure 3-9: 3D AFM and top surface FESEM images of the synthesized polyamide membranes. Roughness data including R_a , R_q , and SAD were estimated using the Nanoscope software.

Figure 3-10 shows cross-section TEM images of coated PES and polyamide TFC membranes mediated with an interlayer. The PES-coated image shows a very thin layer of PDA/GO on the

surface of the support. For all TFC membranes, the polyamide layer formed over the surface of the interlayer and was completely separated from the PES support. The noticeable difference in these images is the structure of polyamide layer, which varied with the concentration of the amine monomer. TFC0 had a thick and rough active layer with empty volumes with various sizes, but increasing TAP concentration decreased the polyamide thickness, with TFC4 showing the lowest thickness and apparently the densest structure.

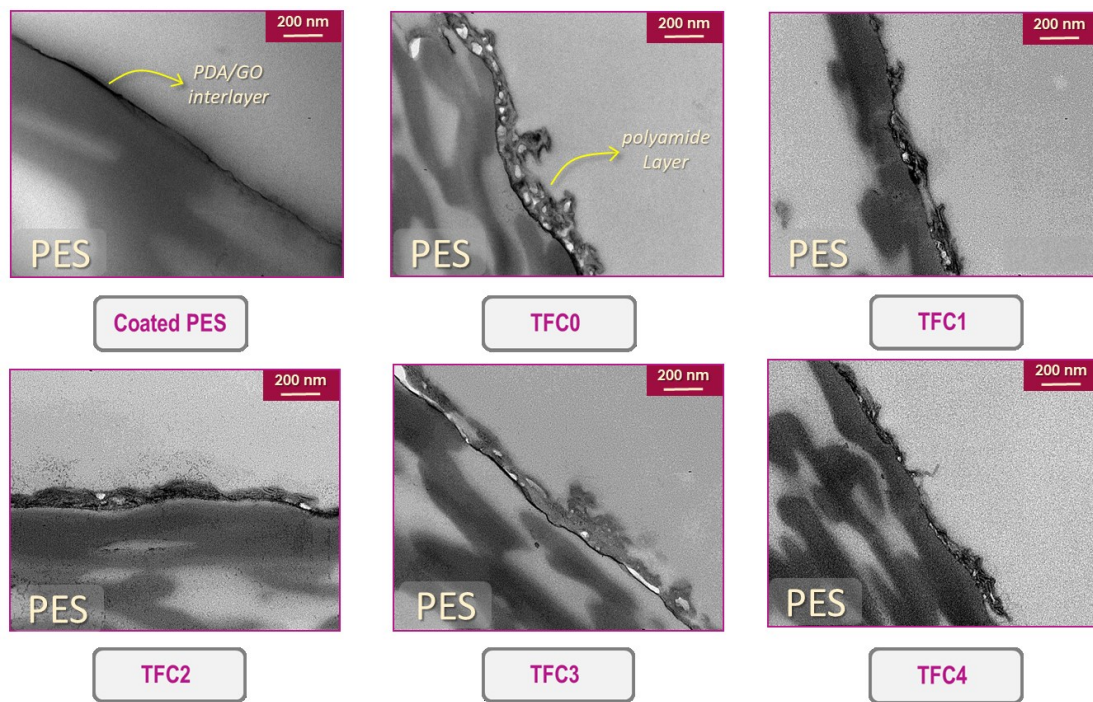


Figure 3-10: Cross-section TEM images of coated PES and polyamide TFC membranes modified with PDA/GO interlayers.

To explore the effect of the interlayer on the formation of the polyamide layer, 3D AFM, FESEM top surface, and cross-section TEM images of TFC4 (with and without the interlayer) are compared in **Figure 3-11**. In the FESEM images, the TFC without the interlayer shows the largest surface features, which may be attributed to differences in the diffusion media for the amine monomer molecules. When interfacial polymerizations occurred on the porous PES support (average pore size of 200 nm) the amine molecules could diffuse more freely to the organic solution. Since the PDA/GO interlayer reduces the cross-sectional area available for the diffusion of the amine monomer molecules, the polyamide top surface morphology looks smoother, without large features. The TEM images show that the interlayer stopped the polyamide layer from

penetrating more deeply into the support pores: the polyamide and PES substrate were completely separated in the TFC membrane made with the interlayer, while the amine solution penetrated into the PES pores, allowing the polymerization to proceed inside the support layer. The formation of polyamide on the surface of the TFC membrane without intruding into the substrate is of great importance for FO filtration because the faster transport of the water molecules in the support layer minimizes the negative effect of internal concentration polarization (ICP) on the water flux.

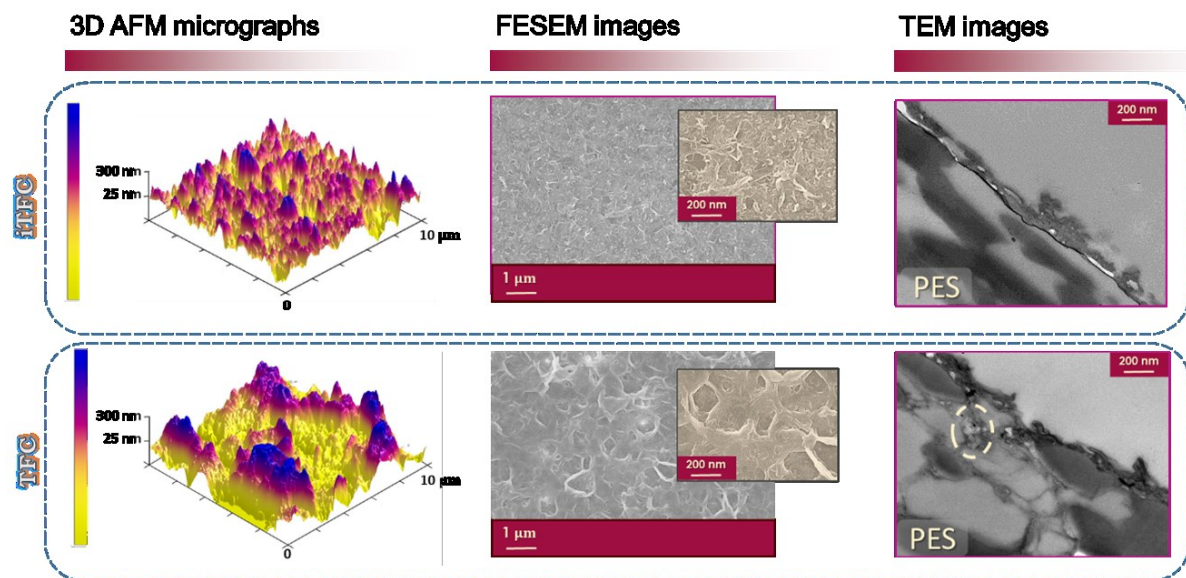


Figure 3-11: 3D AFM, top surface FESEM, and cross-section TEM images of TFC4 with and without PDA/GO interlayer. The TFC membrane modified with an interlayer is called iTFC in this thesis.

3.2.3.2 Chemical characterization

Figure 3-12 shows the FTIR spectra of PES, PDA/GO coated PES, and polyamide membranes. In the PDA/GO spectrum, the peak at 1330 cm^{-1} is attributed to aromatic C-O stretching of PDA. The peak at 1520 cm^{-1} corresponds to C=N stretching in the aromatic structure of PDA. All the spectra have a peak at 1420 cm^{-1} , representing OH in-plane bending and C=C aromatic ring stretching. The high intensity of this peak in the PDA/GO spectrum can be explained by the presence of many OH functional groups in the structure of both PDA and GO. The peak at 1730 cm^{-1} also represents the C=O stretching of carboxylic groups on GO particles [126,148,149]. There are three polyamide characteristic peaks at 1540 cm^{-1} , 1610 cm^{-1} , and 1660 cm^{-1} which were assigned to N-H in-plane bending, C=O stretching, and C=C aromatic ring stretching, respectively [126,150,151]. Finally, the PES spectrum displayed absorption peaks at 1150 cm^{-1} (symmetric SO_2

stretching vibration), 1240 cm^{-1} (asymmetric stretching of C-O-C), and 1485 cm^{-1} and 1580 cm^{-1} (aromatic in-plane ring stretching vibration). The characteristic peaks of PES existed in all spectra, showing IR beam penetration depth.

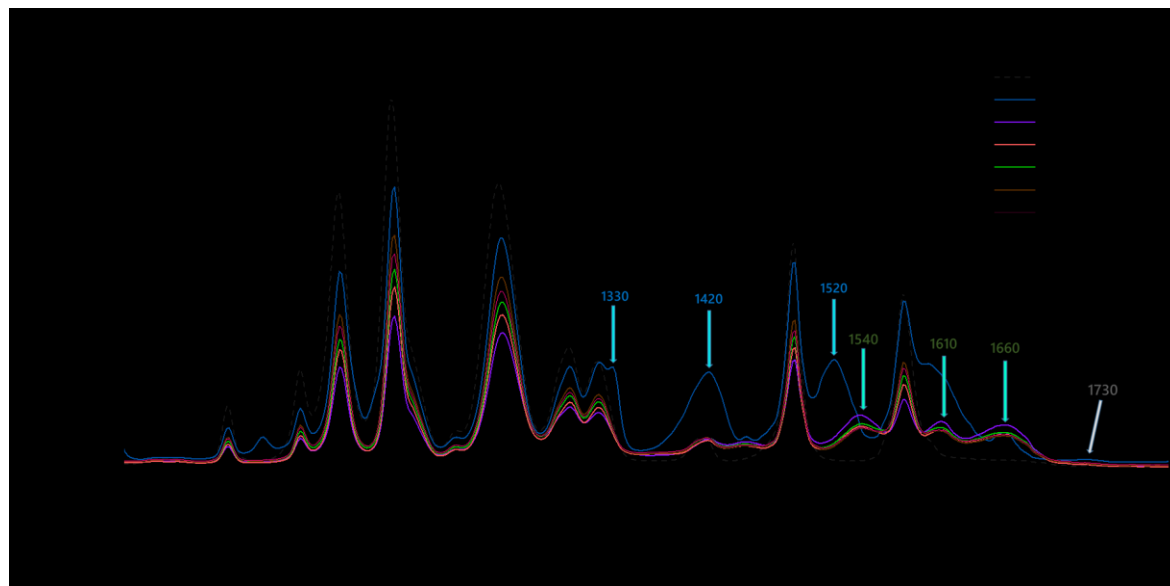


Figure 3-12. FTIR spectra of PES, PDA/GO-coated PES, and polyamide membranes with interlayers. The blue, grey, and green arrows show the characteristic peaks of PDA, GO, and polyamide, respectively.

3.2.3.3. Separation performance of synthesized membranes

Figure 3-13 depicts the water flux and reverse salt flux of the synthesized membranes modified with interlayers in AL-FS and AL-DS configurations. The water flux in the AL-DS configuration is higher than in the AL-FS configuration due to a lower effect of ICP in the PES support layer. When the active layer is facing the feed solution (AL-FS configuration), the presence of NaCl ions in the support layer reduces the effective osmotic pressure. Therefore, the water flux in the AL-DS configuration was higher than in the AL-FS configuration. As the TAP concentration increases, the water flux and reverse salt flux both increased, following the trade-off between water permeability and salt rejection. The reverse salt flux for all membranes was lower than 20 gMH , which kept the effective osmotic pressure constant in the first hour of filtration, without water flux decline.

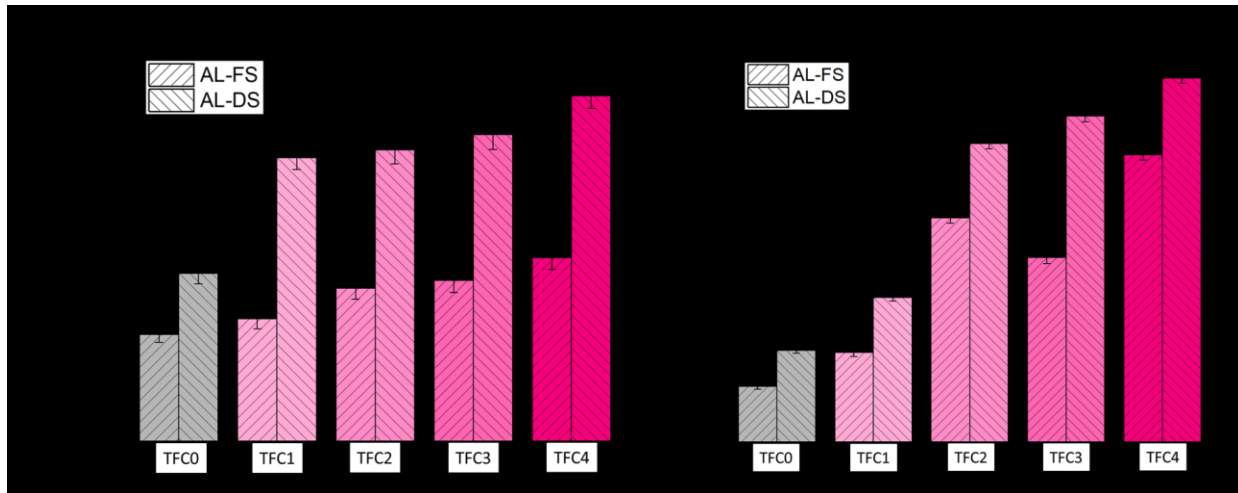


Figure 3-13: Water flux and reverse salt flux in AL-FS and AL-DS of TFC0 and TAP-modified TFC membranes. All membranes had an interlayer.

Figure 3-14 contrasts the performances of TFC0 and TFC3 membranes in the AL-FS configuration from 25-65 °C. The FO filtration was conducted for 1 hour at 25 °C and 65 °C. We adjusted the initial flux to 10 LMH for both membranes by changing the concentration of draw solution. The water flux of the TFC0 and TFC3 membranes increased to 18.3 and 14.2 LMH, respectively. The salt rejection for both membranes also increased, while the reverse salt flux for TFC0 and TFC3 increased to 6.1 and 3.7 gMH, respectively.

As frequently reported in the literature, increasing the temperature in RO processes improves NaCl rejection [152,153]. However, the reverse salt flux for TFC0 and TFC3, with the similar chemistry to RO membranes, increased at high temperature (lower salt rejection). Increasing the temperature intensifies the segmental motions of the polymeric network, allowing more water to diffuse through the membranes [154]. However, RO membranes are subjected to a permanent hydraulic pressure which can compensate the increased free volume inside the polymeric structure. Flux decline of RO membranes at high temperature is an indication of compacting effect of pressure on the membranes at elevated temperatures [147,152,153]. Conversely, our results showed that increasing the temperature in the FO process (without hydraulic pressure) had a negative effect on salt rejection. The increase of reverse salt flux for TFC0 was also higher compared with TFC3. In section 3.1.3.2, we showed that adding TAP increased the cross-linking density of the polyamide structure. Therefore, it is expected that TFC3, with a higher polyamide cross-linking density, maintained its structural integrity at a high temperature compared to a free-

TAP membrane (TFC0). Less plasticizing effect of temperature on the active layer of TFC3 led to lower improvement of water flux and reverse salt flux.

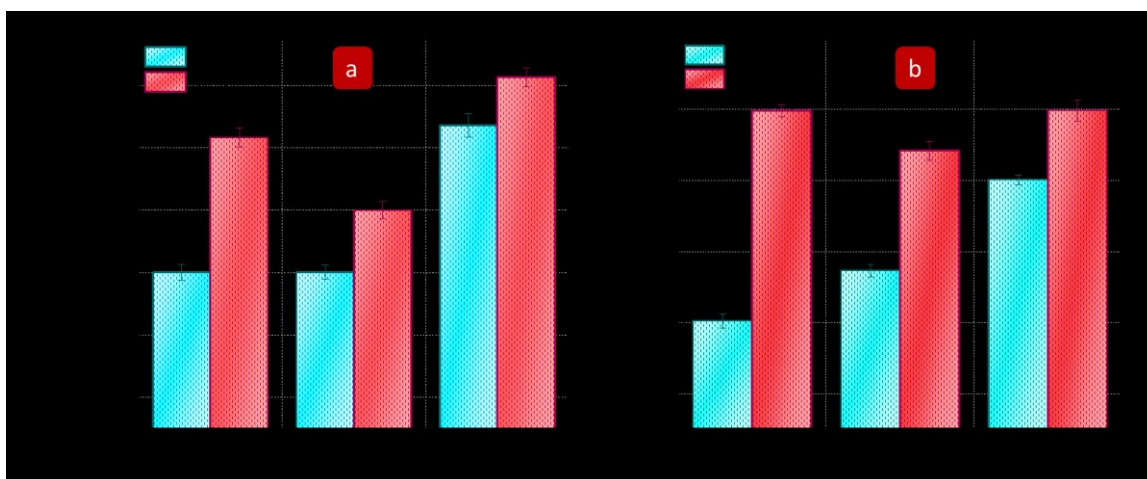


Figure 3-14: (a) The water flux and (b) reverse salt flux of TFC0 and TFC3 membranes in the temperature range of 25-65 °C. The filtrations in AL-FS modes were conducted with two different methodologies: same initial flux and same draw solution concentration (DS: draw solution).

3.3 Conclusion

In this work, we copolymerized two amine monomers, TAP and MPD, with TMC to improve the permeation properties and thermal stability of TFC polyamide membranes for two RO and FO processes. The membranes were made by the interfacial polymerization of TAP, MPD, and TMC at different ratios on a microfiltration PES support.

Polyamide RO TFC membranes had consistent permeate fluxes for 9 hours at 75 °C, proving that the structural integrity of the selective layer was maintained. FTIR and XPS results showed the formation of more amide linkages in the polyamide layer as a consequence of TAP incorporation in the membrane. Higher TAP fractions in the membrane increased the permeate flux more than 3 times, but slightly reduced NaCl rejection. This higher flux agrees with morphological analysis results, in which membranes with higher TAP fractions were thinner and had smoother surfaces. However, the permeability/selectivity trade-off was explained with the possible formed free volume, which is called aggregate pore, interior the polyamide layer structure of TAP-modified membranes.

Polyamide FO TFC membranes were modified with an ultrathin PDA/GO interlayer. The interlayer made the polyamide layer thinner, smoother, and with smaller surface features. TAP-

modified membranes had higher water permeability and thermal stability at high temperatures. TFC membranes made with TAP was less prone to be plasticized at 65 °C, showing less increase in reverse salt flux.

Chapter 4

Exploiting unique features of nanodiamond (ND) particles for fabricating high- performance TFC and TFN membranes[‡]

[‡] This chapter was prepared based on references [150,153].

4.1 Nanodiamond-enabled TFN polyamide membrane for high-temperature water treatment

4.1.1 Introduction

The world is facing pervasive challenges due to the finite freshwater resources in many countries. Although around 70% of our planet is covered with water, only 3% of these resources are suitable freshwater for human needs [155]. In addition, more than 65% of earth's freshwater is locked up in ice caps and glaciers [156]. The universal need is even more substantial when it comes to drinking water. A report of the World Health Organization (WHO) and the United Nations Children's Fund (UNICEF) in June 2019 states that one in three people does not have access to safely managed drinking water worldwide [157]. The inevitable growing demand for clean water, along with climate change and rapid industrialization, are serious threats to available freshwater resources. It is, therefore, essential to treat and recycle municipal and industrial wastewater. Continuous efforts have been devoted to improve the current methods and develop new technologies to provide cost- and energy-efficient water treatment processes [158–160].

RO is a pressure-driven membrane process that has applications spanning from desalination to industrial wastewater treatment [161,162]. For more than four decades, thin-film composite (TFC) membranes have been the most common type of RO membranes [163]. A TFC membrane has a layered structure consisting of an ultrathin cross-linked polyamide layer coated on a mechanically robust porous substrate. The polyamide layer is formed by interfacial polymerization (IP), where two monomers, such as *m*-phenylene diamine (MPD) and trimesoyl chloride (TMC), react at the interface of two immiscible aqueous and organic solutions on the surface of the porous substrate [37,40,164]. One of the main shortcomings of TFC membranes is the inherent trade-off between water permeability and solute selectivity: the higher the water flux, the lower the salt rejection. Moreover, most of the commercial TFC RO membranes suffer from low thermal stability and flux decline at temperatures above 45 °C [165].

Since it is almost certain that the permeation and thermal properties of TFC membranes are governed by the physicochemical characteristics of the top polyamide layer rather than the underlying support [166,167], functional organic and inorganic nanoparticles have been incorporated into the polyamide layer to develop high-performance thin-film nanocomposite

(TFN) membranes. Due to their high mechanical and thermal stability, inorganic nanoparticles (such as zeolite, silica, titanium, carbon nanotube, and graphene oxide) can enhance the structural integrity of the polyamide layer when an appropriate surface modification is applied [104,110,168–170].

Khorshidi et al. [106] introduced well-dispersed oleic acid-modified TiO₂ nanoparticles to the polyamide layer of TFN membranes to tailor their permeation and thermal performance. The addition of 0.0245 wt% modified TiO₂ nanoparticles in a heptane solution led to the production of TFN membranes that had stable flux for 6 hours at 65 °C. The formation of a robust TiO₂/polyamide layer, however, made the TFN membranes less permeable [106]. Covalent attachment of nanoparticles to the polyamide layer was also found to be effective in promoting polymer/filler interactions. Wen et al. [98] incorporated acyl chloride functionalized graphene oxide into poly(piperazine/TMC) TFN membranes. The functionalized graphene oxide particles reacted with the amine groups of piperazine during interfacial polymerization. The fabricated membranes showed stable Na₂SO₄ rejection in the operating temperature range of 30-80 °C. The incorporation of the surface-modified nanoparticles was found to enhance the thermal properties of the polymeric structure of TFNs. Wu et al. [109] showed that adding carboxylated multi-walled carbon nanotubes increased the decomposition temperature of TFN membranes significantly.

Although extensive research has been conducted on the development of TFN membranes, it is still challenging to enhance the thermal stability of these membranes without sacrificing their permeation flux and/or contaminant removal efficiency. In addition, much of the research up to now has been mostly restricted to induce some functional properties, such as antimicrobial activity and biofouling resistance, to the TFN membranes and failed to verify the robustness of the membranes in long-term operation. Given that, it is desirable to introduce novel functional nanomaterials into the polyamide layer and evaluate the integrity of the synthesized TFN membranes under harsh conditions for a longer time.

Detonation ND is a relatively novel carbon nanoparticle with a unique core-shell structure. The diamond core of ND has a dense tetrahedral sp³ carbon structure, rendering it with high thermal, mechanical, and chemical stability. Its graphitic shell, bearing numerous oxygen functional groups and sp² carbons, provides a hydrophilic surface with tunable chemistry for further chemical functionalization [171,172]. Benefiting from these outstanding structural properties, ND has been

recently considered for the fabrication of microfiltration, ultrafiltration, and nanofiltration nanocomposite membranes [173–178]. These studies mainly focused on the hydrophilic nature of the ND particles for the synthesis of membranes with higher water permeability and antifouling propensity. As the selective layer has a key role in TFC membrane performance, it seems to be more beneficial to embed ND particles into the polyamide layer. This approach requires that the nanoparticles be well dispersed in the medium and have good affinity with the polyamide matrix. Qin et al. [179] introduced ND particles in interfacial polymerization to fabricate nanofiltration TFN membranes. The membranes were synthesized by dispersing carboxylated ND particles into the aqueous piperazine solution. With adding 0.05 wt% ND particles, the water flux was increased 70% without sacrificing MgSO_4 rejection compared with pristine TFC membrane. The improvement was justified with the effect of ND particles on increasing the effective surface area of the membranes as well as the enhancement of the hydrophilicity.

In this study, we proposed a new generation of TFN membranes made through the incorporation of surface-functionalized ND particles into the polyamide layer to enhance the permeation properties and thermal stability of TFN membranes. We functionalized the surface of the ND particles with amine groups through a wet chemical process and then dispersed them into an organic monomer suspension. To improve the dispersion of the ND particles, we added ethyl acetate as a co-solvent to the organic solution. Then, the co-solvent assisted interfacial polymerization between MPD and TMC solutions was conducted over a PES support to synthesize the polyamide nanocomposite layer. The effect of ND-MPD particles and ethyl acetate on chemical composition, morphological characteristics, and separation performance of the modified membranes was evaluated at room and elevated temperature (75 °C).

4.1.2 Experimental methods

In order to functionalize the ND particles with MPD groups, 0.5 g of as-received ND powder was first oxidized in a furnace at 420 °C for 2 hours under air. Air oxidization introduced carboxylic groups onto the ND surface (ND-COOH) and homogenized its surface by removing impurities. To facilitate further functionalization, the ND particles were halogenated with thionyl chloride to provide a reactive surface. A volume of 25 mL of thionyl chloride was added to ND-COOH and stirred at 65 °C for 24 hours. Then, the synthesized ND-COCl was washed with tetrahydrofuran to remove unreacted thionyl chloride [180,181]. For amine functionalization, ND-COCl particles

were added to an MPD solution, composed of 20 g of MPD dissolved in 30 mL dimethylformamide, and stirred at 70 °C for 72 hours [182]. **Figure 4-1a** illustrates these reaction steps. MPD-functionalized ND particles (ND-MPD) were washed again with tetrahydrofuran and dried in a vacuum oven at 40 °C overnight. Finally, ND-MPD powder was kept in a vacuum chamber to avoid undesirable moisture absorption.

TFN Polyamide membranes were fabricated by coating a nanocomposite polyamide layer containing ND-MPD particles over the PES support using interfacial polymerization (IP). The polyamide layer was formed by the reaction between an aqueous MPD solution, composed of 2 wt% MPD, 1 wt% triethylamine, and 0.2 wt% sodium dodecyl sulfate, and an organic TMC solution, composed of 0.2 wt% TMC, 6 wt% ethyl acetate, and different loadings of ND-MPD particles. Initially, the ND-MPD powder was added to the solution of heptane and ethyl acetate. Ethyl acetate was used as a polar co-solvent to improve the dispersion of nanoparticles in heptane. The mixture was sonicated with an ultrasound probe sonicator (Q700 Qsonica) with 45% amplitude at room temperature for 45 minutes. Then, a concentrated TMC/heptane solution was added to the mixture to adjust the TMC concentration to 0.2 wt%. TMC solution was selected as the dispersant phase to facilitate the covalently incorporation of MPD functionalized ND particles into the polyamide matrix. The ND-MPD particles partially react with TMC monomers. Considering the presence of abundant TMC monomers, the resulting TMC solution contained two components: (1) ND-MPD particles attached to TMC, and (2) free TMC monomers. Both components can take part in interfacial polymerization and make a polyamide layer. After the preparation of the TMC solution, synthesizing the polyamide layer started with soaking the PES support with the MPD solution for 9 minutes. The impregnated support was rolled using an acrylic roller to remove the excess MPD solution from the support. Then, the TMC solution containing ND-MPD particles was poured over the support, and the polymerization was allowed to proceed for 30 seconds. After that, the excess TMC solution was removed, and the coated membrane was cured in an oven at 60 °C for 4 minutes, followed by rinsing with distilled water for 5 minutes. The curing was performed to stabilize the polyamide layer through evaporating the remained aqueous and organic solvents as well as further interfacial polymerization [40,183]. TFN membranes made by loading 100 ppm, 200 ppm, and 400 ppm of ND-MPD were labelled as TFN100, TFN200, and TFN400. Two TFC membranes (TFC-1 and TFC-2), one without ND-MPD/ethyl acetate and one without ND-MPD, respectively, were also fabricated as the pristine and control membranes.

Figure 4-1b illustrates the incorporation process of ND-MPD particles into the polyamide layer of the TFN membranes.

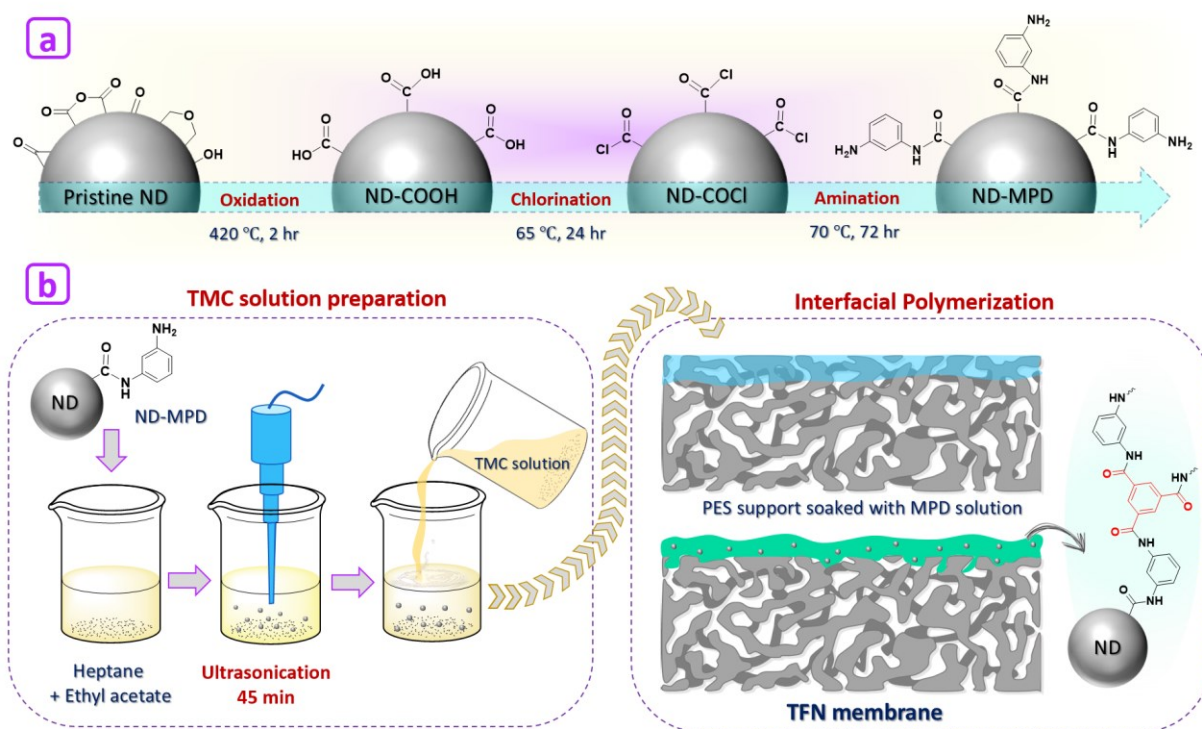


Figure 4-1: (a) Schematic illustration of the functionalization route of ND particles with MPD and (b) Schematic representation of TFN membrane fabrication. The TFN fabrication method is divided into two steps. First, functionalized ND particles were dispersed in a heptane solution containing ethyl acetate followed with the sonication of the suspension. TMC solution was added after the sonication to avoid disturbing the reaction between ND-MPD and TMC. In the second step, the prepared TMC solution was brought into contact with the MPD solution to form an ND/polyamide composite layer.

4.1.3 Results and discussion

4.1.3.1 Characterization of pristine and functionalized ND particles

Figure 4-2 illustrates the TEM and XRD characterizations of the pristine ND. The TEM image of nanoparticles (**Figure 4-2a**) shows that the pristine ND particles were approximately spherical with an average diameter of <10 nm. Their small spherical shapes together with their high surface energy make ND particles likely to self-agglomerate [171]. The XRD spectra, shown in **Figure 4-2b**, indicates two intense ND characteristic peaks at 43.8° and 75.4°, which correspond to diffraction from atomic planes of (111) and (220) of the cubic diamond structure [184,185]. The successful functionalization of ND particles was corroborated with FTIR and TGA measurements. The FTIR spectra of pristine ND, ND-COOH, and ND-MPD are illustrated in **Figure 4-2c**. The

peak at 1740 cm^{-1} corresponds to C=O stretching vibrations of carboxylic groups. The high intensity of the carboxylic group peak in ND-COOH confirms the successful carboxylation of ND. The appearance of an intense peak at 1630 cm^{-1} in the ND-MPD spectrum is attributed to C=O stretching vibrations of the amide group (shifted by electronegative nitrogen atom) [180–182]. This peak can also be ascribed to N–H bending vibrations of primary amines [186]. ND-MPD also showed the peak at 1740 cm^{-1} , which represents the remained carboxylic groups on the surface of amine-functionalized ND. A broad band around 3340 cm^{-1} corresponds to O–H and N–H stretching vibrations [126].

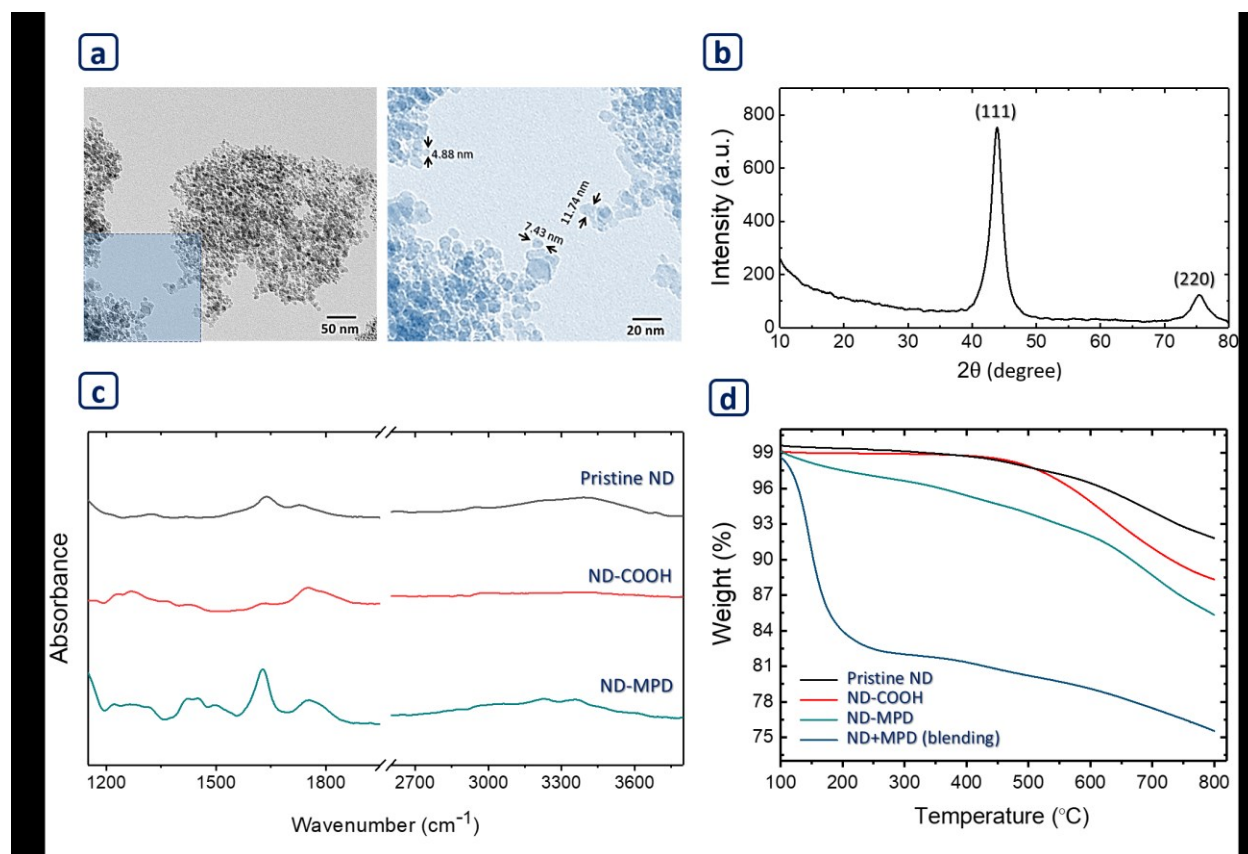


Figure 4-2: (a) TEM images of pristine ND particles dispersed in water. Single nanoparticles are distinguishable due to the fine dispersion of NDs. (b) XRD pattern of pristine ND showing two characteristic peaks of the diamond structure at 43.8° and 75.4° . (c) FTIR spectra of pristine and functionalized ND particles. (d) TG curves of pristine ND, functionalized NDs, and ND+MPD mixture. ND+MPD is a mixture made by simply blending MPD and ND. TGA results are presented from 100°C since the mass loss at $0\text{--}100^\circ\text{C}$ is attributed to the possible absorbed water on the ND particles.

TG curves in **Figure 4-2d** compares the thermal stability of the pristine and functionalized NDs. To evaluate the effectiveness of the surface functionalization process, the ND particles were simply blended with MPD (labelled as ND+MPD in **Figure 4-2d**) with a mass ratio of 4:1. The

pristine ND and ND-COOH showed a stable curve up to 450 °C with a slight mass loss of ~1.1 % and ~0.6 %, respectively, which indicates high thermal stability of the ND particles. The marked gap between pristine ND and ND-COOH at 450-800 °C can be attributed to the decomposition of carboxylic groups of ND-COOH [187]. The amine-functionalized ND, however, exhibited 5.5% mass loss at 100-450 °C, corresponding to the decomposition of amino groups [180,181]. This was also confirmed with the thermal decomposition of the ND+MPD blended sample, where almost 20% of the mass, equal to the exact amount of MPD in the mixture, was lost at 100-450 °C.

4.1.3.2 ATR-FTIR and XRD analysis of synthesized membranes

The surface chemistry of PES support and the synthesized composite membranes was assessed by ATR-FTIR and XRD analyses. As shown in **Figure 4-3a**, the three distinctive peaks at 1535 cm^{-1} (N-H in-plane bending of amide II and C-N stretching), 1610 cm^{-1} (C=C aromatic ring stretching), and 1660 cm^{-1} (C=O stretching of amide I) in TFC and TFN membranes spectra are ascribed to polyamide layer, which are absent in PES spectrum [188,189]. The characteristic peaks of PES support are present in all samples at 1150 cm^{-1} (symmetric SO_2 stretching vibration), 1240 cm^{-1} (asymmetric stretching of C-O-C), 1410 cm^{-1} (C=C aromatic ring stretching), and 1485 and 1580 cm^{-1} (aromatic in-plane ring stretching vibration), due to the large penetration depth of IR beam (ca. 0.5-3 μm) [126,128]. The changes in the areas of the peaks corresponding to polyamide and PES correspond to the formation of polyamide layers with different thicknesses. To provide a quantitative comparison of the synthesized polyamide layer thickness in different membranes, the ATR-FTIR peaks were first deconvoluted, and then the ratio of the area of the polyamide peak at 1660 cm^{-1} to the PES peak at 1150 cm^{-1} was calculated. The results are tabulated in **Figure 4-3a**. The lowest ratio was obtained for the pristine TFC membrane, implying the formation of the thinnest polyamide layer among all membranes. In contrast, the highest value was obtained for TFN100, suggesting the formation of a thicker polyamide layer in the presence of ethyl acetate and minimum loading of ND particles. Accordingly, TFN200 and TFN400 had intermediate ratios of the peak areas. This observation shows that while the presence of ethyl acetate, as a co-solvent, intensified the polymerization reaction, the addition of ND particles moderated the impact of ethyl acetate and resulted in lower polymerization rates with lower polyamide formation compared to the TFN100 membrane.

Figure 4-3b showed the XRD patterns of ND-MPD, TFC-1, and TFN membranes. The major diffraction peak appeared at $2\theta=18.2^\circ$ for all synthesized membranes represents the amorphous structure of PES support [190]. Due to the low concentration of ND particles in the very thin polyamide layer, the characteristic peaks of ND particles were not distinguished in the TFN100 and TFN200 XRD spectra. However, TFN400, with the highest loading of ND, showed a small peak at $2\theta=43.8^\circ$, which can be assigned to the presence of ND particles.

Figure 4-4 shows the high resolution of C 1s and N 1s XPS spectra peaks for TFC-1 and TFN membranes. The C 1s peak spectrum is deconvoluted to five peaks associated to C-H and C-C at 285 eV (carbon bonds in the aromatic rings), C-COOH and C-CONH at 285.7 eV (carbon attached to carboxyl group and amine linkage), -CN- at 286.2 eV (carbon attached to amines and amide linkage), N-C=O at 288.4 eV (amide linkage), O-C=O at 288.5 eV (carbon attached to carboxyl group). The N 1s peak spectrum is deconvoluted to three peaks corresponded to N-C=O at 400.5 eV (amide linkage), R-NH₂ at 398.5 eV (unreacted amine), and -NH³⁺ at 402.1 eV (quaternary nitrogen) [130,191]. The -NH³⁺ peak is attributed to the electrostatic interaction between amine and carboxylic groups [191–193].

Table 4-1 presents the elemental composition as well as the peak area percentages of C 1s and N 1s species. The carbon content was increased from 70.36% to 75.25% for TFC-1 and TFN400, respectively. It can be due to increasing the participation of ND particles in polyamide layer at higher nanoparticle concentrations. To evaluate the cross-linking density, the ratio of unreacted functional groups, that are amine and carboxylic groups, to amide linkage were calculated. According to Table 1, (O-C=O)/(N-C=O) ratio has the maximum value for pristine membrane (TFC-1) compared with TFN membranes, indicating the formation of less amide linkages and more carboxylic groups (hydrolyzed acid chloride groups of TMC). Similar results were obtained for (R-NH₂)/(N-C=O) ratio in N 1s peak species. This comparisons clearly exhibit the effect of functionalized ND particles on the increment of amide linkage formation, and consequently, higher cross-linking density.

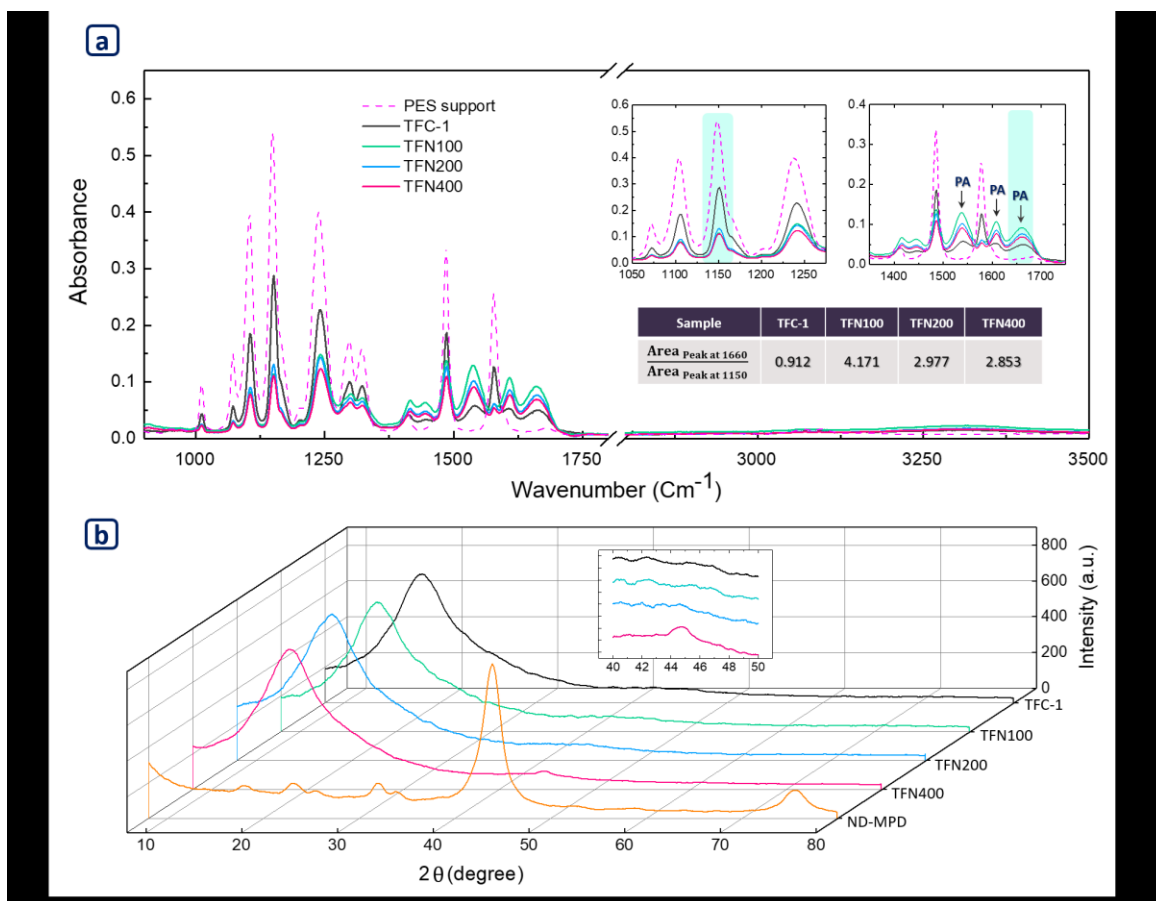


Figure 4-3: (a) FTIR spectra of PES support, TFC-1, and TFN membranes. The area ratios of two highlighted peaks, a polyamide peak at 1660 cm^{-1} and a PES peak at 1150 cm^{-1} , were listed in a table. (b) XRD spectra of ND-MPD, TFC-1, and TFN membranes. Higher magnification of the XRD spectra in the range of $2\theta=40\text{--}50^\circ$ was presented in a separate panel to illustrate the ND characteristic peak for TFN400.

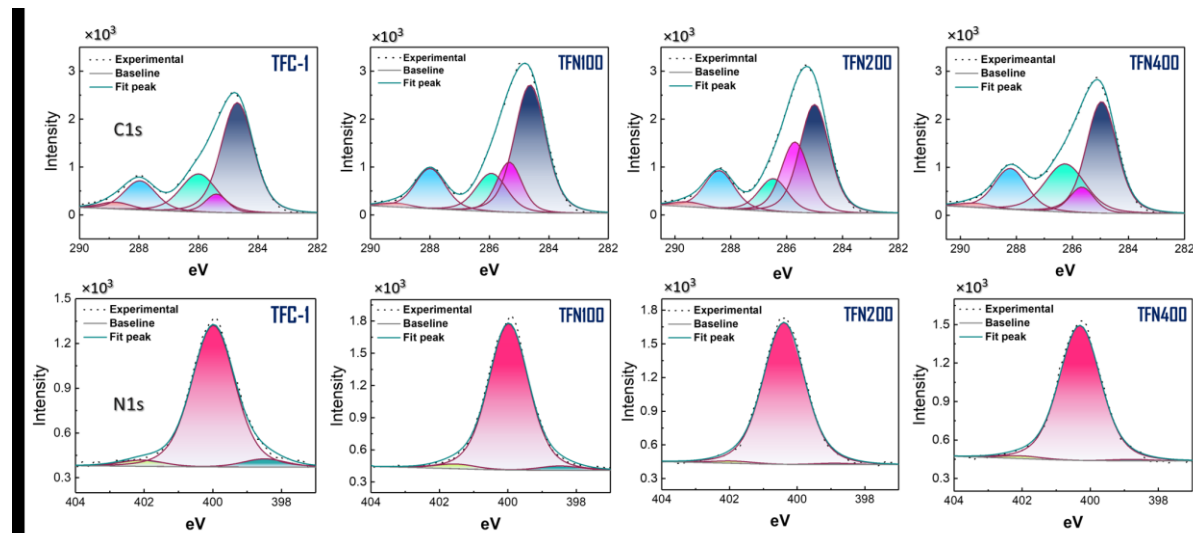


Figure 4-4: Deconvoluted C 1s and N 1s XPS spectra of TFC-1 and TFN membranes.

Table 4-1: Elemental composition and peak area percentage of C 1s and N 1s species

Sample	Atomic concentration (%)			C 1s species (%)						N 1s species (%)			
	Carbon	Nitrogen	Oxygen	C-H, C-C	C- COO, C- CON	-CN-	N- C=O	O- C=O	$\frac{O-C=O}{N-C=O}$	R-NH ₂	N-C=O	$\begin{matrix} - \\ NH_3 \\ + \end{matrix}$	$\frac{R-NH}{N-C=O}$
TFC-1	70.36	10.44	19.20	55.20	6.23	21.08	14.21	3.29	0.232	5.24	90.78	3.98	0.058
TFN100	73.56	11.73	14.70	51.44	16.21	15.22	15.64	1.49	0.095	2.82	94.13	3.06	0.030
TFN200	73.71	11.63	14.66	43.66	26.27	12.86	15.29	1.93	0.126	0.98	97.45	1.57	0.010
TFN400	75.24	10.12	14.64	45.74	8.42	26.11	17.91	1.81	0.101	1.00	97.02	1.97	0.010

3.1.3.3 Morphology characterization

Figure 4-5 illustrates the FESEM top surface morphology of the PES support and the fabricated composite polyamide membranes. The PES support exhibited a uniform porous structure at the top surface. TFC-1 showed a ridge-and-valley structure, which is typical for the polyamide membranes made with interfacial polymerization [32]. In contrast, TFC-2 and all TFN membranes showed bigger surface features with less wrinkled structures. This observation was also confirmed by the 2D and 3D surface topography images of the membranes, presented in **Figure 4-6**. The roughness data indicates that the average roughness (R_a) and root-mean-square roughness (R_q) were increased from 108.4 and 82.6 nm for TFC-1 to 177.5 and 130.0 nm for TFN400, respectively.

The TEM images in **Figure 4-7** illustrate the cross-sectional images of the prepared membranes. The lowest polyamide thickness was observed for the pristine TFC-1 membrane (inset a). In contrast, the polyamide thickness of TFN membranes increased significantly compared to the pristine membrane. The higher polyamide thickness of TFN membranes can be attributed to the use of ethyl acetate as a co-solvent which reduced the solubility difference and the interfacial tension of the aqueous and organic solutions [194,195]. Therefore, the polyamide formation was intensified due to the higher diffusion rate of the MPD monomers to the reaction zone during the interfacial polymerization [36,39]. These observations align well with the ATR-FTIR analysis that showed more polyamide thickness for the membranes synthesized with ethyl acetate. Comparing TFN membranes, the thickness of polyamide layer was almost similar (insets b-d). This can be due to the dominant impact of ethyl acetate compared to ND concentration on the thickness of polyamide layer. The marked effect of ethyl acetate on the thickness of the polyamide layer was also verified by comparing the cross-section FESEM images of TFC-1 and TFN-400 (see the Figure B1 in the Appendix B). Taking a closer look into the TEM images reveals that the TFN membranes with a thick polyamide layer had more voids in their structures compared to the pristine

TFC-1 membrane. It has been suggested that the more polyamide formation during the interfacial polymerization leads to more generation of heat as this reaction is exothermic. The released heat partially evaporates the organic solvent and forms multiscale internal voids within the polyamide structure [134].

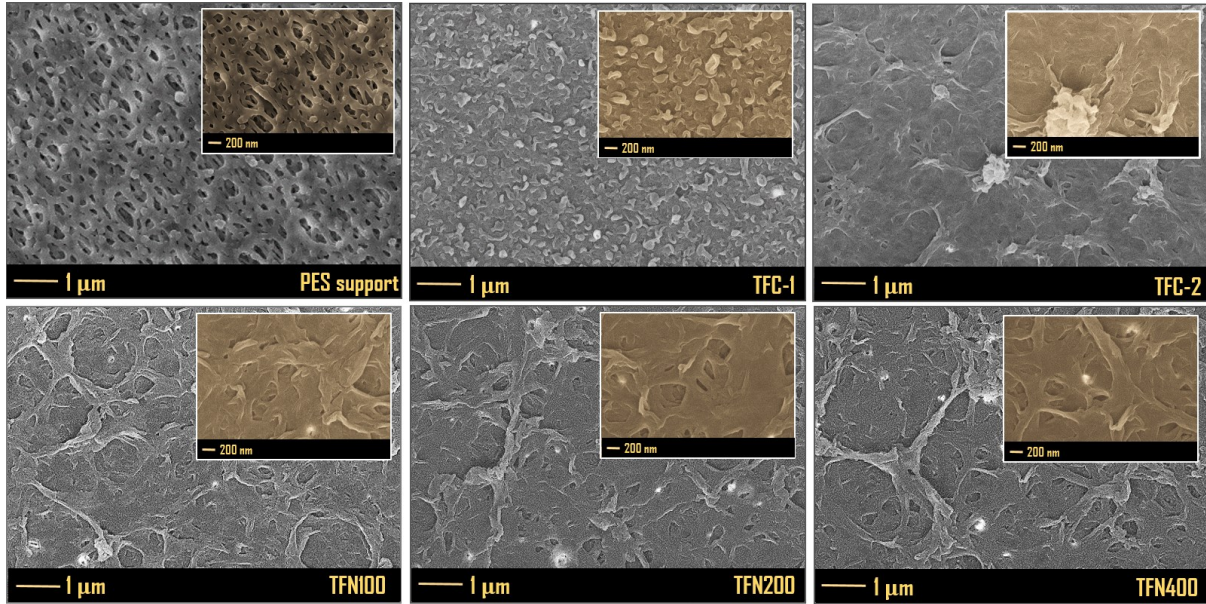


Figure 4-5: FESEM top surface images of PES and TFC/TFN membranes. For all polyamide membranes, it is evident that the surface of PES is covered with a continuous defect-free thin film of polyamide.

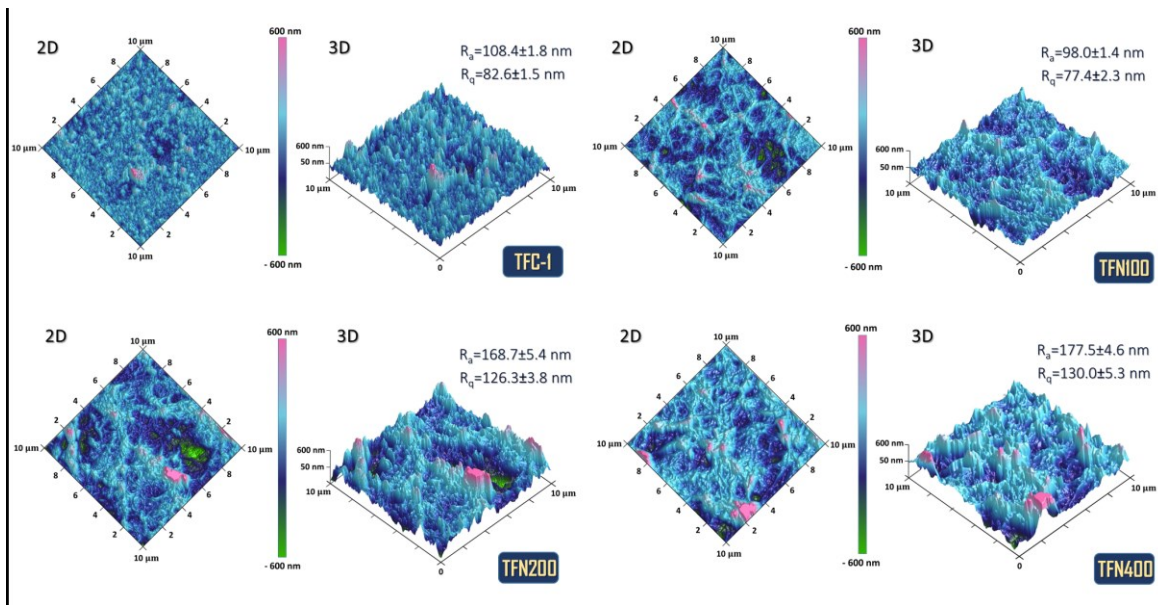


Figure 4-6: 2D and 3D AFM micrographs of synthesized TFC/TFN membranes and roughness data including average roughness (R_a) and root mean square roughness (R_q).

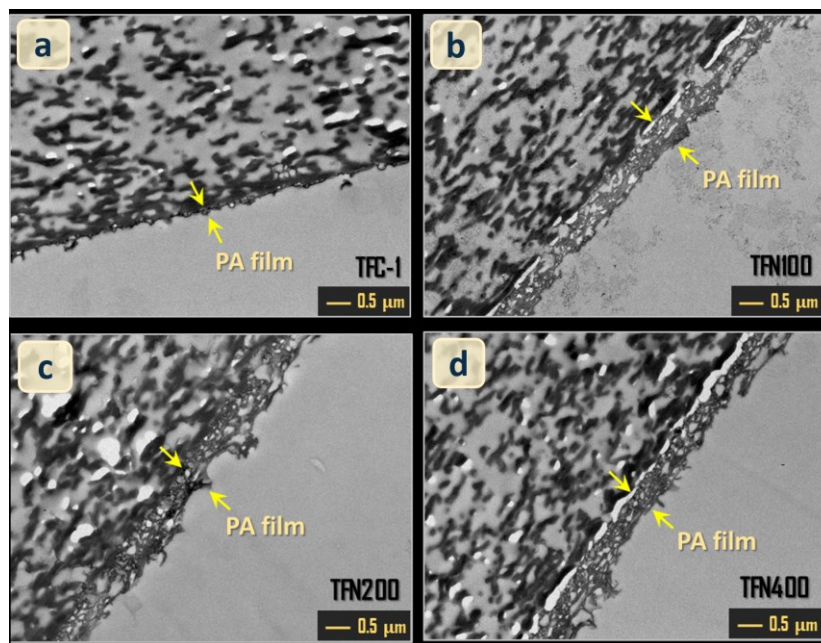


Figure 4-7: TEM cross-section images of TFC-1 and TFN membranes. The formation of more polyamide on top of the dense initial layer for TFN membranes is an indication of intensified MPD diffusion.

4.1.3.4 Separation Performance

Figure 4-8 demonstrates the water flux and NaCl rejection of the fabricated membranes at 25 °C and 75 °C. The performance of lab-synthesized membranes was also compared to a commercial RO polyamide membrane (SUEZ AG). The pristine TFC-1 showed the lowest permeate flux of ~17 LMH at room temperature. The ND-modified TFN membranes showed improved water flux with the highest value of 76.5 LMH at 25 °C for TFN400, which was more than 4.5 times improvement compared with the TFC-1. In addition, TFN400 overcame the typical permeability/selectivity trade-off, where the NaCl rejection increased from 96.5 % for the TFC-1 to 97.3 % for the TFN400. The comparison between the TFN membranes shows that both water flux and NaCl rejection enhanced by increasing the concentration of ND particles in the reacting solution. The high-temperature flux stability of the membranes was evaluated by increasing the operating temperature from 25 °C up to 75 °C followed by a continuous operation for 9 hours. **Figure 4-8a** illustrates that all the membranes showed higher water flux as the temperature ramped up from 25 °C to 75 °C. Considering the continuous operation at 75 °C, the TFC-1 had a stable water flux, whereas all the other membranes experienced some extent of flux decline. The water flux of SUEZ AG decreased from 168 to 131 LMH over 9 hours, showing 22% flux decline. The

TFN membranes demonstrated more stable permeate flux than SUEZ AG, with the lowest flux decline of 13 % for TFN400.

The higher permeation rate of TFN membranes compared to pristine TFC-1 at 25 °C can be attributed to the higher hydrophilicity of ND-modified polyamide films, and possibly the formation of more nano-scale voids within the polyamide network by the addition of ND particles and ethyl acetate. The water contact angle of the membranes decreased from 88.4° for TFC-1 to 58.3° for TFN400, showing 34% reduction (see Figure B2 in the Appendix B). The abundant oxygen functional groups on the surface of the ND particles can serve as favorable spots for hydrogen bonding to accelerate the diffusion of water molecules through the polyamide network. Furthermore, recent studies, using positron annihilation lifetime spectroscopy (PALS) and molecular dynamic (MD) simulation, have shown that the internal free volumes can be divided into “network” and “aggregate” voids. The former is ascribed to small voids ($\sim 4.2\text{-}4.8$ Å in diameter) between the segments in the polyamide network, and the later is referred to the larger voids ($\sim 7.0\text{-}9.0$ Å in diameter) between the polyamide network domains [136,196–200]. Therefore, the enhancement of both the water flux and salt rejection of the TFN400 membrane compared to the pristine TFC-1 membrane can be attributed to the sufficient enlargement of internal “network” and “aggregate” voids within the polyamide layer. The enhancement of the water flux of the membranes over temperature transition is expected due to the fact that the polyamide average free volume increases by higher random thermal motions of the polymer segments. Therefore, the diffusion coefficient of the water molecules through the polyamide networks increases at elevated temperatures. Furthermore, the self-diffusion of water molecules increases considerably at higher temperatures due to the lower viscosity and faster thermal motion.

The flux decline of the membranes over the continuous operation at 75 °C may be attributed to partial collapse/closure of the interconnected voids within their polyamide structure. Hence, the flux stability of the TFC-1 membrane at 75 °C can be justified as this membrane possessed a dense polyamide layer as evidenced by its low initial flux at 25 °C). Accordingly, the higher flux decline of the TFN membranes compared to TFC-1 can be ascribed to the presence of more nano-scale voids within their structure which made them more prone to microscopic compaction. The lower flux decline of TFN400 compared to TFN100 can be related to its higher rigidity and cross-linking density which was introduced by the higher numbers of ND particles in the polyamide matrix. Moreover, it is widely accepted that the incorporation of conductive nanomaterials (e.g., ND

particles) into a polymer promotes the thermal conductivity of the resulting polymer nanocomposites [201–203]. The well-dispersed NDs can potentially act as thermal bridges, and reduce the heat accumulation within the polyamide matrix at high temperatures. The favorable outcome would be the less impact of thermal stresses on the polyamide structure when a higher ND concentration is loaded.

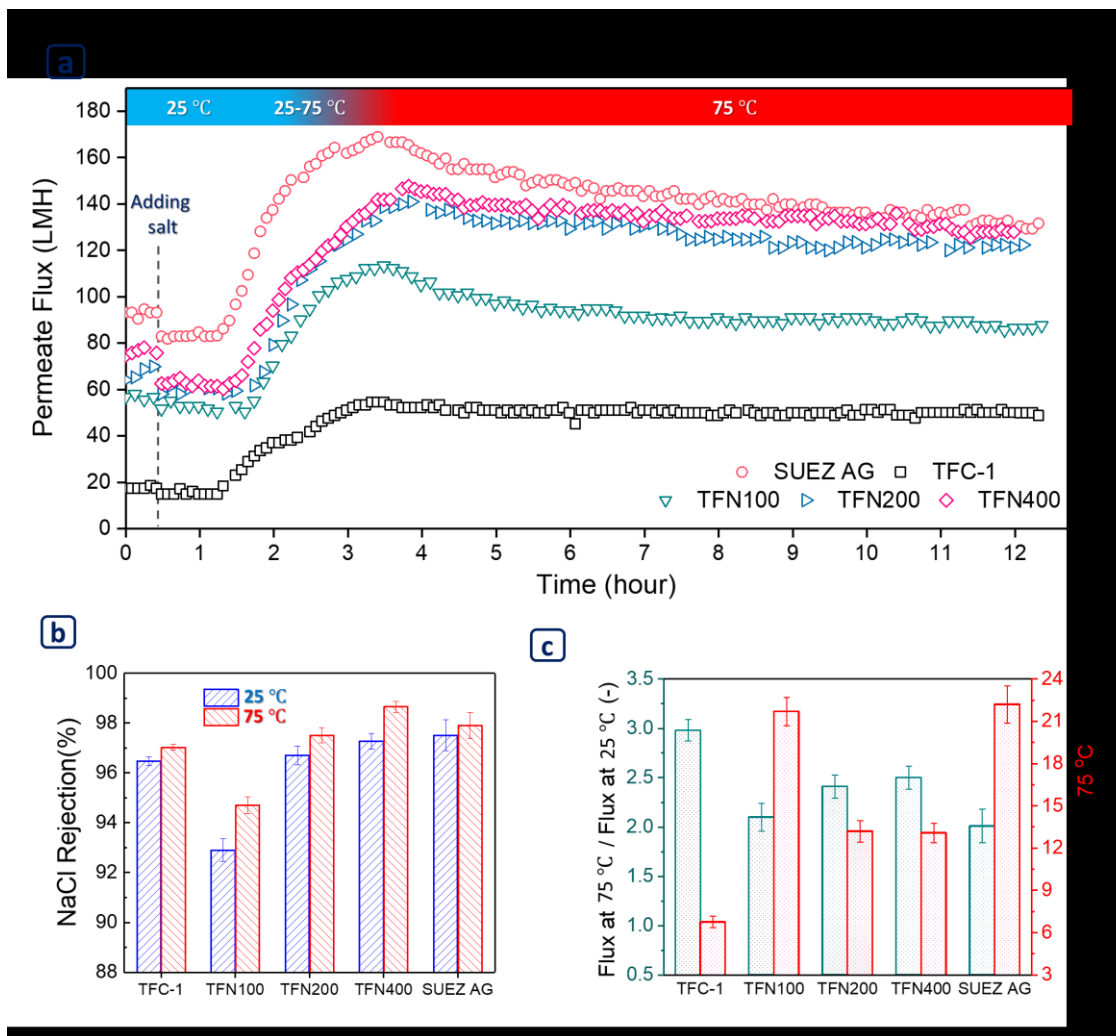


Figure 4-8: (a) Permeate flux of TFC-1, TFN membranes, and SUEZ AG. The filtration started with pure water, and 2000 ppm NaCl solution was added after 30 minutes. Afterward, the feed temperature was increased to 75 °C and kept constant for 9 hours. The transmembrane pressure and feed flow rate were set to 220 psi and 3 LPM during the filtration test. (b) NaCl rejection of the membranes at 25 °C and 75 °C. To obtain the salt rejection percentage at 75 °C, the sample was collected at the end of filtration, and the measurement of the conductivity was conducted the next day when the sample cooled down to room temperature. (c) Permeate flux ratio between 25 °C and 75 °C. The flux at 75 °C was the initial recorded data at high temperature (t=3 hours). The flux decline was calculated at 75 °C for 9 hours (t=3-12 hours).

Figure 4-8c presents further quantification of the response of the membranes to thermal stresses. The left axis shows the ratio of water flux at 75 °C to the water flux at 25 °C, and the

right-axis provides the flux decline over the continuous operation at 75 °C. It can be concluded that a membrane with a larger flux ratio provided a lower flux decline over the continuous operation. TFC-1 and SUEZ AG with the flux ratios of 3.02 and 2.01, respectively, showed the lowest and highest flux decline at 75 °C. A similar trend was observed for ND-modified TFN membranes where TFN400 with a higher flux ratio showed a lower flux decline compared to TFN100. The primary reason for this observation may be the structural variation of the polyamide layer due to thermal stresses over the temperature transition. Therefore, the membranes which were more prone to voids compaction exhibited lower flux ratio during temperature transition up to 75 °C, and larger flux decline after that.

4.2 Nanodiamond-Decorated TFC membranes with antifouling and antibacterial properties

4.2.1 Introduction

Significant changes in water consumption patterns, population growth, climate, and urbanization have exacerbated the environmental stresses on available freshwater resources [204,205]. In 2020, the United Nations World Water Development Report (UN WWDR) stated that global water consumption is increasing at a rate of 1% per year, forecasting a 20 to 30% rise by 2050 compared to the current level of water usage [206]. The global need for a safe and clean water supply has urged many countries to explore more efficient water treatment, recycle, and reuse solutions. Among water treatment processes, membrane technology has come under the spotlight as a single-step energy-efficient method to desalinate and treat wastewater. Membrane technology offers several attractive features such as portability, high-quality end-product, environmental friendliness, and low operating expenses [165,207,208].

Osmotically driven membrane processes rely on osmotic pressure differences across a membrane for water recovery. In the forward osmosis (FO) process, the water is drawn from a dilute feed solution with lower osmotic pressure to a concentrated draw solution with higher osmotic pressure [209,210]. Polyamide thin-film composite (TFC) membranes are the most popular FO membranes due to high water fluxes, low salt passages, and high mechanical stabilities. The high permeability of TFC membranes is attributed to their thin (50-200 nm) polyamide selective layer, which is formed on a microporous substrate [36]. One of the main obstacles to the

use of FO TFC membranes in wastewater treatment is fouling caused by the deposition/attachment of colloidal particles, organic matter, and solute macromolecules onto the membrane surface. Fouling reduces the performance and lifetime of forward osmosis TFC membranes, hindering their widespread applications for wastewater reclamation [211–213].

Most surface modification methods employed to reduce the fouling of polyamide membranes rely on physical coating or chemical grafting of functional materials on the membrane surface to change its hydrophilicity, surface charge, and roughness [214–218]. The physical coating method, while being versatile, inexpensive, and adaptable to many substrates, suffers from the weak attachment of coatings to the membrane surface and from leaching during cross-flow filtration. The need to make more durable coatings has drawn attention to chemical grafting methods. In this method, hydrophilic macromolecules are either *grafted to* or *grafted from* the membrane surface. The first method refers to tethering hydrophilic polymers to the membrane surface, while the latter to growing polymer chains from the surface. In either method, the need for post-treatment steps, such as plasma or UV treatment, to ensure grafting, as well as the potential danger of releasing grafted materials to the environment, raises concerns about the cost, scalability, and environmental friendliness of these approaches.

Recently, multiple investigations reported an efficient technique to modify the surface of the polyamide layer without post-fabrication treatments [111,219–221]. In the *chemically induced grafting*, the unreacted dangling acyl chloride (COCl) functional groups that remain from the polyamide polymerization step are modified via nucleophilic substitution reaction with amine-terminated modifiers. Lu et al. [219] modified the polyamide surface with an amine-terminated polyethylene glycol derivative (Jeffamine) to make TFC membranes harder to foul with organic compounds. The Jeffamine-modified membranes had a significantly lower flux decline than the pristine membrane in filtering an alginate solution. The antifouling properties were ascribed to low membrane/foulant interactions, and to higher hydrophilicity of amine-modified TFC membranes.

Inorganic nanoparticles are usually unsuitable for coating polyamide because they are incompatible with the membrane surface and tend to agglomerate during the coating process [222]. Yin et al. [220] coated the surface of a polyamide TFC membrane with silver nanoparticles by first reacting the polyamide layer with $\text{NH}_2\text{-(CH}_2\text{)}_2\text{-SH}$ (cysteamine), then by attaching antibacterial silver nanoparticles over the polyamide layer by Ag-S chemical bonding. The affinity of surface

chemistry between the nanoparticles and the membrane is a critical prerequisite to translate the properties of inorganic nanoparticles to the antifouling properties of polymeric membranes.

This study aims to graft amine-functionalized ND particles to the untreated surface of polyamide membranes to enhance the antifouling and antibacterial properties. ND nanoparticle has a crystalline diamond structure and a heterogeneous graphitic shell. The surface characteristics of the ND particles in terms of available functional groups, such as carbonyls, carboxyls, phenols, pyrones, and sulfonic acids, determine their colloidal properties, surface charge, and intermolecular interactions with the host medium. The presence of oxygen-containing functional groups makes ND particles more hydrophilic. Moreover, the graphitic shell of ND particles, with sp^2 hybridization of carbon atoms, provides tunable surface chemistry for further functionalization [176,203,223–225]. In addition, their low toxicity, high chemical stability, and antibacterial properties make ND particles interesting for a broad range of applications [153,171,174,175]. ND is also a noncytotoxic antibacterial agent that interferes with biofilm formation [226]. Etemadi et al. [178] showed that amine-functionalized ND and polyethylene glycol-functionalized ND increased the antibacterial and biofilm-disrupting activity of cellulose acetate membranes by reducing the filamentous bacteria/membrane adhesion. Recently, our group developed high-performance thin film nanocomposite membranes through incorporating ND particles *within* the selective layer [153]. The ND particles showed excellent compatibility with the polymeric matrix during the polymerization. ND particles increased water permeability during filtration with a stable separation performance.

In this work, we showed how TFC membranes could be made more resistant to fouling by grafting ND particles onto the polyamide selective layer. We also proposed a facile method to fabricate ND-modified TFC membranes. The ND particles were first functionalized with ethylenediamine (EDA) to provide adequate surface chemistry for membrane functionalization. Then, the amine-functionalized ND particles were grafted to freshly synthesized polyamide TFC membranes by reacting them with the unreacted acyl chloride functional groups on their surfaces. The membranes' fouling resistance was assessed with a series of forward osmosis filtrations. The enhanced fouling tolerance of the ND-coated TFCs was explained based on the surface chemical composition, wettability, and surface roughness.

4.2.2 Experimental methods

Surface functionalization of ND was carried out with EDA through carboxylation, chlorination, and amination. The carboxylic groups of the ND particles were converted to EDA-terminated functionalities through a wet chemical process (**Figure 4-9**). The details of the functionalizing procedure were presented in our previous publication [181]. An ultra-thin selective layer was fabricated over the porous PES support with a step-growth polymerization between MPD and TMC at the interface of DI water and n-heptane [166]. First, the PES substrate was soaked with the aqueous MPD solution containing 2 wt.% MPD, 1 wt.% TEA, and 0.2 wt.% SDS for 9 minutes. After removing the excess amine solution from the PES surface using a roller, a 0.4 wt.% TMC solution was poured on the substrate for 30 seconds reaction. The TFC membranes were then functionalized with amine-functionalized ND particles.

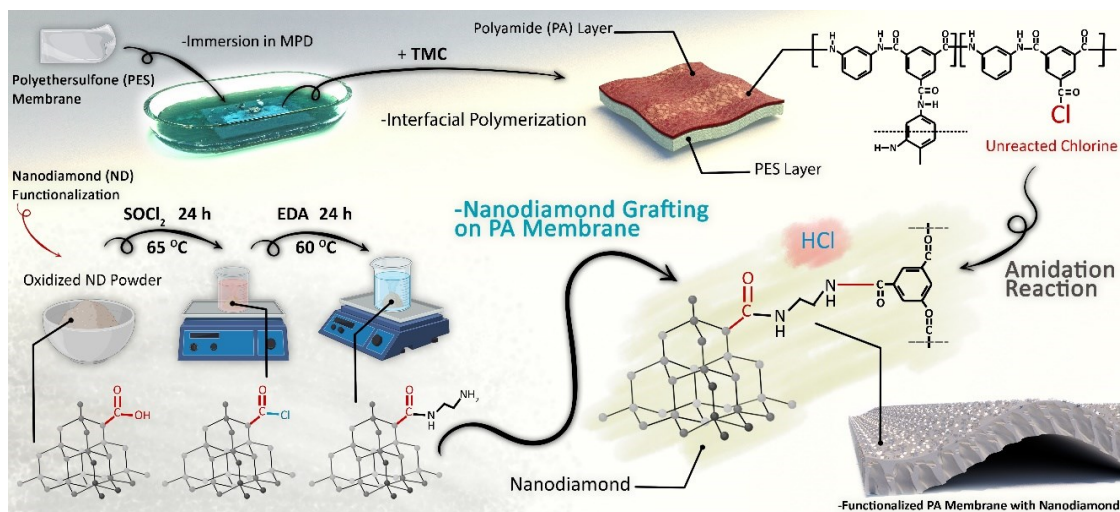


Figure 4-9: Schematic representation of interfacial polymerization, ND particle functionalization, and ND particle grafting over the polyamide surface. The ND particles were modified with EDA in order to provide a reactive surface with polyamide COCl groups. The surface of polyamide membrane was coated with ND particles through formation of amide linkages between ND-EDA particles and unreacted COCl groups.

Initially, a desired concentration of the ND-EDA powder (250, 500, and 1000 ppm) was loaded in 15 ml of ethanol, followed by sonication in a water bath for 10 minutes. After that, the ND-EDA dispersion was poured over the polyamide layer to allow the free amine groups of the ND-EDA particles to react with the acyl chloride groups of the polyamide surface. After 10 minutes, the membranes were rinsed two times with pure ethanol to remove the unreacted ND-EDA particles, and cured in an oven (Thermo Scientific Heratherm™, USA) at 60°C for 4 minutes. The membranes were stored in distilled water at room temperature.

The ND-modified membranes prepared with 250 ppm, 500 ppm, and 1000 ppm of ND-EDA were labeled TFC-250, TFC-500, and TFC-1000, respectively. To evaluate the effect of ethanol and functionalized ND particles, a pristine TFC membrane (TFC-0) and a control ethanol-modified TFC membrane (TFC-EtOH) were also fabricated. The TFC-EtOH membrane was made with a pure ethanol solution, following the same procedure used to make the ND surface-modified membranes. The chemical grafting of the TFC membranes with ND-EDA is illustrated in **Figure 4-9**.

4.2.3 Results and discussion

4.2.3.1 FTIR and TEM Analysis of ND Particles

Figure 4-10a shows the FTIR spectra of the ND, carboxylated ND, and EDA-modified ND (ND-EDA). ND-EDA particles show two peaks at 1530 cm^{-1} (C-N stretching and in-plane bending vibrations of the N-H bond in the amine groups) and 1670 cm^{-1} (C=O stretching vibration of the amide groups), indicating the presence of EDA modifier. The peak at 1670 cm^{-1} is shifted to the right due to the presence of electronegative nitrogen atoms [180,181]. The peak at 1740 cm^{-1} in ND-EDA and carboxylated ND particles is attributed to the free acid band of the carboxylic groups [126]. The TEM image of the ND particles in **Figure 4-10b** shows that they are spherical with diameters lower than 10 nm. The crystalline diamond core and the graphitic shell can be distinguished in the TEM image.

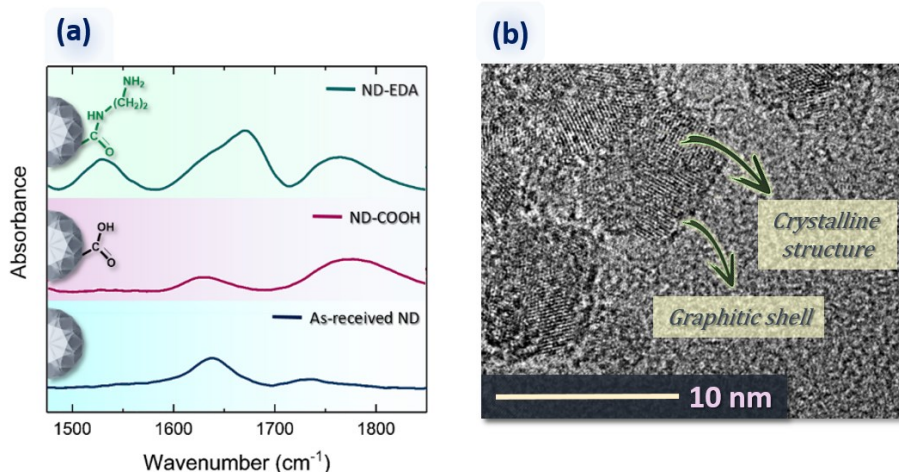


Figure 4-10: (a) FTIR spectra of pristine ND, carboxylated ND, and ND-EDA particles and (b) TEM image of nanoparticles. The spherical shape of ND particles represents both diamond core and graphitic shell structures.

4.2.3.2 FTIR and XPS results of fabricated TFC membranes

Figure 4-11a compares the FTIR spectra of the PES, TFC-0, TFC-EtOH, and ND-modified TFC membranes. The polyamide peaks at 1660 cm^{-1} ($\text{C}=\text{O}$ stretching of amide I), 1610 cm^{-1} (aromatic amide ring stretching), and 1540 cm^{-1} ($\text{C}-\text{N}$ stretching/ $\text{N}-\text{H}$ in-plane bending of amide II) in TFC membranes confirms the formation of polyamide over the PES substrate [36,115,227–229]. The intensity of the polyamide peaks increases as the concentration of the nanoparticles increase, which is related to the formation of amide linkages between amine-terminated ND particles and the COCl groups in the polyamide layer. **Figure 4-11b** is a schematic depicting the polyamide membranes before and after ND functionalization.

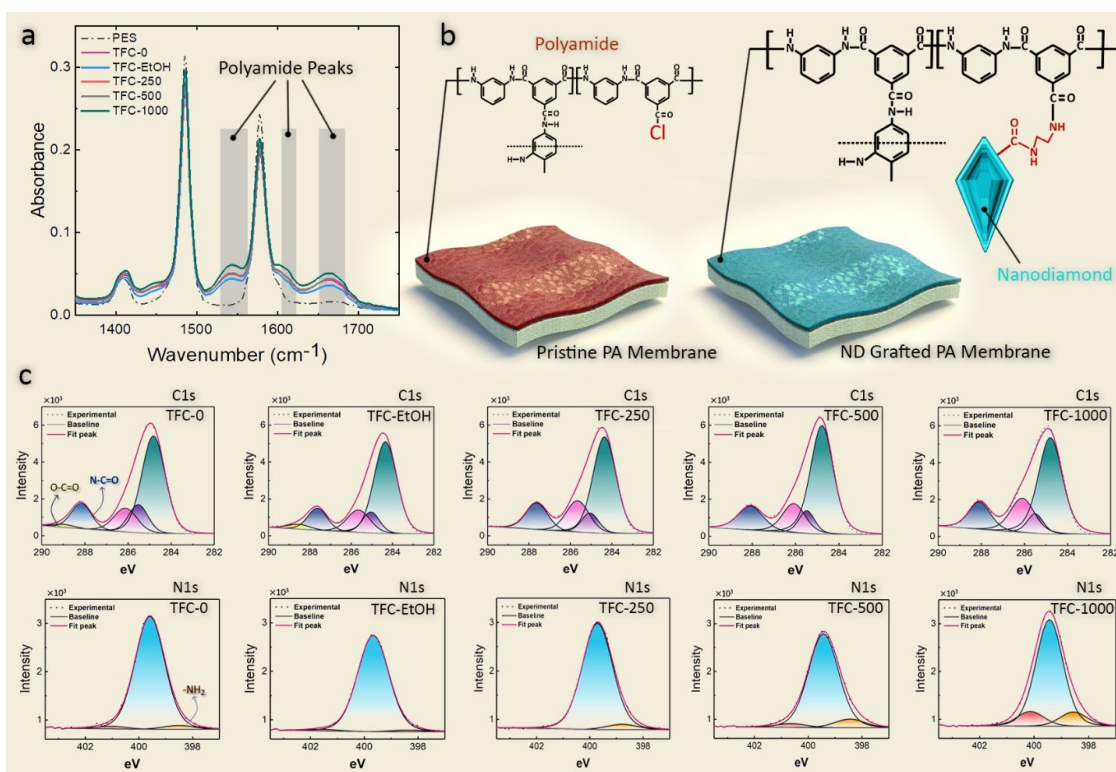


Figure 4-11: (a) FTIR spectra of PES and fabricated membranes, (b) schematic of TFC membranes before and after ND grafting, and (c) deconvoluted carbon and nitrogen XPS peaks of all synthesized membranes.

Figure 4-11c shows the XPS carbon (C 1s) and nitrogen (N 1s) spectra of the membranes. The functional group ratio of the deconvoluted C 1s and N 1s peaks is summarized in **Table 4-2**. The C 1s peak comprises peaks of C-H/C-C at 285 eV, C-COOH/C-CONH at 285.7 eV, CN- at 286.2 eV, N-C=O at 288.4 eV, and O-C=O at 288.5 eV. The N 1s peak comprises peaks of R-NH₂ at 398.5 eV, N-C=O at 400.5 eV, and $-\text{NH}_3^+$ at 402.1 eV [130,153,191]. Further explanation for

each peak is presented in our previous work [153]. The O-C=O peak area percentage, which correlates with the content of carboxylic groups, decreases as the ND concentration increases because of the reaction between aminated ND particles and unreacted COCl functional groups on the polyamide layer (the ND particles stop the hydrolysis of the COCl group by forming amide linkages). The O-C=O peak for TFC-1000 vanishes completely, indicating that nearly all COCl functional groups were consumed for the highest ND loading. Comparing the R-NH₂ peak in the N 1s species, the TFC-500 and TFC-1000 membranes had a substantially higher peak area percentage than the pristine TFC membrane, likely because of presence of free amine groups of the functionalized ND particles. These FTIR and XPS analyses indicate that the ND particles were covalently bonded to the membrane surface.

Table 4-2: Peak area percentages of deconvoluted carbon and nitrogen peaks.

Membrane	Functional group ratio (carbon) (%)					Functional group ratio (Nitrogen) (%)		
	C-H/C-C	C-COO/C- CON	CN-	N-C=O	O-C=O	R-NH ₂	N-C=O	-NH ₃ ⁺
TFC-0	57.43	13.76	14.08	12.94	1.81	2.18	94.53	3.28
TFC-EtOH	59.72	10.35	14.64	12.13	3.16	1.51	96.74	1.74
TFC-250	57.26	8.81	18.67	15.00	0.26	4.81	94.73	0.47
TFC-500	61.17	6.98	17.24	14.39	0.25	8.09	88.28	3.63
TFC-1000	56.98	7.73	20.36	14.96	0.00	10.45	78.96	10.86

4.2.3.3 Morphological evaluation of the synthesized M

Figure 4-12 compares the FESEM and TEM images of the PES, TFC-0, TFC-EtOH, and ND-modified membranes. The polyamide layers in the TFC-0 and TFC-EtOH membranes showed nodular features resulting from the heterogeneous MPD diffusion in interfacial polymerization [166,230]. Polyamide was also formed in the larger pores of the substrate. Since the monomer concentrations and polymerization conditions were the same for all membranes, the polyamide surface was similar for the TFC-0 and TFC-EtOH membranes. Attaching the ND particles to the membranes, however, changed their surface morphologies, especially for TFC-1000, which is covered with a layer of ND particles. It seems that the ND particles agglomerated on top of the initially attached ND layer, especially when higher ND loadings were used.

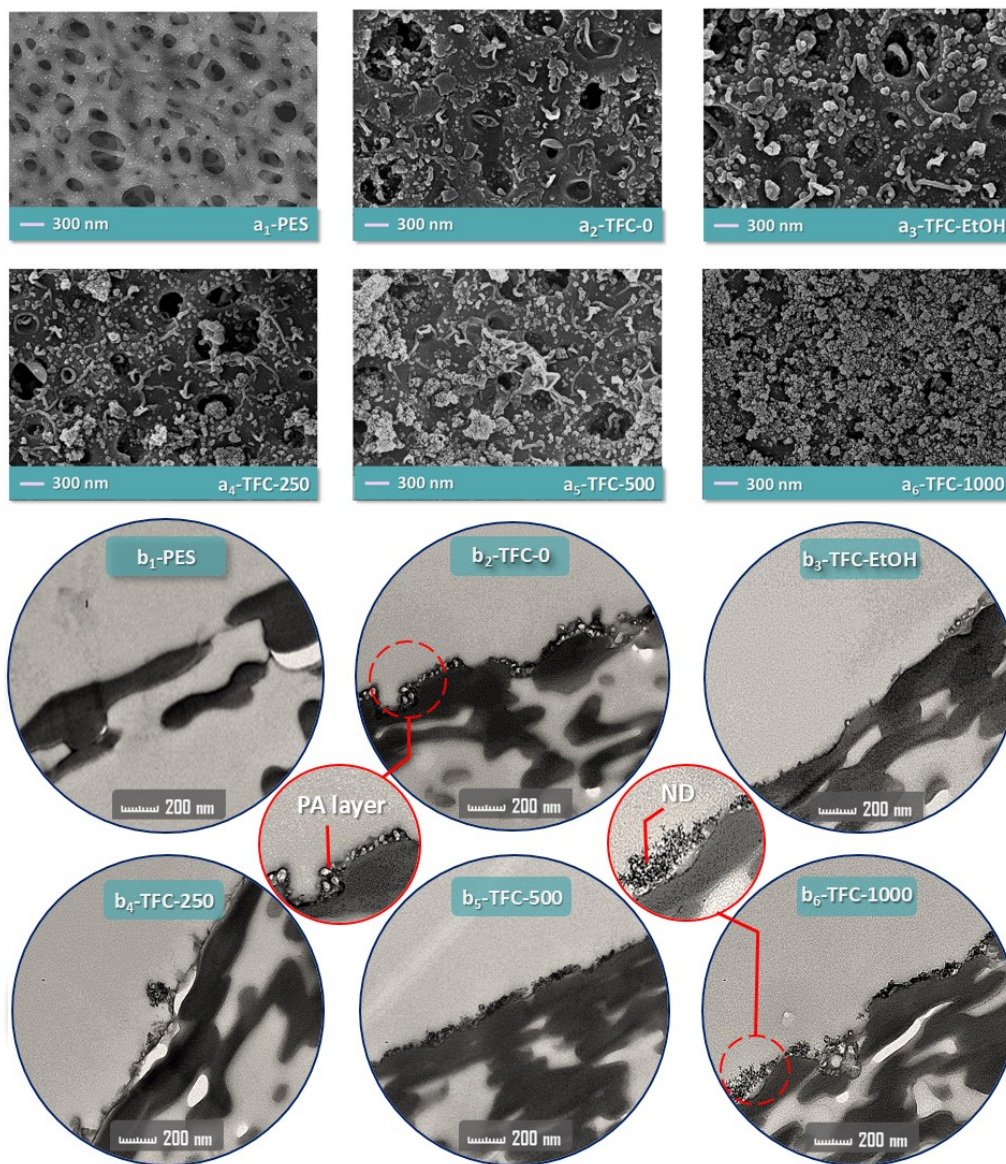


Figure 4-12: (a) Top surface FESEM and (b) cross-section TEM images of PES, TFC-0, TFC-EtOH, and ND-modified membranes. The membranes modified with ND particles show the presence of nanoparticles on the top surface, which become more distinguishable at higher ND loadings. The polyamide layer in panel b₂-TFC-0 represents the internal void structure which is mostly covered in the TEM images of ND-modified TFC membranes.

The cross-sectional TEM images reveal that the polyamide thickness in all TFC membranes are similar. The ND-modified TFC membranes, especially for higher ND loadings, revealed the nanoparticles over the membrane surface. The TFC-500 and TFC-1000 membranes showed high loading of NDs over the membrane surface, implying the deposition of multiple layers of ND particles on the initially covalently bonded ND particles. TEM images of all TFC membranes

showed that the polyamide layer formed continuously on the top surface and inside the pores of the PES support. It indicated that the visible pores on the surface of TFC-0, TFC-EtOH, and TFC-250 were filled with polyamide during the polymerization.

Figure 4-13 contrasts the 3D AFM surface topography, surface roughness (R_a and R_q), and water contact angle of the TFCs. The 3D AFM surface topographies show that the membranes have a ridge-and-valley surface structure [231]. The roughness data indicate that the ND layer smoothed the polyamide surface because the nanoparticles filled the “valleys” of the polyamide surface. The water contact angle results show that the surface wettability of the membranes increased when more ND particles were added to the polyamide surface. The water contact angle depends on the surface chemistry and on the morphology of the polyamide layer. Wenzel's model states that for a surface with a contact angle of less than 90° (a wettable surface), a rise in surface roughness should reduce the water contact angle [131]. Our contact angle results, however, show the lowest contact angle was measured for the smoothest membrane (TFC-1000). This observation highlights how the hydrophilicity of the nanoparticles increases the surface wettability of TFC membranes. The impact of chemical heterogeneities induced by hydrophilic function groups to the surface dominates the effect of physical heterogeneities.

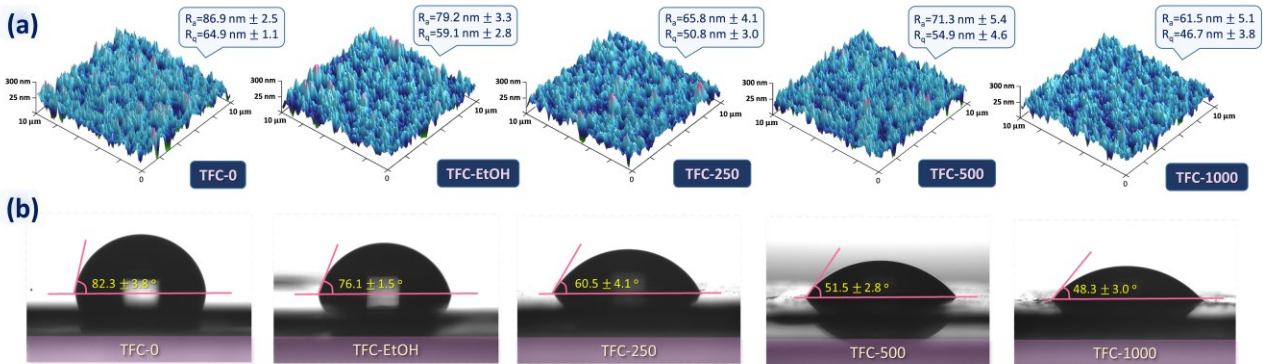


Figure 4-13: (a) 3D AFM images, R_a : average roughness, and R_q : root mean square roughness, (b) water contact angle of membranes. All the 3D AFM images are presented with a same z-axis aspect ratio to give a better visual comparison.

4.2.3.4 Transport performance of the membranes

Figure 4-14(a and b) shows the water flux of the TFC membranes at different draw solution concentrations in two different configurations: active layer facing feed solution (AL-FS) and active layer facing draw solution (AL-DS). In both configurations, the water flux increased with

increasing the draw solution concentration. It is due to the buildup of a larger osmotic driving force. However, the water flux increased non-linearly with a lower slope at higher NaCl concentrations, because Na^+ and Cl^- ions accumulated on the polyamide layer in the AL-DS configuration (external concentration polarization, ECP) and within the PES layer in the AL-FS configuration (internal concentration polarization, ICP), which reduced the effective osmotic pressure gradient across the membranes [232]. This effect intensified at higher concentrations of the draw solution. Furthermore, the water flux was higher in the AL-DS than in the AL-FS configuration, revealing the more significant effect of ICP in AL-FS compared to ECP in AL-DS on the effective osmotic driving force. The water fluxes through all ethanol-treated membranes (TFC-EtOH and ND-modified TFCs) were higher than in the pristine TFC-0 membrane. The water flux, however, decreased when the loading of ND particles increased. The higher water fluxes of the EtOH-treated membranes are likely a result of the plasticization of the polyamide layer by ethanol [233]. As the polyamide layer swells, the free volume in the polymeric structure increases, making it easier for water to permeate. In addition, ethanol can remove smaller polymer chains that were not bonded to the polyamide network during interfacial polymerization [220]. The reduction of the water flux for ND-coated TFCs, especially at higher loadings, can be related to the additional resistance of the ND layer against water permeation. The size of the covalently attached NDs and their agglomerates are presumably larger than the size of the water channels in the polyamide selective layer. Therefore, a likely explanation for the flux decline can be the additional transport resistance imposed by the ND layer.

Figure 4-14(c and d) compares the reverse salt flux and specific salt flux in both membrane configurations with a 2 M NaCl draw solution. The ethanol-treated TFC membranes (TFC-EtOH and ND-modified TFCs) exhibited higher reverse salt fluxes in both modes than the pristine TFC-0 membrane, which might be related to the swelling effect of alcohol on the selective layer. The TFC-250 and TFC-500 membranes had reverse salt fluxes similar to the TFC-EtOH membrane, showing that ND grafting did not affect salt separation substantially. Higher loadings of ND particles, however, improved salt selectivity: TFC-1000 had the lowest reverse salt flux among all ethanol-treated membranes.

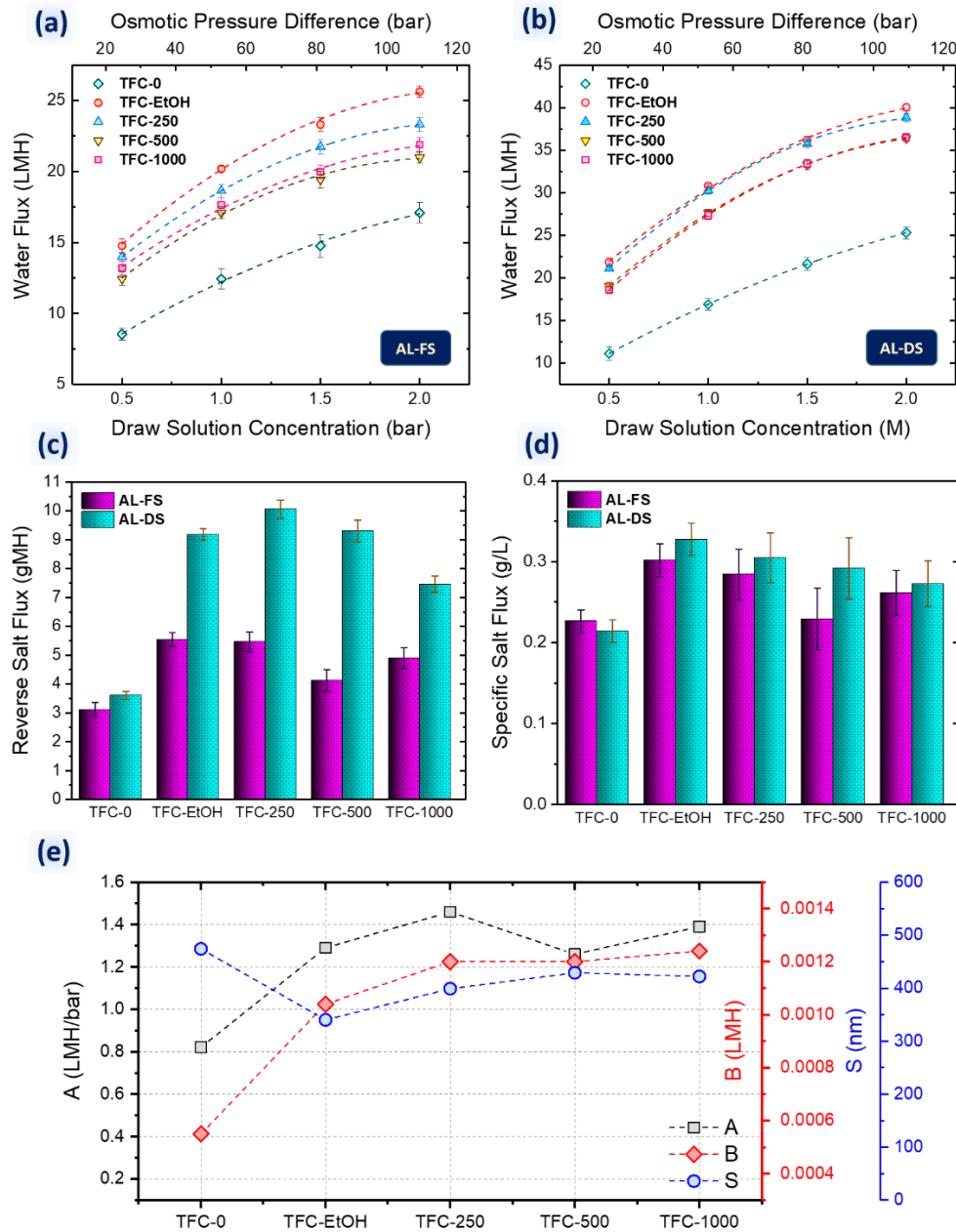


Figure 4-14: (a) Water flux in AL-FS configuration, (b) Water flux in AL-DS configuration, (c) reverse salt flux, (d) specific salt flux, and (e) transport parameters for TFC-0, TFC-EtOH, and ND-modified membranes. All the forward osmosis filtrations in AL-FS and AL-DS configurations were performed with 1 M NaCl draw solution and deionized water as the feed solution. The reported water flux in panel a and b is the flux at the beginning of the filtrations. The reverse salt flux is also calculated by measuring the NaCl concentration in feed solution during 2 hours filtration.

Figure 4-14e shows the transport parameters (A , B , and S) of the TFC membranes. The water and solute permeability parameters followed a trend similar to water flux and reverse salt flux in

which the ethanol-treated membranes had higher water permeation and lower salt selectivity. The structural parameter, S , is one of the important parameters of PES support. The lower structural parameter indicates less severe internal concentration polarization in the support layer of TFC membranes. Since similar PES supports were used to fabricate all TFC membranes, the structural parameter showed an average value of 412.8 nm with ± 43.8 nm variation.

4.2.3.5 Antifouling properties of ND-modified membranes

Figure 4-15(a and b) shows the water flux during the filtration in the AL-FS configuration for SA-CaCl₂ and BSA-CaCl₂ feed solutions. The flux of the TFC-0 and TFC-EtOH membranes declined substantially in the initial 30 minutes of filtration of the SA solution because the organic foulant was accumulated on the membrane. In contrast, the fluxes of the ND-modified membranes declined gradually over the fouling experiments and stabilized after 150 minutes. Moreover, the flux decline was lower for the TFC membranes with higher ND loadings: TFC-0 had the highest (42%) and TFC-1000 had the least (15%) flux declines of all membranes.

Figure 4-15b shows that the membranes experienced lower flux declines with the BSA solution, suggesting that the BSA foulant attaches less effectively onto the membrane surfaces. The TFC-0 and TFC-EtOH membranes had similar flux declines in the first 30 minutes, followed by a gradual decline until the end of the experiments. All the ND-modified membranes were more resistant to BSA fouling, with less than 11% flux decline in 180 minutes. **Figure 4-15c** illustrates that more alginate gel was formed over the membrane surface of the pristine membrane at the end of filtration with SA than with the TFC-1000 membrane.

The fouling mechanism of polyamide membranes can explain why the SA solution caused more fouling than the BSA solution. The presence of Ca²⁺ ions has a major impact on the fouling severity of these membranes because Ca²⁺ ions form cross-linked foulant networks through binding with the carboxylic groups of the foulants. Ca²⁺ ions can also link foulants and carboxylic groups of the polyamide layer (hydrolyzed COCl groups), forming an adhesive fouling layer. These Ca²⁺ attachments are known as Ca²⁺ bridging effect [234,235]. Therefore, the content of carboxylic groups in the foulant and on the polyamide layer can affect the extent of fouling. The BSA molecules have a much lower fraction of carboxylic groups than those of SA. Hence, fewer cross-linked structures form when the feed solution contains BSA and CaCl₂, leading to less fouling and lower flux decline. TFC membranes coated with nanoparticles had a lower flux decline, likely

because of the fewer carboxylic groups on the ND-modified polyamide layer. As shown by XPS analysis, the amine-functionalized ND particles consumed the COCl groups at the polyamide surface. Therefore, fewer COCl functional groups remained to be hydrolyzed and converted to COOH when rinsing with water. This led to the reduction of adhesion spots on the polyamide layer for Ca^{2+} to make bridges between the membrane and the foulant molecules. The existence of multiple carboxylic groups on the TFC-0 and TFC-EtOH membranes made them more prone to fouling with the foulants. In addition, the hydrophilic ND particles make a hydration layer, and therefore hinder the accumulation of hydrophobic SA and BSA foulants on the surface. Finally, A smoother polyamide film (based on roughness data) is expected to experience less fouling because it has fewer ridges and valleys where foulant molecules can be deposited [236].

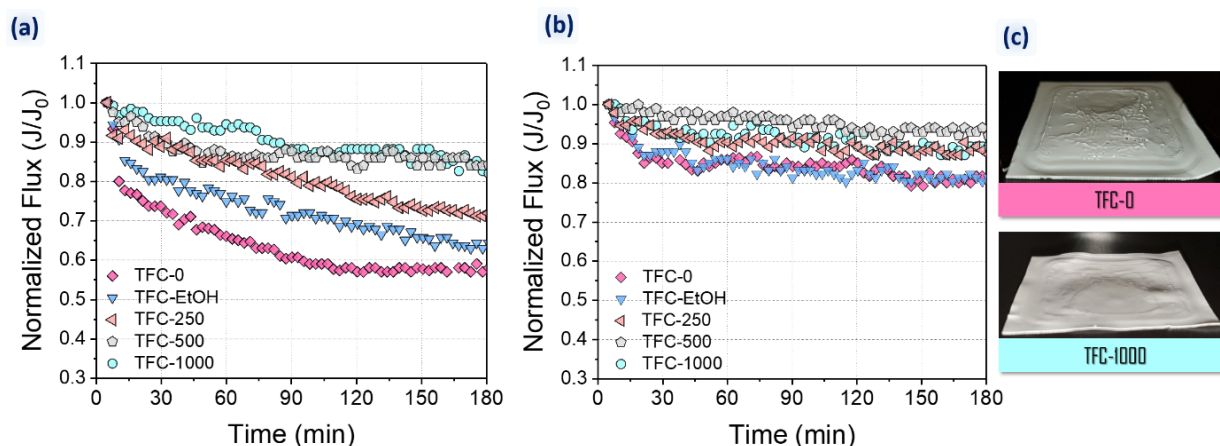


Figure 4-15: Water flux of synthesized membranes with (a) SA feed solution and (b) BSA feed solution, (c) formation of alginate gel on TFC-0 and TFC-1000 membranes after 180 minutes fouling experiment. The abrupt flux decline of TFC-0 in the initial 30 minutes of the filtration is an indication of alginate cake layer formation. Fouling experiments started with 18 ± 1 LMH water flux for all TFC membranes to exclude the effect of hydrodynamic flow condition on the fouling.

4.2.3.6 Stability of grafted ND particles

The release rate of ND particles is an indication of the stability and lifetime of the ND layer. **Figure 4-16** shows the leaching rate of ND particles, measured by the total organic carbon (TOC) over 16 days. On day 1, the release rate of pristine (TFC-0) and ND-modified membranes differed significantly. The release from the pristine membrane is caused by unreacted monomers and residual solvents. The release from the ND-modified TFC membranes is related to the detachment of ND particle agglomerates, unreacted monomers, and residual solvents. It seems that the number of loosely detached ND particles is higher than covalently attached ND particles as many

nanoparticles formed agglomerates over the initially attached layer by weak interactions. However, the leaching curves of all TFC membranes behaved similarly after day 4, suggesting that the ND particles remained on the surface after the loosely attached ND particles were released. The FESEM and TEM analyses showed that the agglomerated ND particles accumulated on top of the covalently-bonded ND layer. The ND agglomerates can be released from the membrane due to their weak interparticle electrostatic interaction, but not the covalently-bonded ND particles.

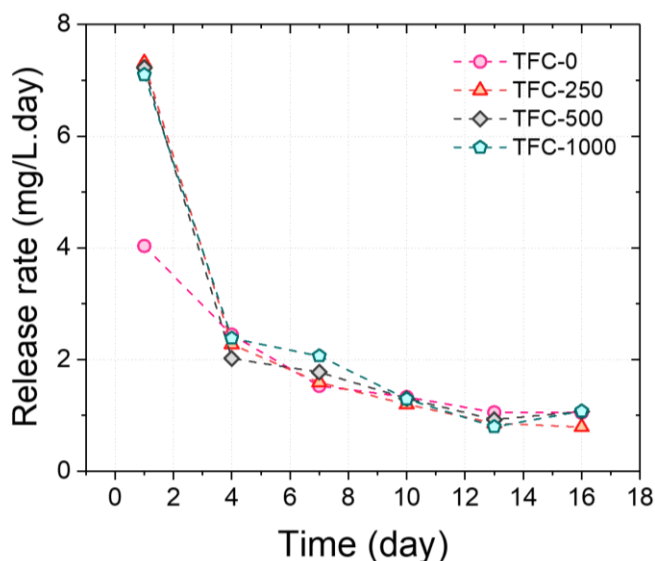


Figure 4-16: The release rate of ND particles, evaluated by total organic carbon, for the fabricated membranes. The samples were collected each three days for the analysis. The vials of the samples were refilled with pure water every day to report the release data daily.

4.2.3.7 Antibacterial activity of the ND membranes

Figure 4-17a shows a schematic of the colony plating and confocal microscopy tests. The membranes were first exposed to *E. coli* cultures for 3 hours, and then monitored through the colony plating (**Figure 4-17(b₁-b₆)**) and confocal microscopy (**Figure 4-17(c₁-c₆)**) analyses. *E. coli* was used as one of the common gram-negative bacteria for study of the efficiency of antibacterial agents [237,238]. Control samples were used to calculate the mortality rate of *E. coli* in contact with the membranes. The colony plating test showed that the TFC-1000, TFC-500, and TFC-250 membranes inactivated 63.7%, 59.7%, and 52.4% of the bacteria, respectively, while the TFC-0 and TFC-EtOH membranes inactivated only 1.3% and 14%, respectively. Confocal microscopy results confirmed these findings: The TFC-1000, TFC-500, and TFC-250 membranes

showed 52.1%, 51.9%, and 48.3% mortality rates, respectively, while the TFC-0 and TFC-EtOH membranes inhibited a negligible fraction of *E. coli*.

These results confirm that the ND particles significantly increased the bacterial inactivation rates of the membranes. ND had already been proven to be a promising antibacterial agent [239,240], and this finding was reflected in the performance of the TFC-1000, TFC-500, and TFC-250 membranes [241]. The colony plating and confocal analysis indicate that higher grafted nanoparticles increase the antibacterial activity of the membranes, but the small difference in inactivation rates between the TFC-1000 and TFC-500 membranes suggests that the membrane surface approaches saturation at this concentration range for inactivating bacteria.

The antibacterial activity of the membranes can be related to the remaining hydroxyl and carbonyl groups on the ND surface (see **Figure 4-9**), since they have been listed as strong antibacterial agents on ND particles by Wehling et al. [239]. These oxygen-containing groups may attach to the intracellular components of the bacteria or bind to their cell walls. This bondage inhibits vital proteins and enzymes, which leads to a rapid collapse of the bacterial metabolism and death [239]. Physical interactions among ND particles and bacteria can be another mechanism for *E. coli* death, as Chatterjee et al. [242] showed in their study. They also mentioned that the interaction of ND with bacteria might be due to the highly reactive surface of ND particles. This increases the chance for a physical hit to the bacterial outer membrane, and eventually causes death.

Disc inhibition zone tests (**Figure 4-17(d₁-d₆)**) demonstrate the antibacterial behavior of the modified TFCs. Inhibition zones form when ions or other antibacterial agents can move away from the membrane by diffusion [243–246]. None of the membranes (black circles in panels d₂-d₆) showed any inhibition zone surrounding them (in the perimeter of the membranes). This supports the idea that the ND particles are strongly bonded over the polyamide layer. The bondage of nanoparticles to the membrane surface affects the long-term activity of polymeric membranes, especially for anti-biofouling studies. Based on the antibacterial activity of the membranes, it can be concluded that not only functionalization of membranes with ND particles increase the antibacterial activity of the membrane but may also guarantee their long-term performance in the presence of bacteria.

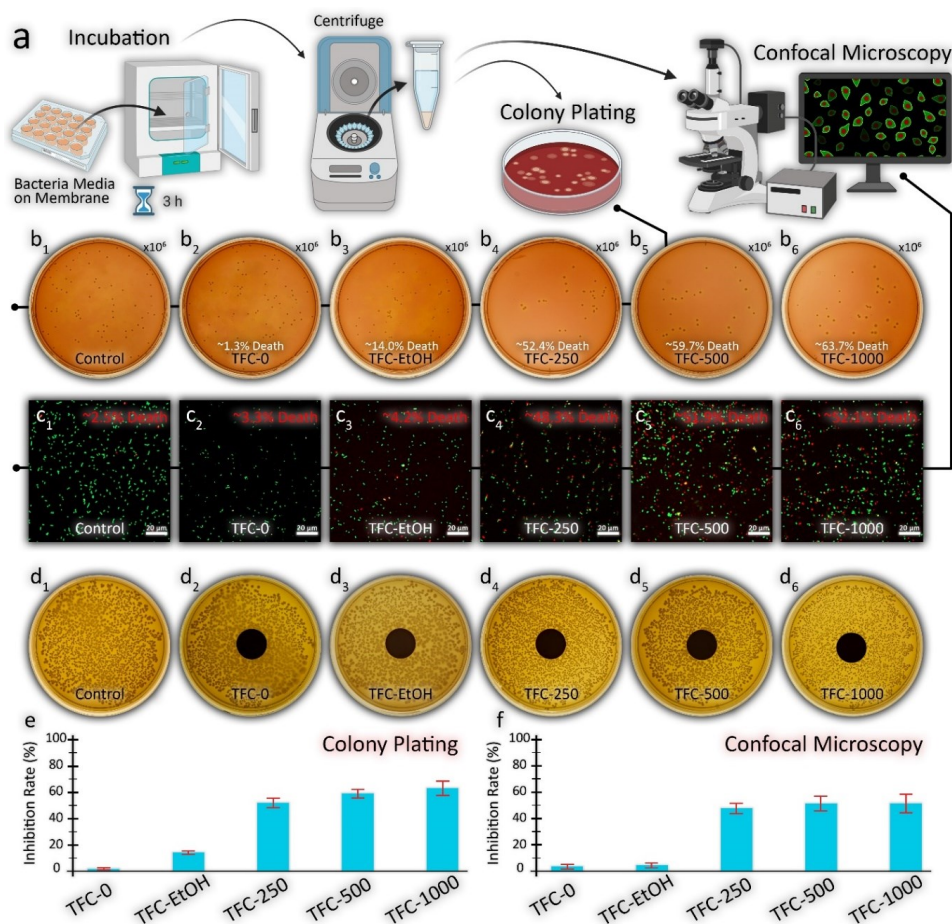


Figure 4-17: The antibacterial assessment of the ND membranes. (a) schematic illustration of colony plating and confocal microscopy tests preparation steps, (b1-b6) colony plating test of the membranes. The Solution for these plates has been 10⁻⁶ diluted. (c1-c6) confocal microscopy test of the membranes (green and red areas represent the live and dead bacteria, respectively). The mortality rate is the ratio of the red area to the total red and green area calculated using ImageJ software, and (d1-d6) inhibition zone test of the membranes (black circles (d2-d6) are the membrane samples). Bacteria inhibition rates of the membranes in (e) colony plating and (f) confocal microscopy tests.

4.3 Conclusion

In this study, we showed how the unique features of ND particles can be exploited for enhancing permeability, thermal stability, antifouling, and antibacterial properties.

First, we incorporated surface-functionalized ND particles into the polyamide layer of TFN membranes for the first time. FTIR and TG analysis indicated the successful functionalization of ND particles with MPD. Ethyl acetate was used as the co-solvent of the organic TMC solution to facilitate the dispersion of ND particles in the polyamide matrix. FTIR and morphological characterization of the synthesized membranes highlighted the significant effect of ethyl acetate on the formation of a thicker polyamide layer. The synergetic effects of ethyl acetate and ND

particles dramatically improved the membrane permeation and broke the trade-off between permeability and salt rejection. The improvement in the permselectivity of TFN membranes increased with the incorporation of more NDs into the polyamide matrix. With an increase of ND particles concentration from 100 to 400 ppm, water flux and NaCl rejection improved 22.8% and 4.4%, respectively. The addition of diaminated ND particles also contributed to the stability and integrity of the polyamide network at elevated temperature through increasing the cross-linking density as well as the heat dissipation effect. In the second phase of the work, a series of ND-modified TFC membranes were synthesized by covalently bonding amine-functionalized ND particles to polyamide layers to explore whether the ND particles formed an antifouling and antibacterial layer. Ethylenediamine was used as the surface modifier to improve the affinity between the functional groups of ND particles and the polyamide. The ND particles reduced fouling of the TFC membranes with SA and BSA organic foulants by decreasing the electrostatic and hydrophobic foulant/membrane interactions, and by reducing the membrane roughness. The ND particles also imparted antibacterial activity to the membranes by killing *E. coli* bacteria cells.

Chapter 5

High-temperature cross-flow filtrations of commercial reverse osmosis membranes: guidelines for characterization[§]

[§] This chapter was prepared based on a manuscript entitled as “High-Temperature Cross-flow Filtrations of Commercial Reverse Osmosis Membranes: Guidelines for Characterization” submitted to the Canadian Journal of Chemical Engineering

5.1 Introduction

Many industries produce massive volumes of contaminated water at high temperatures, which must be treated, recycled, and reused. Seasonal and daily temperature fluctuations may also affect the temperature of the water flowing to the treatment facilities [165,247]. For example, in the province of Alberta in Canada, in-situ oil extraction processes produce highly contaminated water at high temperatures. Steam-assisted gravity drainage (SAGD), as the front-runner technology for oil extraction in Alberta, consumes 2-3 barrels of water to extract one barrel of oil. Most water treatment technologies perform optimally at room temperature [114,248]. In the case of membrane filtration, the low thermal stability of most commercial polymeric membranes is their main limiting factor. Therefore, the hot wastewater must be cooled down before being treated by a membrane filtration process, which increases capital and operating costs when dealing with hot streams [249,250]. Consequently, there is a growing demand for the development of water treatment techniques that operate at high temperatures and, thus, improve heat integration of the overall process. From the viewpoint of cost and energy savings, it is often essential for the membrane to be operated at the highest allowable temperature.

Polyamide thin-film composites (TFC) are the industry-standard multilayer structure of RO and nanofiltration membranes. They are widely used in different separation applications such as municipal and industrial wastewater reclamation or seawater desalination [21,106,251]. TFC membranes are commonly developed by coating an ultrathin crosslinked polyamide layer on the top of a microporous support [38,150]. The nanoscale polyamide layer is formed via an interfacial polymerization between a diamine-containing monomer (such as m-phenylenediamine) and a triacyl chloride monomer (such as trimesoyl chloride). The three functional groups on the trimesoyl chloride molecules form the 3-dimensional crosslinked polyamide network needed for high salt rejection from water. Any change in monomer type, interfacial reaction time, or peripheral conditions may largely impact the final film characteristics [40,211].

Most commercial polymeric TFC membranes are recommended to be used below 45 °C. The unfavorable separation performance, and in an extreme scenario the catastrophic failure, of TFC membranes when the feed solution temperature exceeds 45 °C restricts their direct use in the effective treatment of streams like hot condensates, boiler-water blowdowns, textile and sugar effluents, laundry wastewater, annealing baths, high-temperature mining wastewater, and water

produced in the oil and gas industries [165]. In some food industries, water streams must be kept at an elevated temperature (up to 90°C) to prevent biological contamination [252]. In pharmaceutical processes, the membranes should be exposed to high-temperature (up to 95°C) water streams for sanitization purposes. This operation is mostly done at hydraulic pressures as low as 60 psi for several hours. In some industries, the saturation of aqueous solutions with different salts requires keeping the unit at high temperatures; otherwise, the solubility limit of critical compounds may be reached. In the SAGD process, the produced water temperature is as high as ~150 °C and a large amount of energy is wasted to cool down the water from this temperature to below 70 °C (or lower) for water treatment, and then heating it again up to ~220 °C to produce steam [7].

It has been reported that increasing the process temperature is favorable for water recovery but deteriorates the separation performance of the membranes. Increasing the filtration temperature affects the membrane properties and the mobilities of solvents and solutes [253]. Some researchers investigated the effect of temperature on solute transport through nanofiltration membranes [254]. Nanofiltration polyamide membranes rejected less uncharged solutes at higher temperatures, which is justified by an increase in the pore radius of the membranes at elevated temperatures, leading to lower steric exclusion of the solute molecules. Roy et al. [253] studied the effect of temperature on monovalent and divalent ions transport in nanofiltration membranes. Solute transport through the membranes via three mechanisms—convection, molecular diffusion, and electromigration—was found to increase at higher temperatures. Higher temperatures also reduced the dielectric exclusion of solutes because the pore dielectric constant at elevated temperatures decreases. The authors concluded that higher solute transport at elevated temperatures could be due to a change in membrane properties (e.g., increased polymer chain mobility at higher temperatures), lower solvent viscosity (higher convection flow rates), and higher ion diffusivity. However, our recent studies on fabricating novel thermally stable RO membranes [106,153,255] showed that the NaCl rejection *increased* at higher temperatures. Such an opposite trend for NaCl rejection in RO membranes compared to nanofiltration membranes can be justified by the difference in solute transport mechanism through the dense polyamide layer of these two types of membranes. We attributed the increase in NaCl rejection with temperature primarily to the plasticizing effect of temperature on collapsing internal free volumes of the polyamide structure. Indeed, physical or chemical changes of polymeric materials with temperature should be

considered in justifying the performance of RO membranes at elevated temperatures. The thermal stability of a polymeric membrane depends strongly on polymer properties such as aromaticity, crosslinking degree, chain interactions, and stiffening functional groups [84,165]. Improving the crosslink density of the polyamide layer by using new monomers and fabrication of a fully aromatic polyamide structure have already been investigated [87,255]. Further studies showed that incorporating some inorganic fillers like TiO₂, carbon nanotubes (CNT), and ND particles could improve the thermal and mechanical characteristics of TFC membranes [102,109,152,153]. Nevertheless, the first step in designing state-of-the-art thermally stable RO membranes is to develop laboratory protocols for high-temperature testing similar to industrial RO operations.

This study aims to test three flat-sheet commercial RO membranes in a simulated SAGD operation environment at high temperatures (70-80 °C). The main objectives are to: (i) understand the thermal stability of available commercial RO membranes in the market, (ii) develop standard operating protocols to test RO membranes at high temperatures, (iii) and provide insights regarding the fabrication of thermally stable RO TFC membranes.

5.2 Results and discussion

5.2.1 High-temperature filtrations of flat-sheet membranes

5.2.1.1 Long-term performance of the membranes at high temperature

In this paper, we used AG, AK, and AD symbols to label these membranes (see **Figure 5-1**). The flat-sheet membranes were used for filtration after overnight soaking the coupon samples in isopropanol (IPA) and water solution with a volume ratio of 1:4.

Figure 5-2 compares the water flux and NaCl rejection of the commercial RO membranes in the temperature range of 25-75 °C. The performance of the membranes was also evaluated at 75 °C for 15 hours. The NaCl rejection was measured at 25 °C, at the beginning of high-temperature filtration at 75 °C, and at the end of the filtration. The flux of the membranes increased by increasing the temperature. The water flux reached the highest value with different rates. The AG and AD membranes showed the lowest and highest water flux ratios at 75 °C to the water flux at 25 °C, respectively. All RO membranes experienced flux decline during 15 hours of filtration at 75 °C. The AD membrane showed a 15.81 % flux decline at high temperature, indicating its high stability in a long-term operation. However, the brackish water membranes (AK and AG) showed

22.08 % and 27.58 % flux declines, respectively. We noticed that the membranes with a higher flux ratio in the transition zone (25-75 °C) had a lower flux decline at 75 °C after 15 hours of filtration. The NaCl rejection increased for all the membranes when the temperature increased.



Figure 5-1: Commercial polyamide TFC membranes used in this study. SUEZ AG and SUEZ AK are standard and low-pressure brackish water RO membranes, respectively. SUEZ AD is designed for delivering high NaCl rejection at seawater operating conditions.

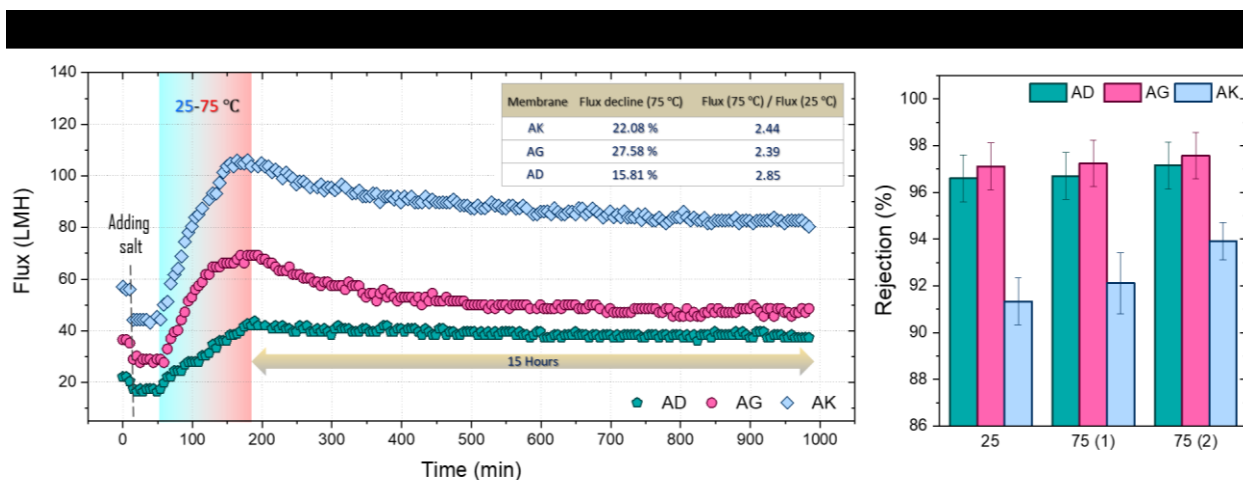


Figure 5-2: Water flux and NaCl rejection of the AK, AG, and AD membranes in a long-term (15 hours) filtration. The permeate samples at high temperature were collected and allowed to be cooled down to room temperature for conductivity measurement.

At higher temperatures, the diffusion rate of all feed solution components, including water molecules, through the membrane film increases. Besides, higher temperatures reduce the solvent viscosity and density, facilitating fast permeation through the membrane. These two phenomena increase the water flux during filtration in the temperature transition zone [100,255,256]. Furthermore, at high temperatures, the intensified segmental motions of the polymeric network allow the formation of more water channels inside the polyamide membranes [153]. The flux decline at high temperatures can be explained by the low thermal resistance of the polymeric

structure of the membranes. The plasticizing effect of the temperature on the membranes, subjected to a permanent hydraulic pressure, leads to the collapse of the internal voids of the membrane structure, and consequently, less free volume. The AD membrane, designed for seawater desalination (800 psi operating pressure), possesses a dense polyamide layer with low permeability. The rigid selective layer resisted better against thermal stresses at elevated temperature than brackish water membranes (AG and AK) with selective layers more prone to structural variations at high temperatures.

The increase in NaCl rejection at 75 °C might be attributed to the different impact of temperature on the diffusion of water molecules and NaCl ions at high temperatures. As the water permeation rate is faster than the salt passage at high temperatures, the rejection percentage increases, i.e., the quality of permeate water is improved when filtering hot feed streams [51]. Moreover, the compaction of the polymeric structure at elevated temperatures, which has a detrimental effect on water flux at 75 °C, improves the salt rejection of the membranes.

5.2.1.2 Cyclic tests

Figure 5-3 contrasts the water flux and NaCl rejection of the three RO TFC membranes in cyclic operations for three days. The performance of the membranes on day 1 resembled the long-term performance of the membranes in the initial 4 hours. However, on days 2 and 3, the flux decline at 75 °C decreased for all the membranes. This observation implies that high temperature had less market effect on the heat-treated membranes. Another indication of the more stable performance of the membranes in cycles 2 and 3 is the more linear flux increment in the temperature transition zones (25-75 °C). A linear trend of water flux during the temperature increment can be explained by the less structural variation of polyamide due to thermal stresses. It should be noted that the overall flux decline of the membranes in the three cycles is higher than that in long-term operation for 15 hours, indicating the deteriorating effect of temperature variations during cycles. The water flux of the membranes at 25 °C had a decreasing trend for all the membranes in three cycles as well. The NaCl rejection was measured at points 1-4, as shown in **Figure 5-3** (panel 1). The rejection for all the membranes increased at higher temperatures. However, NaCl rejection of AD membrane decreased in cycles 2 and 3.

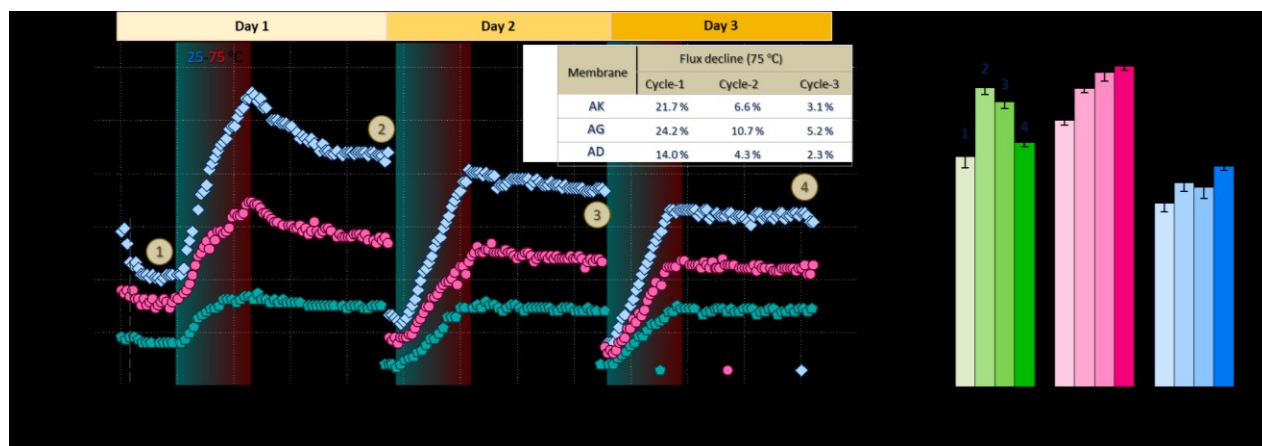


Figure 5-3: Water flux and salt rejections of cyclic operations of AK, AG, and AD membranes in three days. The flux decline of the membranes at 75 °C for each cycle was calculated and listed in a Table in the first panel. After finishing each cycle, the feed solution was cooled down slowly overnight.

5.2.1.3 Stepwise temperature increment

Figure 5-4 shows the water flux and NaCl rejection of the membranes in the range of 25-75 °C with 10 °C intervals.

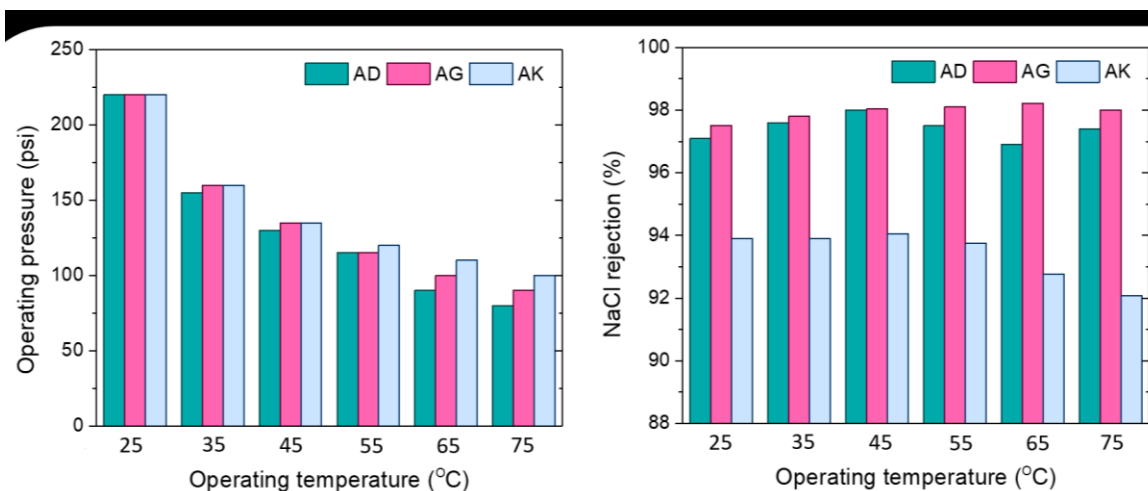


Figure 5-4: (a) The trans-membrane pressure of the membranes at different operating temperatures. The water flux was set to 35 LHM, 72 LMH, and 112 LMH for AD, AG, and AK membranes, respectively, and (b) NaCl rejection of the membranes at different temperatures.

The operating pressure was adjusted to deliver the same initial water flux at each temperature level. The initial flux for AD, AG, and AK was set to 35 LHM, 72 LMH, and 112 LMH, respectively. As can be observed in **Figure 5-4**, the operating pressure decreased by elevating the temperature. The NaCl rejections for AD and AG showed low variations by elevating the temperatures. However, the salt rejection of AK decreased at higher temperatures. This

observation is contrary to the obtained results in long-term performance and cyclic operations, in which the NaCl rejection increased at higher temperatures. By ruling out the effect of pressure on the membrane at higher temperature levels, the structural compaction of the polyamide is lower, leading to more consistent rejection results.

5.2.1.4 Permeability measurement of membranes at different temperatures

The pure water permeability of TFC RO membranes at different temperatures was measured by varying the transmembrane pressure. **Figure 5-5** depicts the water flux of AD and AG membranes at 150, 175, 200, and 225 psi in the temperature range of 25-75 °C. The slope of the curve at each temperature level is the permeability of the membranes, as illustrated in the left panel of **Figure 5-5**. The permeability of the membranes (flux normalized with the pressure) was increased at elevated temperatures for both AD and AG membranes, again emphasizing the impact of temperature increment water permeation through the membrane. This result highlights that high-temperature water filtration can be more beneficial from an energy and cost-saving perspective than room-temperature water filtration.

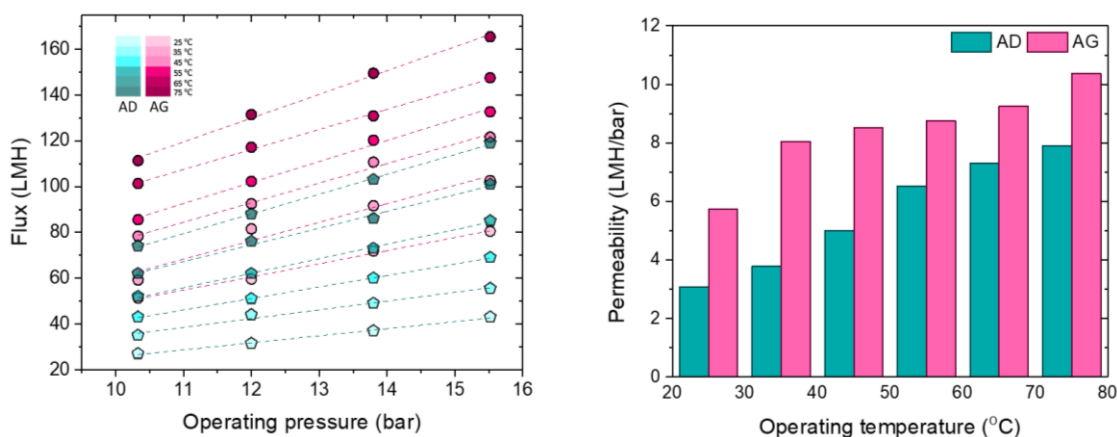


Figure 5-5: The water permeability of membranes at different temperatures. The permeability was reported by calculating the slope of flux/pressure curves.

5.2.2 The effect of temperature on the morphological characteristics of TFC membranes

Figure 5-6 shows the top surface FESEM and 3D topography AFM images of as-received membranes, the membranes after filtration at room temperature, and the membranes after filtrations at high temperature for 15 hours. **Table 5-1** summarizes the roughness data, including R_a (average roughness) and R_q (root mean square roughness).

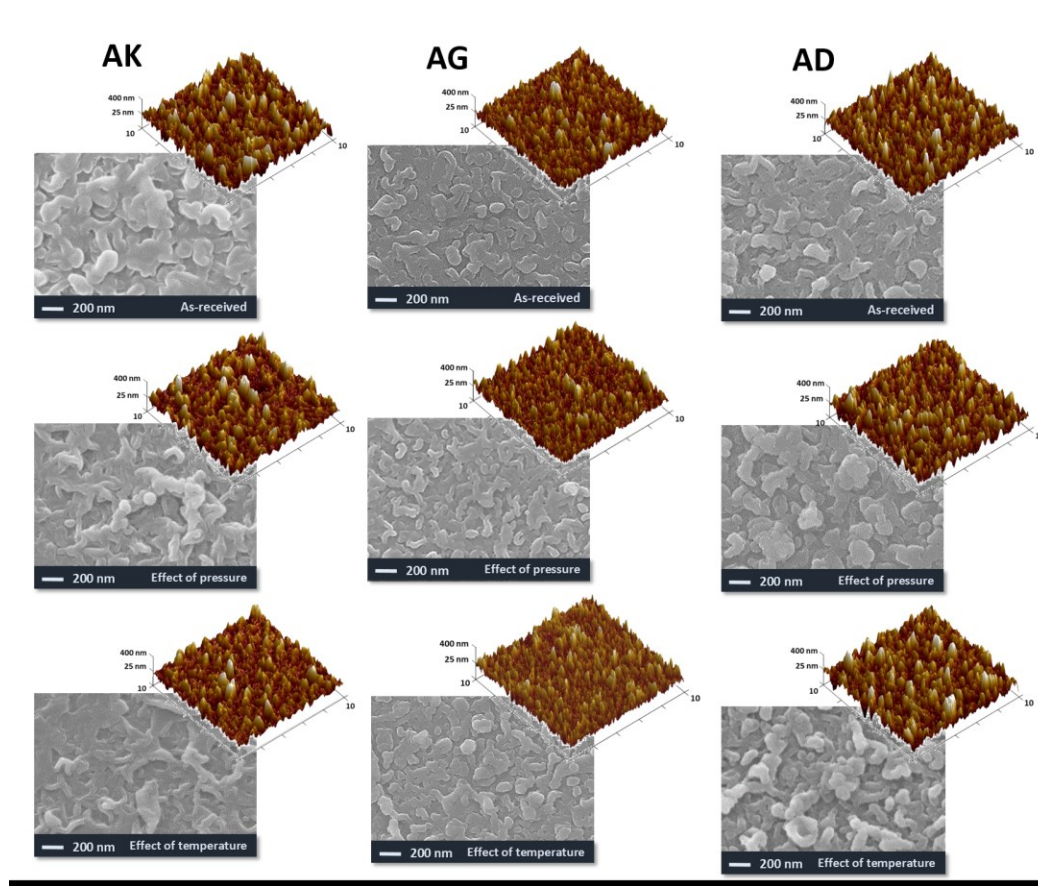


Figure 5-6: Top surface FESEM and 3D topography AFM images of AK, AG, and AD membranes.

As shown in **Figure 5-6**, all the images show the typical morphology of the polyamide layer: ridge-and-valley structure [41,257]. The morphology of the membranes was affected by the pressure and temperature. The AK membrane showed a smoother surface after filtration at room and high temperatures. However, the AG membrane had lower variation compared with the AK membrane. In contrast, the AD membrane revealed a rougher surface after filtration at elevated temperatures. This observation shows the different effects of temperature on the polyamide layer for AK, AG, and AD membranes.

Table 5-1: The roughness data including Ra: average roughness and Rq: root mean square roughness of AK, AG, and AD membranes

Membrane	R _a (nm)			R _q (nm)		
	As-received	Pressure-effect	Temp-effect	As-received	Pressure-effect	Temp-effect
AK	76.2	70.3	61.5	96.6	92.2	79.2
AG	59.9	57.7	58.5	76.5	73.5	73.1
AD	72.3	70	83.6	91.2	88.5	105.7

To further evaluate the effect of filtration temperature on morphology and thickness of the polyamide layer, the cross-sectional TEM images of RO membranes were taken before and after 15 hours of high-temperature filtration. **Figure 5-7** shows that the polyamide layer with a spongy structure containing internal voids completely covered the polysulfone (PSf) support. The internal voids in the polyamide layer are formed due to solvents' evaporation during interfacial polymerization [134,166]. With increasing the filtration temperature, AG and AK membranes experienced considerable compaction of selective layer after a long-term operation. AK membrane showed the highest structural compaction of the selective layer, while the AD membrane had almost the same thickness of polyamide before and after high-temperature filtration. This observation agrees with the long-term filtration results, in which AD membrane revealed lower flux decline compared with AG and AK membranes.

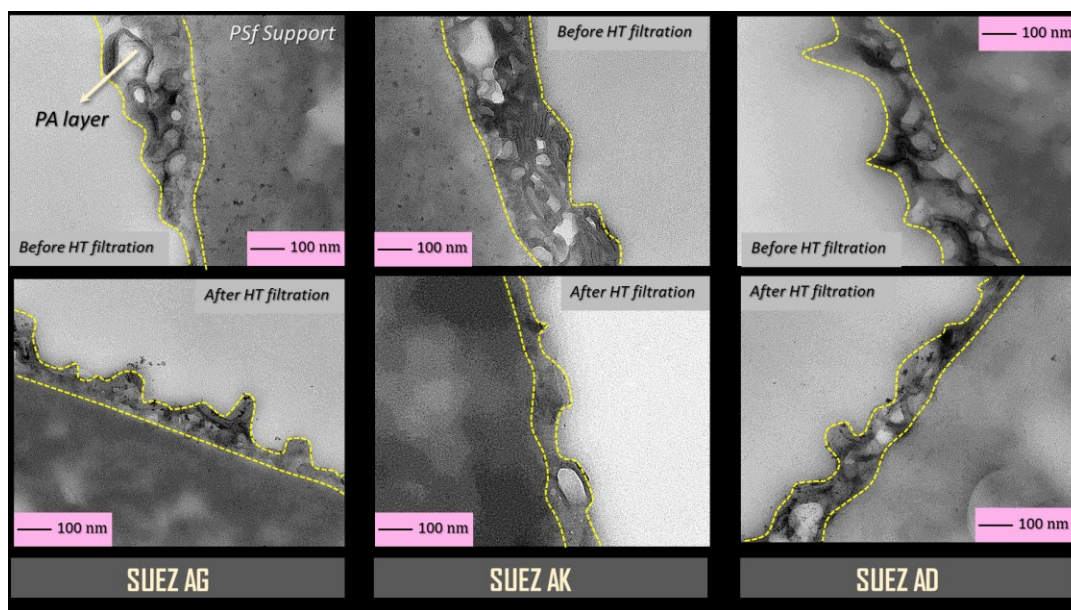


Figure 5-7: Cross-section TEM images of AG, AK, and AD membranes before and after high-temperature filtrations. The polyamide layer contrasts with PSf support by its spongy structure with internal voids.

5.2.3 The effect of temperature on the chemical composition of TFC membranes

Figure 5-8 illustrates the FTIR spectra of as-received membranes, the membranes after filtration at room temperature, and the membranes after filtrations at high temperature for 15 hours. In AK and AG membranes, two peaks at 3350 cm^{-1} and 1100 cm^{-1} were removed after room and high-temperature filtration, which can be attributed to the washing of the preservative materials

(glycerol) from the polyamide surface. The peaks at 3350 cm^{-1} and 1100 cm^{-1} correspond to O-H stretching and alcoholic C-O asymmetric stretching vibration of glycerol, respectively [258]. The intensity of the peaks was also reduced after filtration for AK and AG spectra. AD membrane exhibits the same spectra before and after high-temperature filtrations, showing high stability of the selective layer at high temperatures. From the FTIR analysis, it can be concluded that the temperature does not significantly affect the chemical composition of the polyamide layer.

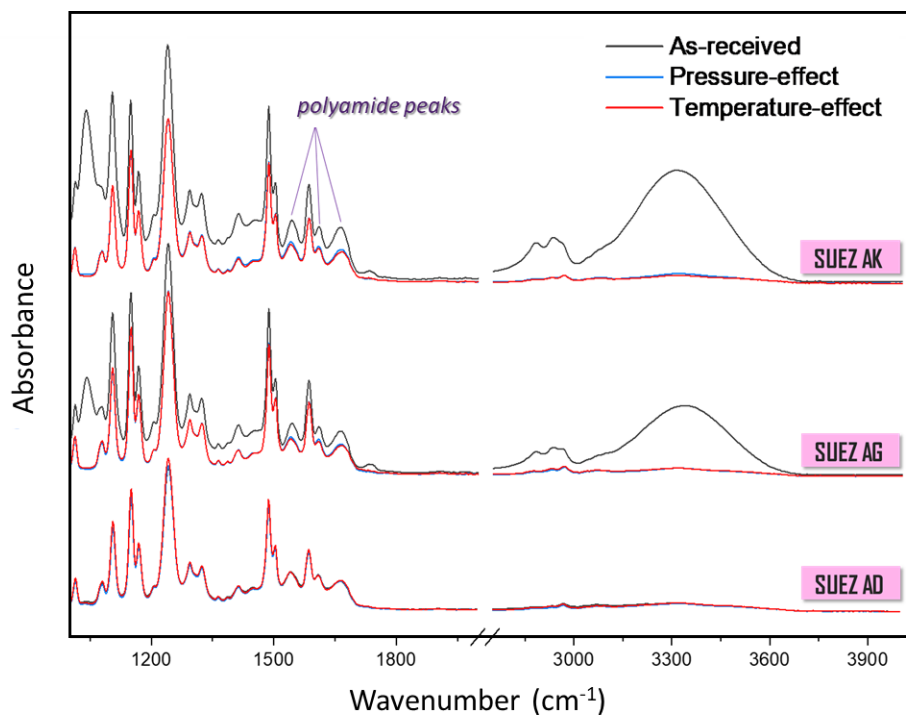


Figure 5-8: FTIR spectra of AG, AK, and AD membranes before and after room and high-temperature filtrations.

5.3 Conclusion

Employing currently available industry-standard RO membranes for industrial and commercial high-temperature applications is still a big challenge, suggesting a high demand for the development of thermally stable membranes by modifying the chemical and morphological structure of the polyamide layer. Understanding the contributing factors on separation performance at elevated temperatures as well as establishing standard protocols for high-temperature testing are critical prerequisites for developing novel thermally stable membranes. In this study, three commercial membranes were tested following four different high-temperature filtration methodologies. The results showed that the brackish water membranes (AG and AK) experienced

a higher flux decline during filtration at high temperatures. The AD membrane, a seawater desalination membrane, performed more stably at higher temperatures. However, fabricating highly permeable RO membranes (such as AG and AK) with robust polymeric selective layers and high thermal tolerance remains a challenge since available thermally stable membranes (such as AD), designed for specific applications, provide low water recovery.

Chapter 6

Conclusion and future work

6.1 Conclusion

The present thesis is a comprehensive study on the development of novel thin film composite (TFC) and thin film nanocomposite (TFN) membranes with improved water permeability and thermally stability. We provided insights on polymer material selection, characterization techniques, promising progresses, major challenges, and potential future trends.

In many industrial applications, the contaminated process water must be treated at high temperatures for the sustainability and energy efficiency of water recycling processes. Commercially available TFC membranes suffer from limited thermal resilience at temperatures above 45 °C, resulting in short working lifetimes. This limitation has motivated researchers to improve the thermal stability of TFC membranes through three primary approaches: (i) tuning the chemistry of the selective layer, (ii) enhancing the thermal properties of the porous sublayer, and (iii) incorporating nanomaterials into both the selective and support layers of TFC membranes.

Among different approaches, efforts on modifying the selective layer have gained momentum due to the critical role it plays on the overall separation performance. Synthesis parameters were modified to develop new polyamide layers with higher cross-linking degree and rigidity. Furthermore, employing other strategies, such as using novel sublayers or well-dispersed nanoparticles was also found to increase the separation performance and thermal tolerance of TFC membranes. Major challenges for the development of robust TFC and TFN membranes still remain: (i) how to overcome the trade-off between thermal stability and permselectivity of membranes, primarily caused by the low reactivity of new monomers with stabilized resonance structure and severe aggregation of nanoparticles, and (ii) how to develop reliable methods to characterize the individual layers of composite membranes.

First, we synthesized novel TFC reverse osmosis (RO) polyamide membranes by modifying the chemical structure of their selective layers. Triaminopyrimidine (TAP) was used to synthesize a polyamide selective layer with high cross-linking density over a microporous polyethersulfone (PES) support. The addition of TAP to the classic *m*-phenyldiamine (MPD)/trimesoyl chloride (TMC) combination improved the permeation of the membranes remarkably. All synthesized TFC membranes showed consistent permeate flux for 9 hours of operation at 75 °C with only a slight reduction in salt rejection. In the second phase of this work, we synthesized TAP-modified TFC

membranes on PES support. We also modified the support layer with a polydopamine (PDA)/graphene oxide (GO) interlayer to regulate the structure of polyamide layer during interfacial polymerization. TAP-modified membranes had higher permeability and thermal stability at 65 °C compared to a free-TAP TFC membrane.

In the second part of this thesis, we reported a design strategy for the development of thermally-stable RO thin film TFN membranes embedded with nanodiamond (ND) particles. The surface of ND particles was first functionalized by MPD. Then ND-MPD particles were dispersed into a TMC organic solution. To improve the dispersion state of ND particles, ethyl acetate, as a polar co-solvent, was added to the organic solution. The polyamide composite layer containing different loadings of ND particles were synthesized through interfacial polymerization. The chemical characterization of functionalized ND proved the successful amination of nanoparticles with MPD. The reactive functional groups and the hydrophilic surface of NDs intensified the interactions of nanoparticles with the polymer matrix and enhanced the surface wettability of the TFN membranes. The contact angle measurement showed a maximum decrease from 88.4° for the pristine membrane to 58.3° for the TFN membrane fabricated with 400 ppm ND particles. The addition of ND particles and ethyl acetate created larger surface features on the polyamide surface of TFN membranes. The average roughness of the membranes increased from 108.4 nm to 107.5 nm for the pristine and TFN membranes, respectively. The ND-modified TFN membranes showed higher water flux (up to 76.5 LMH) compared to pristine membrane (17 LMH) at ambient temperature. The TFN membrane with highest loading of ND particles overcame the trade-off relation between water flux and NaCl rejection with 76.5 LMH and 97.3%. Furthermore, the TFN membrane prepared with 400 ppm MPD functionalized ND particles exhibited the lowest flux decline (13%) over a 9 hours filtration test at elevated temperature (75 °C) compared with other TFN membranes.

TFC membranes could also benefit from outstanding structural properties of ND particles to be more hydrophilic and fouling resistant at the surface. We reported an effective and scalable method to reduce the fouling of polyamide TFC membranes by grafting amine-functionalized ND particles. The surface chemistry of ND was modified to improve the compatibility of nanoparticles with the polyamide membranes. Fouling experiments with sodium alginate (SA) and bovine serum albumin (BSA) showed that the ND layer substantially reduced fouling of the membranes. The flux of the ND-modified membrane made with a solution containing 1000 ppm ND particles

declined only by 15% (SA) and 9% (BSA) after 180 minutes of filtration, while the flux of the pristine TFC membrane declined by 42% (SA) and 21% (BSA). The ND particles increased the antibacterial activity of the membrane, increasing the inactivation and mortality rate of *Escherichia coli* (*E. coli*) bacteria cells among the synthesized membranes. Because they are easy to make and have antifouling and antibacterial properties, these membranes can be applied in a broad range of forward osmosis water reclamation applications.

Finally, high-temperature separation performance of three commercial RO TFC polyamide membranes were evaluated with a series of filtrations at elevated temperatures. Morphological and physiochemical characterizations were performed to study the impact of high-temperature filtration on the chemical composition and morphological characteristics of the membranes. An increment in the temperature deteriorated the membrane performance in terms of water flux and salt rejection. Flux decline at high temperatures was recognized as the primary concern of high-temperature filtrations, restricting the applications of commercial membranes for long-term operations. This work presented valuable guidelines for researchers to take steps to advance the development of polymeric membranes with higher stability at elevated temperatures.

6.2 Contributions to knowledge

This research can open up new pathways to develop advanced TFC polyamide membranes. We introduced a new library of thermally stable membranes. The synthetic methods and materials selection were based on the targeted application: high-temperature water treatment. The effect of cross-linking density of the polyamide selective layer on the performance of TFC membranes at high temperature/pressure was well studied. We showed how improving the cross-linking density of polyamide layer using a new multifunctional monomer enhanced the resistance of membranes at elevated temperatures.

For the first time, ND particles functionalized with one of the common polyamide monomers (MPD) were incorporated into the selective layer. We maximized the compatibility of ND particles with the host polymer matrix. ND-MPD particles showed high capability of improving cross-linking density of polyamide layer (by consumption of unreacted functional groups). The method of functionalization and fabrication method can elaborate research works in the field of developing novel TFN membranes.

This research also presented novel approaches to quantify FTIR and XPS results to have an evaluation of cross-linking density of polyamide layer. We compared the content of amide linkages and unreacted functional group. The formation of more amide linkages indicated higher cross-linking density. For the first time, we characterized the chemistry and morphology of polyamide layer before and after long-term high-temperature filtration. The flux decline of polyamide membranes at high temperature was attributed to the morphological structure variations, and not the chemistry changes. This results lead future researches to be more focused on polyamide structure to develop thermally stable TFC membranes.

For the first time, a long-term operation of RO TFC membranes with different methods was conducted. Our suggestions for high temperature water treatment give a baseline for more researches in this field. Having standard protocols helps industrial membrane suppliers and membrane researchers to guarantee their products to be used for real high-temperature applications. In this PhD work, we provided some solutions for high-temperature water treatment considering the vital need for reducing the energy consumption and greenhouse gas emission.

6.3 Future work

High-temperature water treatment is a growing need across many industries. Despite recent advances in the development of thermally stable TFC membranes, some performance challenges remain. Modification of the polymer chemistry of both selective and substrate layers to achieve higher thermal stability should not affect the basic requirements of membranes to provide useful fluxes of clean water with minimum fouling. Adding pendant groups to the polymer backbone to restrict segmental motion of the polymer chains may increase the thermal stability of the membrane. However, pendant group modification may also increase free volume within the polymer network and adversely influence separation efficiency. Additionally, polymer structural modification may either improve or deteriorate other key membrane element features such as pH stability, chemical resilience, oxidant compatibility, operating pressure limits [103,259].

Certain chemical modification strategies have been successful in developing thermally stable polymers. However, these strategies may not be viable for the fabrication of high-performance membranes. For instance, linear polymers such as polyamide Kevlar fibers have extraordinary thermal properties ($T_g \sim 345^\circ\text{C}$), but form membranes with higher free volume and lower rejection efficiency compared to conventional, nonlinear and highly cross-linked TFC polyamide

membranes. The tradeoff between stability and separation performance limits choices of polymers that can be used for the development of thermally stable membranes.

The support layer of TFC polyamide membranes must also be thermally robust so that the integrity of the porous structure at high temperatures is maintained. Thermally induced creep of polymer macromolecules may lead to shrinkage and collapse of the micropores in the support structure. Polymers with a stiff backbone structure or firm three-dimensional network are able to resist structural deformation at high temperatures. Hence, exploring more thermally stable and cost-efficient polymers to be utilized as substrates of TFCs is the topic of ongoing research.

The significant challenges for the development of nanocomposite membranes are the severe aggregation of the nanoparticles and their weak compatibility with polymer network [169,260]. For TFN membranes, large clusters of nanoparticles cannot be accommodated in a thin polyamide layer of 100-300 nm. The aggregation of nanoparticles leads to the formation of non-selective voids at the interface of the polymer and nanoparticles, which significantly reduces the rejection percentage [261]. Given that, the research for fabricating robust TFN membranes has been centered on the development of efficient strategies for surface functionalization of nanomaterial and their dispersion in various solvents and reacting solutions.

One of the main obstacles toward precise thermal characterization of individual layers of TFC membrane is the firm attachments of the thin polyamide layer to its thick sublayer. Hence, the thermal behavior observed by most of the thermal analysis techniques would be mainly related to the substrate rather than the top thin layer. Nano-TA has shown promising results to exclusively measure the glass transition temperature of the selective layer of TFC membranes. In addition, dissolution of the substrate into an appropriate solvent such as dichloromethane was proposed to produce an isolated polyamide layer. [105,262]. However, the probable drawback of this method is the change in the thermal properties of the polyamide selective layer during the dissolution process. Hence, to be able to use other methods such as DSC and TGA, there is a critical need for developing standard protocols to separate the selective layer from the substrate. The need to treat high-temperature contaminated water in different industries in the forthcoming years is expected to grow, spurring the interest in the development of advanced thermally stable TFC membranes with a wide range of applications. Although the prospects for developing novel thermally tolerant TFCs are promising, several challenges must still be addressed. For instance, no standard protocols

exist to evaluate the thermal stability of TFC membranes for water treatment. New long-term high-temperature water filtration tests and thermal characterization methods for ultra-thin polyamide selective layers can provide valuable insights to researchers trying to develop novel thermally stable TFC membranes.

Given the latest technical developments and remaining challenges of thermally stable TFC membranes critically reviewed in this article, the following suggestions for future research can be made:

1. The thermal properties of a polymer are strongly correlated to its chemical structure. The primary bond energy and secondary valence forces that exist between the atoms in a polymer chain are the main sources of polymer thermal stability. High thermal stability can also be attained by taking the advantage of resonance stabilization of aromatic structures (for instance, for carbocyclic and heterocyclic groups). Therefore, polymer scientists have attempted to develop novel polymers with stronger chemical bonds (adding halogens and inorganic elements, such as silicon and phosphorus, in the polymer backbone) and incorporating chain stiffening aromatic structures. Strategies to develop thermally stable polymers may include amine and acid chloride monomers that contain halogens, inorganic element, or carbocyclic/heterocyclic structures.

2. The incorporation of inorganic nanofillers in the membranes may reduce intermolecular chain mobility, thereby increasing the thermal stability of the nanocomposite structure. Weak interaction between the polymer chains and inorganic materials, however, may sacrifice the permselectivity of the synthesized membranes. Hence, developing strategies for surface functionalization of nanomaterials, preferentially anchoring the same amine and acid chloride functional groups of monomers to nanofillers, will increase their contribution to the interfacial polymerization reaction and thus improves their compatibility with the polyamide matrix.

3. The most commonly used and commercially available membrane materials for water treatment use polyamide as the top selective layer, due to its higher water permeability and better selectivity compared to integrally skinned asymmetric membranes. Development of new methods to create thin selective layers with other thermally stable polymers is a promising research area. These methods may include physical spray coating or other in-situ polymerization reaction schemes. Free-radical interfacial polymerization was conducted to fabricate ultrafiltration

membrane, as well as, surface modified porous membranes. In this method, the monomer and the initiator were dissolved separately in aqueous and organic phase. The polymerization starts at the interface by activation of monomers by initiators. This method looks promising to introduce various types of monomers.

4. Even though traditional polyamide membranes perform remarkably well, they unfortunately have low chlorine resistance, poor thermal stability, and high fouling propensity. Polyester TFC is a new family of TFC membranes that have recently received attentions. The polyester membranes showed higher chlorine resistance and more negative surface charge compared with polyamide membranes. The fabrication method of polyester TFC membranes is similar to polyamide membranes as well (interfacial step-growth polymerization). Polyester TFC membrane can be an alternative to traditional TFC membrane specially for developing thermally stable and antifouling membranes.

6.4 List of contributions

6.4.1 Journal papers

- 1. P. Karami**, B. Khorshidi, M. McGregor, J.T. Peichel, J.B.P. Soares, M. Sadrzadeh, Thermally stable thin film composite polymeric membranes for water treatment: a review, *Journal of Cleaner Production* 250 (220) 119447.
- 2. P. Karami**, B. Khorshidi, J.B.P. Soares, M. Sadrzadeh, Fabrication of highly permeable and thermally-stable reverse osmosis thin film composite polyamide membranes, *ACS Applied Materials and Interfaces* 12(2) (2020) 2916-2925.
- 3. P. Karami**, Md.M.H. Mizan, B. Khorshidi, J.B.P. Soares, M. Sadrzadeh, Triammonopyrimidine modified forward osmosis polyamide membranes mediated with graphen oxide/polydopamine interlayer, Ready for submission.
- 4. P. Karami**, B. Khorshidi, L. Shamaei, E. Beaulieu, J.B.P. Soares, M. Sadrzadeh, Nanodiamond-enabled thin-film nanocomposite polyamide membranes for high-temperature water treatment, *ACS Applied Materials and Interfaces* 12(47) (2020) 53274-53285.

5. **P. Karami**, S. Aghapour Aktij, B. Khorshidi, M. Dadashi Firouzjaei, A. Asad, M. Elliott, A. Rahimpour, J.B.P. Soares, M. Sadrzadeh, Nanodiamond-decorated thin film composite membranes with antifouling and antibacterial properties, *Desalination* 522 (2022) 115436.
6. **P. Karami**, S. Aghapour Aktij, M. Rastegar, B. Khorshidi, F. Mohammadtabar, J. Peichel, M. McGregor, T. Reinders, A. Rahimpour, J.B.P. Soares, M. Sadrzadeh, High-temperature cross-flow filtrations of commercial reverse osmosis membranes: guidelines for characterization, Submitted to *Canadian Journal of Chemical Engineering*.

6.4.2 Conference presentations

1. **P. Karami**, B. Khorshidi, J.B.P. Soares, M. Sadrzadeh, High-temperature Water Treatment using Novel Thin Film Composite Membranes, 11th Western Canadian Symposium on Water Quality Research, May 10th, 2019, Edmonton, AB, Canada
2. **P. Karami**, B. Khorshidi, M. Sadrzadeh, J.B.P. Soares, Improving the Thermal Stability of Thin Film Composite Membranes by Modifying the Structure of the Selective Layer - ACS National Meeting & Expo, Chemistry & Water, August 25-29th 2019, San Diego, CA, USA
3. **P. Karami**, B. Khorshidi, M. Sadrzadeh, J.B.P. Soares, Taking the Unique Advantages of Nanodiamond Particles to Enhance Perm-selectivity of Thin Film Nanocomposite Membranes for High-Temperature Water Treatment - Canadian Chemical Engineering Conference - October 25-30th 2020, Ottawa, Canada
4. **P. Karami**, B. Khorshidi, J.B.P. Soares, M. Sadrzadeh, Significant Improvement of Permeability/Selectivity of Polyamide Thin Film Nanocomposite Membranes using Surface-Functionalized Nanodiamonds, 12th International Congress on Membranes and Membrane Processes, December 7-11th 2020, London, UK
5. **P. Karami**, B. Khorshidi, M. Sadrzadeh, J.B.P. Soares, Antifouling thin film composite membranes by grafting nanodiamond particles over the polyamide selective layer - Canadian Chemical Engineering Conference - October 24-27h 2021, Montreal, Canada

References

- [1] A.Y. Hoekstra, Water scarcity challenges to business, *Nat. Clim. Chang.* 4 (2014) 318–320. doi:10.1038/nclimate2214.
- [2] M. Hightower, S.A. Pierce, The energy challenge, *Nature*. 452 (2008) 285–6. doi:10.1038/452285a.
- [3] Global Risks Report, 14th ed., World Economic Forum, 2019.
- [4] M.A. Shannon, P.W. Bohn, M. Elimelech, J.G. Georgiadis, B.J. Mariñas, A.M. Mayes, Science and technology for water purification in the coming decades., *Nature*. 452 (2008) 301–10. doi:10.1038/nature06599.
- [5] A. Fakhru'l-Razi, A. Pendashteh, L.C. Abdullah, D.R.A. Biak, S.S. Madaeni, Z.Z. Abidin, Review of technologies for oil and gas produced water treatment, *J. Hazard. Mater.* 170 (2009) 530–551.
- [6] E.T. Igunnu, G.Z. Chen, Produced water treatment technologies, *Int. J. Low-Carbon Technol.* 9 (2014) 157–177.
- [7] M. Sadrzadeh, J. Hajinasiri, S. Bhattacharjee, D. Pernitsky, Nanofiltration of oil sands boiler feed water: Effect of pH on water flux and organic and dissolved solid rejection, *Sep. Purif. Technol.* 141 (2015) 339–353. doi:10.1016/j.seppur.2014.12.011.
- [8] J. Lian, F. Zhou, B. Chen, M. Yang, S. Wang, Z. Liu, S. Niu, Enhanced adsorption of molybdenum (VI) onto drinking water treatment residues modified by thermal treatment and acid activation, *J. Clean. Prod.* 244 (2020) 118719.
- [9] M.J. Luján-Facundo, M.I. Iborra-Clar, J.A. Mendoza-Roca, M.I. Alcaina-Miranda, Pharmaceutical compounds removal by adsorption with commercial and reused carbon coming from a drinking water treatment plant, *J. Clean. Prod.* 238 (2019) 117866.
- [10] C.C. Small, A.C. Ulrich, Z. Hashisho, Adsorption of acid extractable oil sands tailings organics onto raw and activated oil sands coke, *J. Environ. Eng.* 138 (2012) 833–840.
- [11] W. Zubot, M.D. MacKinnon, P. Chelme-Ayala, D.W. Smith, M.G. El-Din, Petroleum coke adsorption as a water management option for oil sands process-affected water, *Sci. Total Environ.* 427 (2012) 364–372.
- [12] J.C. Anderson, S.B. Wiseman, N. Wang, A. Moustafa, L. Perez-Estrada, M. Gamal El-Din, J.W. Martin, K. Liber, J.P. Giesy, Effectiveness of ozonation treatment in eliminating toxicity of oil sands process-affected water to *Chironomus dilutus*, *Environ. Sci. Technol.* 46 (2012) 486–493.
- [13] M.G. El-Din, H. Fu, N. Wang, P. Chelme-Ayala, L. Pérez-Estrada, P. Drzewicz, J.W. Martin, W. Zubot, D.W. Smith, Naphthenic acids speciation and removal during petroleum-coke adsorption and ozonation of oil sands process-affected water, *Sci. Total Environ.* 409 (2011) 5119–5125.
- [14] P. Gautam, S. Kumar, S. Lokhandwala, Advanced oxidation processes for treatment of leachate from hazardous waste landfill: A critical review, *J. Clean. Prod.* 237 (2019) 117639.
- [15] L. Rizzo, G. Lofrano, C. Gago, T. Bredneva, P. Iannece, M. Pazos, N. Krasnogorskaya, M. Carotenuto, Antibiotic contaminated water treated by photo driven advanced oxidation processes: Ultraviolet/H₂O₂ vs ultraviolet/peracetic acid, *J. Clean. Prod.* 205 (2018) 67–75.
- [16] K. Barbusinski, K. Kalemba, D. Kasperczyk, K. Urbaniec, V. Kozik, Biological methods for odor treatment--A review, *J. Clean. Prod.* 152 (2017) 223–241.

- [17] A. Saidi-Mehrabad, Z. He, I. Tamas, C.E. Sharp, A.L. Brady, F.F. Rochman, L. Bodrossy, G.C.J. Abell, T. Penner, X. Dong, others, Methanotrophic bacteria in oilsands tailings ponds of northern Alberta, *ISME J.* 7 (2013) 908–921.
- [18] G.T. Tellez, N. Nirmalakhandan, J.L. Gardea-Torresdey, Performance evaluation of an activated sludge system for removing petroleum hydrocarbons from oilfield produced water, *Adv. Environ. Res.* 6 (2002) 455–470.
- [19] S. Vuppala, I. Bavasso, M. Stoller, L. Di Palma, G. Vilardi, Olive mill wastewater integrated purification through pre-treatments using coagulants and biological methods: Experimental, modelling and scale-up, *J. Clean. Prod.* 236 (2019) 117622.
- [20] S.A. Hosseini, M. Vossoughi, N.M. Mahmoodi, M. Sadrzadeh, Efficient dye removal from aqueous solution by high-performance electrospun nanofibrous membranes through incorporation of SiO₂ nanoparticles, *J. Clean. Prod.* 183 (2018) 1197–1206.
- [21] M. Rastgar, A. Shakeri, A. Karkooti, A. Asad, R. Razavi, M. Sadrzadeh, Removal of trace organic contaminants by melamine-tuned highly cross-linked polyamide TFC membranes, *Chemosphere.* 238 (2020) 124691. doi:10.1016/j.chemosphere.2019.124691.
- [22] E.W. Allen, Process water treatment in Canada's oil sands industry: I. Target pollutants and treatment objectives, *J. Environ. Eng. Sci.* 7 (2008) 123–138.
- [23] E. Drioli, L. Giorno, *Encyclopedia of membranes*, Springer, 2016.
- [24] M. Mulder, *Basic Principles of Membrane Technology*, Springer Netherlands, Dordrecht, 1996. doi:10.1007/978-94-009-1766-8.
- [25] A. Keucken, G. Heinicke, K. Persson, S. Köhler, Combined coagulation and ultrafiltration process to counteract increasing NOM in brown surface water, *Water.* 9 (2017) 697.
- [26] F. Mohammadtabar, B. Khorshidi, A. Hayatbakhsh, M. Sadrzadeh, Integrated Coagulation-Membrane Processes with Zero Liquid Discharge (ZLD) Configuration for the Treatment of Oil Sands Produced Water, *Water.* 11 (2019) 1348.
- [27] M. Rastgar, A. Bozorg, A. Shakeri, M. Sadrzadeh, Substantially improved antifouling properties in electro-oxidative graphene laminate forward osmosis membrane, *Chem. Eng. Res. Des.* 141 (2019) 413–424. doi:10.1016/J.CHERD.2018.11.010.
- [28] C. Fritzmann, J. Löwenberg, T. Wintgens, T. Melin, State-of-the-art of reverse osmosis desalination, *Desalination.* 216 (2007) 1–76. doi:10.1016/j.desal.2006.12.009.
- [29] J.E. Cadotte, Interfacially synthesized reverse osmosis membrane, U.S. Patent 4277344 A, 1981.
- [30] R.E. Larson, J.E. Cadotte, R.J. Petersen, The FT-30 seawater reverse osmosis membrane-element test results, *Desalination.* 38 (1981) 473–483. doi:10.1016/S0011-9164(00)86092-0.
- [31] I. Pinnau, B. D. Freeman, *Membrane Formation and Modification*, American Chemical Society, Washington, DC, 1999. doi:10.1021/bk-2000-0744.
- [32] B. Khorshidi, T. Thundat, B.A. Fleck, M. Sadrzadeh, Thin film composite polyamide membranes: Parametric study on the influence of synthesis conditions, *RSC Adv.* 5 (2015) 54985–54997. doi:10.1039/C5RA08317F.
- [33] F. Esfandian, M. Peyravi, A.A. Ghoreyshi, M. Jahanshahi, A.S. Rad, Fabrication of TFC nanofiltration membranes via co-solvent assisted interfacial polymerization for lactose recovery, *Arab. J. Chem.* (2017).
- [34] M. Kadhom, B. Deng, Synthesis of high-performance thin film composite (TFC) membranes by controlling the preparation conditions: Technical notes, *J. Water Process Eng.* (2018).

- [35] M. Mulder, Phase Inversion Membranes, *Membr. Prep.* 3 (2000) 3331–3346.
- [36] B. Khorshidi, T. Thundat, B.A. Fleck, M. Sadrzadeh, A novel approach toward fabrication of high performance thin film composite polyamide membranes, *Sci. Rep.* 6 (2016) 22069.
- [37] Y. Song, J.-B. Fan, S. Wang, Recent progress in interfacial polymerization, *Mater. Chem. Front.* 1 (2017) 1028–1040.
- [38] M. Elimelech, W. a Phillip, The future of seawater desalination: energy, technology, and the environment., *Science* (80-.). 333 (2011) 712–717. doi:10.1126/science.1200488.
- [39] B. Khorshidi, B. Soltannia, T. Thundat, M. Sadrzadeh, Synthesis of thin film composite polyamide membranes: Effect of monohydric and polyhydric alcohol additives in aqueous solution, *J. Memb. Sci.* 523 (2017) 336–345.
- [40] B. Khorshidi, T. Thundat, D. Pernitsky, M. Sadrzadeh, A parametric study on the synergistic impacts of chemical additives on permeation properties of thin film composite polyamide membrane, *J. Memb. Sci.* 535 (2017) 248–257.
- [41] D.H.N. Perera, Q. Song, H. Qiblawey, E. Sivaniah, Regulating the aqueous phase monomer balance for flux improvement in polyamide thin film composite membranes, *J. Memb. Sci.* 487 (2015) 74–82. doi:10.1016/j.memsci.2015.03.038.
- [42] F. Pacheco, R. Sougrat, M. Reinhard, J.O. Leckie, I. Pinnau, 3D visualization of the internal nanostructure of polyamide thin films in RO membranes, *J. Memb. Sci.* 501 (2016) 33–44. doi:10.1016/j.memsci.2015.10.061.
- [43] C. Ba, J. Economy, Preparation of PMDA/ODA polyimide membrane for use as substrate in a thermally stable composite reverse osmosis membrane, *J. Memb. Sci.* 363 (2010) 140–148.
- [44] W.J. Lau, A.F. Ismail, N. Misdan, M.A. Kassim, A recent progress in thin film composite membrane: a review, *Desalination.* 287 (2012) 190–199.
- [45] R. Toczyłowska-Mamińska, Limits and perspectives of pulp and paper industry wastewater treatment--A review, *Renew. Sustain. Energy Rev.* 78 (2017) 764–772.
- [46] J. Sójka-Ledakowicz, T. Koprowski, W. Machnowski, H.H. Knudsen, Membrane filtration of textile dyehouse wastewater for technological water reuse, *Desalination.* 119 (1998) 1–9.
- [47] A.-S. Jönsson, J. Wennerbeck, Treatment of high-temperature rinsing water from a degreasing plant by reverse osmosis, *Desalination.* 114 (1997) 175–181.
- [48] G. Hurwitz, D.J. Pernitsky, S. Bhattacharjee, E.M. V Hoek, Targeted Removal of Dissolved Organic Matter in Boiler-Blowdown Wastewater: Integrated Membrane Filtration for Produced Water Reuse, *Ind. Eng. Chem. Res.* 54 (2015) 9431–9439.
- [49] M. Sadrzadeh, J. Hajinasiri, S. Bhattacharjee, D. Pernitsky, Nanofiltration of oil sands boiler feed water: Effect of pH on water flux and organic and dissolved solid rejection, *Sep. Purif. Technol.* 141 (2015) 339–353.
- [50] L. Zhu, F. Zeng, A Condensation Heating Model for Evaluating Early-Period SAGD Performance, *Transp. Porous Media.* 104 (2014) 363–383.
- [51] M.J.H. Snow, D. de Winter, R. Buckingham, J. Campbell, J. Wagner, New techniques for extreme conditions: high temperature reverse osmosis and nanofiltration, *Desalination.* 105 (1996) 57–61.
- [52] M. Fabiyi, A. Larrea, Effect of High Temperature Operations on Wastewater Treatment: Reviewing the Resilience of High Temperature Industrial Wastewater Treatment Systems Using Microbiological Population Studies and Kinetic Dynamics, *Proc. Water Environ. Fed.* 2015 (2015) 1658–1669.

- [53] J.M. Gohil, P. Ray, A review on semi-aromatic polyamide TFC membranes prepared by interfacial polymerization: Potential for water treatment and desalination, *Sep. Purif. Technol.* (2017).
- [54] A. Birca, O. Gherasim, V. Grumezescu, A.M. Grumezescu, Introduction in thermoplastic and thermosetting polymers, in: *Mater. Biomed. Eng.*, Elsevier, 2019: pp. 1–28.
- [55] K.-F. Au, *Advances in knitting technology*, Elsevier, 2011.
- [56] R.B. Seymour, C.E. Carraher, *Structure-property relationships in polymers*, Plenum Press, 1984.
- [57] W.A. Lee, G.J. Knight, Ratio of the glass transition temperature to the melting point in polymers, *Br. Polym. J.* 2 (1970) 73–80. doi:10.1002/pi.4980020112.
- [58] T.R. Crompton, *Thermal stability of polymers*, 2012.
- [59] C.L. Beyler, M.M. Hirschler, Thermal decomposition of polymers, *SFPE Handb. Fire Prot. Eng.* 2 (2002) 111–131.
- [60] J.E. Mark, *Physical properties of polymers handbook*, Springer, 2007.
- [61] J.M.S. S. Kavesh, Meaning and Measurement of Crystallinity: A Review, *Polym. Eng. & Sci.* 9 (1969).
- [62] K.R. Beck, R. Korsmeyer, R.J. Kunz, An overview of the glass transition temperature of synthetic polymers, *J. Chem. Educ.* 61 (1984) 668.
- [63] A. Kumar, R.K. Gupta, *Fundamentals of polymer engineering, Effect of Chemical Structure on Polymer Properties*, CRC Press, 2018.
- [64] M. Walczak, *Role and properties of the confined amorphous phase of polymers*, Paris, ENSAM, 2012.
- [65] L.T. Cureton, E. Napadensky, C. Annunziato, J.J. La Scala, The effect of furan molecular units on the glass transition and thermal degradation temperatures of polyamides, *J. Appl. Polym. Sci.* 134 (2017).
- [66] S. Ray, R.P. Cooney, *Thermal Degradation of Polymer and Polymer Composites*, Second Edi, Elsevier Inc., 2012. doi:10.1016/B978-1-4377-3455-3.00007-9.
- [67] S. Mani, R. Khare, Effect of Chain Flexibility and Interlayer Interactions on the Local Dynamics of Layered Polymer Systems, *Macromolecules.* 51 (2018) 576–588.
- [68] K. Kunal, C.G. Robertson, S. Pawlus, S.F. Hahn, A.P. Sokolov, Role of chemical structure in fragility of polymers: a qualitative picture, *Macromolecules.* 41 (2008) 7232–7238.
- [69] D.J. Kemmish, *Practical guide to high performance engineering plastics*, Smithers Rapra, 2011.
- [70] D. Kemmish, *Update on the Technology and Applications of Polyaryletherketones - Properties and processing of polyaryletherketones*, ISmithers Canada, 2010.
- [71] K.J. Smith, Poly (ether ketone) and Poly (ether sulfone) Synthesis, *Encycl. Polym. Nanomater.* (2015) 1687–1692.
- [72] M. Biron, *Thermoplastics and Thermoplastic Composites - 7-Plastics Solutions for Practical Problems, (Second Edition): William Andrew Publishing*, (2013) 831–984.
- [73] K. Scott, *Handbook of industrial membranes*, Elsevier, 1995.
- [74] R.R. Mather, Synthetic textile fibres: polyolefin, elastomeric and acrylic fibres, in: *Text. Fash.*, Elsevier, 2015: pp. 115–138.
- [75] R.G.M. Van Der Sman, Predictions of Glass Transition Temperature for Hydrogen Bonding

- Biomaterials, *J. Phys. Chem. B.* 117 (2013) 16303–16313. doi:10.1021/jp408184u.
- [76] M. Gilbert, Relation of Structure to Thermal and Mechanical Properties, in: *Brydson's Plast. Mater.* (Eighth Ed., Elsevier, 2017: pp. 59–73.
 - [77] G. Yu, B. Li, J. Liu, S. Wu, H. Tan, C. Pan, X. Jian, Novel thermally stable and organosoluble aromatic polyamides with main chain phenyl-1, 3, 5-triazine moieties, *Polym. Degrad. Stab.* 97 (2012) 1807–1814.
 - [78] Y.-C.K. Hui-Min Wang Sheng-Huei Hsi, Synthesis and characterization of wholly aromatic polyamides containing halogen-substituted triphenylamine moiety, (2010).
 - [79] G. Wypych, *Handbook of polymers*, Elsevier, 2016.
 - [80] K. V Kodre, S.R. Attarde, P.R. Yendhe, R.Y. Patil, V.U. Barge, Differential scanning calorimetry: A review, *Res. Rev. J. Pharm. Anal.* 3 (2014) 11–22.
 - [81] R.E. Wetton, P.J. Corish, DMTA studies of polymer blends and compatibility, *Polym. Test.* 8 (1988) 303–312.
 - [82] L.W. Hill, Dynamic mechanical analysis of property development during film formation, in: *ACS Publications*, 2001.
 - [83] J.D. Menczel, R.B. Prime, *Thermal analysis of polymers: fundamentals and applications*, John Wiley & Sons, 2014.
 - [84] M. Reza kazemi, M. Sadrzadeh, T. Matsuura, Thermally stable polymers for advanced high-performance gas separation membranes, *Prog. Energy Combust. Sci.* 66 (2018) 1–41.
 - [85] S.H. Maruf, D.U. Ahn, A.R. Greenberg, Y. Ding, Glass transition behaviors of interfacially polymerized polyamide barrier layers on thin film composite membranes via nano-thermal analysis, *Polymer (Guildf.)* 52 (2011) 2643–2649.
 - [86] A. Instruments, Nano thermal analysis, (n.d.).
 - [87] J. Wei, X. Jian, C. Wu, S. Zhang, C. Yan, Influence of polymer structure on thermal stability of composite membranes, *J. Memb. Sci.* 256 (2005) 116–121.
 - [88] B. Khorshidi, J. Hajinasiri, G. Ma, S. Bhattacharjee, M. Sadrzadeh, Thermally resistant and electrically conductive PES/ITO nanocomposite membrane, *J. Memb. Sci.* 500 (2016) 151–160.
 - [89] M. Yavari, S. Maruf, Y. Ding, H. Lin, Physical aging of glassy perfluoropolymers in thin film composite membranes. Part II. Glass transition temperature and the free volume model, *J. Memb. Sci.* 525 (2017) 399–408. doi:10.1016/J.MEMSCI.2016.08.033.
 - [90] D.J. Mohan, L. Kullová, A study on the relationship between preparation condition and properties/performance of polyamide TFC membrane by IR, DSC, TGA, and SEM techniques, *Desalin. Water Treat.* 51 (2013) 586–596.
 - [91] J.M. Dodda, T. Remiš, M. Tomáš, P. Novotný, Effect of alternation of polyamide selective layers in the formation and performance of thin-film composite membranes, *Desalin. Water Treat.* 57 (2016) 8720–8729.
 - [92] D.-J. Liaw, P.-N. Hsu, W.-H. Chen, S.-L. Lin, High glass transitions of new polyamides, polyimides, and poly (amide– imide) s containing a triphenylamine group: synthesis and characterization, *Macromolecules.* 35 (2002) 4669–4676.
 - [93] K. Luo, Y. Wang, J. Yu, J. Zhu, Z. Hu, Semi-bio-based aromatic polyamides from 2, 5-furandicarboxylic acid: toward high-performance polymers from renewable resources, *RSC Adv.* 6 (2016) 87013–87020.

- [94] R. Han, Formation and characterization of (melamine–TMC) based thin film composite NF membranes for improved thermal and chlorine resistances, *J. Memb. Sci.* 425 (2013) 176–181.
- [95] C. Wu, S. Zhang, D. Yang, X. Jian, Preparation, characterization and application of a novel thermal stable composite nanofiltration membrane, *J. Memb. Sci.* 326 (2009) 429–434.
- [96] R. Han, S. Zhang, L. Hu, S. Guan, X. Jian, Preparation and characterization of thermally stable poly (piperazine amide)/PPBES composite nanofiltration membrane, *J. Memb. Sci.* 370 (2011) 91–96.
- [97] L. Hu, S. Zhang, R. Han, X. Jian, Preparation and performance of novel thermally stable polyamide/PPENK composite nanofiltration membranes, *Appl. Surf. Sci.* 258 (2012) 9047–9053.
- [98] P. Wen, Y. Chen, X. Hu, B. Cheng, D. Liu, Y. Zhang, S. Nair, Polyamide thin film composite nanofiltration membrane modified with acyl chlorided graphene oxide, 535 (2017) 208–220. doi:10.1016/j.memsci.2017.04.043.
- [99] N. Misdan, W.J. Lau, C.S. Ong, A.F. Ismail, T. Matsuura, Study on the thin film composite poly (piperazine-amide) nanofiltration membranes made of different polymeric substrates: Effect of operating conditions, *Korean J. Chem. Eng.* 32 (2015) 753–760.
- [100] S. Guan, S. Zhang, R. Han, B. Zhang, X. Jian, Preparation and properties of novel sulfonated copoly (phthalazinone biphenyl ether sulfone) composite nanofiltration membrane, *Desalination*. 318 (2013) 56–63.
- [101] J. Han, D. Yang, S. Zhang, L. Wang, X. Jian, Preparation and performance of SPPES/PPES hollow fiber composite nanofiltration membrane with high temperature resistance, *Desalination*. 350 (2014) 95–101.
- [102] B. Rajaeian, A. Rahimpour, M.O. Tade, S. Liu, Fabrication and characterization of polyamide thin film nanocomposite (TFN) nanofiltration membrane impregnated with TiO₂ nanoparticles, *Desalination*. 313 (2013) 176–188.
- [103] N. Rakhshan, M. Pakizeh, The effect of chemical modification of SiO₂ nanoparticles on the nanofiltration characteristics of polyamide membrane, *Korean J. Chem. Eng.* 32 (2015) 2524–2533.
- [104] M. Namvar-Mahboub, M. Pakizeh, Development of a novel thin film composite membrane by interfacial polymerization on polyetherimide/modified SiO₂ support for organic solvent nanofiltration, *Sep. Purif. Technol.* 119 (2013) 35–45.
- [105] M. Fathizadeh, A. Aroujalian, A. Raisi, Effect of added NaX nano-zeolite into polyamide as a top thin layer of membrane on water flux and salt rejection in a reverse osmosis process, *J. Memb. Sci.* 375 (2011) 88–95.
- [106] B. Khorshidi, I. Biswas, T. Ghosh, T. Thundat, M. Sadrzadeh, Robust fabrication of thin film polyamide-TiO₂ nanocomposite membranes with enhanced thermal stability and anti-biofouling propensity, *Sci. Rep.* 8 (2018) 784.
- [107] Y.H. Kotp, Y.A. Shebl, M.S. El-Deab, B.E. El-Anadouli, H.A. Shawky, Performance enhancement of PA-TFC RO membrane by using magnesium silicate nanoparticles, *J. Inorg. Organomet. Polym. Mater.* (2017) 1–14.
- [108] H. Li, W. Shi, Q. Du, R. Zhou, H. Zhang, X. Qin, Improved separation and antifouling properties of thin-film composite nanofiltration membrane by the incorporation of cGO, *Appl. Surf. Sci.* 407 (2017) 260–275.
- [109] H. Wu, B. Tang, P. Wu, MWNTs/polyester thin film nanocomposite membrane: an approach to overcome the trade-off effect between permeability and selectivity, *J. Phys. Chem. C*. 114 (2010) 16395–16400.

- [110] T. Ormanci-Acar, F. Celebi, B. Keskin, O. Mutlu-Salmanlı, M. Agtas, T. Turken, A. Tufani, D.Y. Imer, G.O. Ince, T.U. Demir, Fabrication and characterization of temperature and pH resistant thin film nanocomposite membranes embedded with halloysite nanotubes for dye rejection, *Desalination*. 429 (2018) 20–32.
- [111] Q. Guo, J. Li, T. Chen, Q. Yao, J. Xie, Antimicrobial thin-film composite membranes with chemically decorated ultrasmall silver nanoclusters, *ACS Sustain. Chem. Eng.* 7 (2019) 14848–14855.
- [112] S.F. Seyedpour, A. Rahimpour, G. Najafpour, Facile in-situ assembly of silver-based MOFs to surface functionalization of TFC membrane: A novel approach toward long-lasting biofouling mitigation, *J. Memb. Sci.* 573 (2019) 257–269.
- [113] A. Tiraferri, N.Y. Yip, A.P. Straub, S. Romero-Vargas Castrillon, M. Elimelech, A method for the simultaneous determination of transport and structural parameters of forward osmosis membranes, *J. Memb. Sci.* 444 (2013) 523–538. doi:10.1016/j.memsci.2013.05.023.
- [114] M. Hayatbakhsh, M. Sadrzadeh, D. Pernitsky, S. Bhattacharjee, J. Hajinasiri, Treatment of an in situ oil sands produced water by polymeric membranes, *Desalin. Water Treat.* 57 (2016) 14869–14887.
- [115] B. Khorshidi, T. Thundat, B.A. Fleck, M. Sadrzadeh, Thin film composite polyamide membranes: parametric study on the influence of synthesis conditions, *RSC Adv.* 5 (2015) 54985–54997.
- [116] H. Huang, S. Lin, L. Zhang, L. Hou, Chlorine-resistant polyamide reverse osmosis membrane with monitorable and regenerative sacrificial Layers, *ACS Appl. Mater. Interfaces.* 9 (2017) 10214–10223. doi:10.1021/acsami.6b16462.
- [117] S.-M. Xue, C.-H. Ji, Z.-L. Xu, Y.-J. Tang, R.-H. Li, Chlorine resistant TFN nanofiltration membrane incorporated with octadecylamine-grafted GO and fluorine-containing monomer, *J. Memb. Sci.* 545 (2018) 185–195.
- [118] H. Choi, A.A. Shah, S.-E. Nam, Y.-I. Park, H. Park, Thin-film composite membranes comprising ultrathin hydrophilic polydopamine interlayer with graphene oxide for forward osmosis, *Desalination*. 449 (2019) 41–49.
- [119] A. Tiraferri, Y. Kang, E.P. Giannelis, M. Elimelech, Highly hydrophilic thin-film composite forward osmosis membranes functionalized with surface-tailored nanoparticles, *ACS Appl. Mater. Interfaces.* 4 (2012) 5044–5053.
- [120] N. Misdan, A.F. Ismail, N. Hilal, Recent advances in the development of (bio) fouling resistant thin film composite membranes for desalination, *Desalination*. 380 (2016) 105–111.
- [121] S. Abdikheibari, W. Lei, L.F. Dumée, N. Milne, K. Baskaran, Thin film nanocomposite nanofiltration membranes from amine functionalized-boron nitride/polypiperazine amide with enhanced flux and fouling resistance, *J. Mater. Chem. A.* 6 (2018) 12066–12081.
- [122] H. Hoseinpour, M. Jahanshahi, M. Peyravi, A. Nozad, Feasibility study of a novel copolyamide thin film composite membrane assisted by melamine in terms of acid and thermal stability, *J. Ind. Eng. Chem.* 46 (2017) 244–257.
- [123] A. Bera, R.M. Gol, S. Chatterjee, S.K. Jewrajka, PEGylation and incorporation of triazine ring into thin film composite reverse osmosis membranes for enhancement of anti-organic and anti-biofouling properties, *Desalination*. 360 (2015) 108–117.
- [124] K.P. Lee, G. Bargeman, R. de Rooij, A.J.B. Kemperman, N.E. Benes, Interfacial polymerization of cyanuric chloride and monomeric amines: pH resistant thin film composite polyamine nanofiltration membranes, *J. Memb. Sci.* 523 (2017) 487–496.
- [125] R.P. Chapman, P.R. Averell, R.R. Harris, Solubility of melamine in water, *Ind. Eng. Chem.* 35

- (1943) 137–138.
- [126] B. Stuart, *Infrared spectroscopy: Fundamental and applications*, Google Sch. (2004).
 - [127] L.-F. Liu, X. Huang, X. Zhang, K. Li, Y.-L. Ji, C. Yu, C.-J. Gao, Modification of polyamide TFC nanofiltration membrane for improving separation and antifouling properties, *RSC Adv.* 8 (2018) 15102–15110.
 - [128] C.Y. Tang, Y.-N.N. Kwon, J.O. Leckie, Effect of membrane chemistry and coating layer on physiochemical properties of thin film composite polyamide RO and NF membranes, *Desalination.* 242 (2009) 149–167. doi:10.1016/j.desal.2008.04.003.
 - [129] J.F. Watts, J. Wolstenholme, *An introduction to surface analysis by XPS and AES, An Introd. to Surf. Anal. by XPS AES*, by John F. Watts, John Wolstenholme, Pp. 224. ISBN 0-470-84713-1. Wiley-VCH, May 2003. (2003) 224.
 - [130] S. Karan, Z. Jiang, A.G. Livingston, Sub--10 nm polyamide nanofilms with ultrafast solvent transport for molecular separation, *Science* (80-.). 348 (2015) 1347–1351.
 - [131] M.F. Ismail, B. Khorshidi, M. Sadrzadeh, New insights into the impact of nanoscale surface heterogeneity on the wettability of polymeric membranes, *J. Memb. Sci.* 590 (2019) 117270.
 - [132] Y. Cui, X.-Y. Liu, T.-S. Chung, Ultrathin polyamide membranes fabricated from free-standing interfacial polymerization: Synthesis, modifications, and post-treatment, *Ind. Eng. Chem. Res.* 56 (2017) 513–523.
 - [133] H. Yan, X. Miao, J. Xu, G. Pan, Y. Zhang, Y. Shi, M. Guo, Y. Liu, The porous structure of the fully-aromatic polyamide film in reverse osmosis membranes, *J. Memb. Sci.* 475 (2015) 504–510.
 - [134] X.-H. Ma, Z.-K. Yao, Z. Yang, H. Guo, Z.-L. Xu, C.Y. Tang, M. Elimelech, Nanofoaming of Polyamide Desalination Membranes To Tune Permeability and Selectivity, *Environ. Sci. Technol. Lett.* 5 (2018) 123–130.
 - [135] B. Ukrainsky, G.Z. Ramon, Temperature measurement of the reaction zone during polyamide film formation by interfacial polymerization, *J. Memb. Sci.* 566 (2018) 329–335.
 - [136] S.H. Kim, S.-Y. Kwak, T. Suzuki, Positron annihilation spectroscopic evidence to demonstrate the flux-enhancement mechanism in morphology-controlled thin-film-composite (TFC) membrane, *Environ. Sci. Technol.* 39 (2005) 1764–1770.
 - [137] J. Xu, H. Yan, Y. Zhang, G. Pan, Y. Liu, The morphology of fully-aromatic polyamide separation layer and its relationship with separation performance of TFC membranes, *J. Memb. Sci.* 541 (2017) 174–188.
 - [138] I.L. Alsvik, M.-B. Hägg, Pressure retarded osmosis and forward osmosis membranes: materials and methods, *Polymers* (Basel). 5 (2013) 303–327.
 - [139] W. Suwaileh, N. Pathak, H. Shon, N. Hilal, Forward osmosis membranes and processes: A comprehensive review of research trends and future outlook, *Desalination.* 485 (2020) 114455.
 - [140] B. Khorshidi, A. Bhinder, T. Thundat, D. Pernitsky, M. Sadrzadeh, Developing high throughput thin film composite polyamide membranes for forward osmosis treatment of SAGD produced water, *J. Memb. Sci.* 511 (2016) 29–39. doi:10.1016/j.memsci.2016.03.052.
 - [141] L. Deng, Q. Wang, X. An, Z. Li, Y. Hu, Towards enhanced antifouling and flux performances of thin-film composite forward osmosis membrane via constructing a sandwich-like carbon nanotubes-coated support, *Desalination.* 479 (2020) 114311. doi:10.1016/j.desal.2020.114311.
 - [142] B. Kim, G. Gwak, S. Hong, Review on methodology for determining forward osmosis (FO) membrane characteristics: Water permeability (A), solute permeability (B), and structural parameter

- (S), *Desalination*. 422 (2017) 5–16. doi:10.1016/j.desal.2017.08.006.
- [143] R. Dai, J. Li, Z. Wang, Constructing interlayer to tailor structure and performance of thin-film composite polyamide membranes: A review, *Adv. Colloid Interface Sci.* 282 (2020) 102204.
 - [144] Z. Wang, Z. Wang, S. Lin, H. Jin, S. Gao, Y. Zhu, J. Jin, Nanoparticle-templated nanofiltration membranes for ultrahigh performance desalination, *Nat. Commun.* 9 (2018) 1–9.
 - [145] W. Zhao, H. Liu, Y. Liu, M. Jian, L. Gao, H. Wang, X. Zhang, Thin-film nanocomposite forward-osmosis membranes on hydrophilic microfiltration support with an intermediate layer of graphene oxide and multiwall carbon nanotube, *ACS Appl. Mater. Interfaces*. 10 (2018) 34464–34474.
 - [146] G. Han, S. Zhang, X. Li, N. Widjojo, T.-S. Chung, Thin film composite forward osmosis membranes based on polydopamine modified polysulfone substrates with enhancements in both water flux and salt rejection, *Chem. Eng. Sci.* 80 (2012) 219–231.
 - [147] P. Karami, B. Khorshidi, J.B.P. Soares, M. Sadrzadeh, Fabrication of Highly Permeable and Thermally-Stable Reverse Osmosis Thin Film Composite Polyamide Membranes, *ACS Appl. Mater. Interfaces*. (2019) acsami.9b16875. doi:10.1021/acsami.9b16875.
 - [148] X. Teng, Y. Guo, D. Liu, G. Li, C. Yu, J. Dai, A polydopamine-coated polyamide thin film composite membrane with enhanced selectivity and stability for vanadium redox flow battery, *J. Memb. Sci.* 601 (2020) 117906.
 - [149] D. He, Z. Peng, W. Gong, Y. Luo, P. Zhao, L. Kong, Mechanism of a green graphene oxide reduction with reusable potassium carbonate, *RSC Adv.* 5 (2015) 11966–11972.
 - [150] P. Karami, S.A. Aktij, B. Khorshidi, M.D. Firouzjaei, A. Asad, M. Elliott, A. Rahimpour, J.B.P. Soares, M. Sadrzadeh, Nanodiamond-decorated thin film composite membranes with antifouling and antibacterial properties, *Desalination*. 522 (2022) 115436.
 - [151] M. Rastgar, A. Karkooti, A. Sohrabi, P. Karami, N. Nazemifard, M. Sadrzadeh, Osmotic dewatering accelerates inherent sluggish kinetics of electro-Fenton process: Toward sustainable removal of organic contaminants, *Chem. Eng. J.* 394 (2020) 125043.
 - [152] B. Khorshidi, I. Bi, T. Ghosh, T. Thundat, Robust fabrication of thin film polyamide-TiO₂ nanocomposite membranes with enhanced thermal stability and anti-biofouling propensity, *Sci. Rep.* 8:784 (2018) 1–10. doi:10.1038/s41598-017-18724-w.
 - [153] P. Karami, B. Khorshidi, L. Shamaei, E. Beaulieu, J.B.P. Soares, M. Sadrzadeh, Nanodiamond-Enabled Thin-Film Nanocomposite Polyamide Membranes for High-Temperature Water Treatment, *ACS Appl. Mater. Interfaces*. 12 (2020) 53274–53285.
 - [154] P. Karami, B. Khorshidi, M. McGregor, J.T. Peichel, J.B.P. Soares, M. Sadrzadeh, Thermally stable thin film composite polymeric membranes for water treatment: A review, *J. Clean. Prod.* 250 (2020) 119447.
 - [155] S. Thatai, R. Verma, P. Khurana, P. Goel, D. Kumar, Water quality standards, its pollution and treatment methods, in: *A New Gener. Mater. Graphene Appl. Water Technol.*, Springer, 2019: pp. 21–42.
 - [156] V.G. Gude, Desalination and water reuse to address global water scarcity, *Rev. Environ. Sci. Bio/Technology*. 16 (2017) 591–609.
 - [157] World Health Organization (WHO), 1 in 3 people globally do not have access to safe drinking water – UNICEF, WHO, (n.d.). <https://www.who.int/news-room/detail/18-06-2019-1-in-3-people-globally-do-not-have-access-to-safe-drinking-water-unicef-who>.
 - [158] M.G. Buonomenna, Membrane processes for a sustainable industrial growth, *RSC Adv.* 3 (2013)

5694–5740.

- [159] K. Arola, B. der Bruggen, M. Mänttari, M. Kallioinen, Treatment options for nanofiltration and reverse osmosis concentrates from municipal wastewater treatment: A review, *Crit. Rev. Environ. Sci. Technol.* 49 (2019) 2049–2116.
- [160] L. Shamaei, B. Khorshidi, M.A. Islam, M. Sadrzadeh, Industrial waste lignin as an antifouling coating for the treatment of oily wastewater : Creating wealth from waste, *J. Clean. Prod.* (2020). doi:10.1016/j.jclepro.2020.120304.
- [161] L. Shamaei, B. Khorshidi, M.A. Islam, M. Sadrzadeh, Development of antifouling membranes using agro-industrial waste lignin for the treatment of Canada's oil sands produced water, *J. Memb. Sci.* 611 (2020) 118326. doi:10.1016/j.memsci.2020.118326.
- [162] B. Khorshidi, S. Shabani, M. Sadrzadeh, Prospects of nanocomposite membranes for water treatment by osmotic-driven membrane processes, *Nanocomposite Membr. Water Gas Sep.* (2020) 257–297. doi:10.1016/B978-0-12-816710-6.00011-0.
- [163] J.E. Cadotte, R.S. King, R.J. Majerle, R.J. Petersen, Interfacial synthesis in the preparation of reverse osmosis membranes, *J. Macromol. Sci.* 15 (1981) 727–755.
- [164] M.J.T. Raaijmakers, N.E. Benes, Current trends in interfacial polymerization chemistry, *Prog. Polym. Sci.* 63 (2016) 86–142.
- [165] P. Karami, B. Khorshidi, M. McGregor, J.T. Peichel, J.B.P. Soares, M. Sadrzadeh, Thermally stable thin film composite polymeric membranes for water treatment: A review, *J. Clean. Prod.* (2019) 119447. doi:10.1016/j.jclepro.2019.119447.
- [166] P. Karami, B. Khorshidi, J.B.P. Soares, M. Sadrzadeh, Fabrication of Highly Permeable and Thermally-Stable Reverse Osmosis Thin Film Composite Polyamide Membranes, *ACS Appl. Mater. Interfaces.* (2019) acsami.9b16875. doi:10.1021/acsami.9b16875.
- [167] B. Soltannia, M.A. Islam, J.-Y. Cho, F. Mohammadtabar, R. Wang, V.A. Piunova, Z. Almansoori, M. Rastgar, A.J. Myles, Y.-H. La, others, Thermally stable core-shell star-shaped block copolymers for antifouling enhancement of water purification membranes, *J. Memb. Sci.* 598 (2020) 117686.
- [168] X. Gao, Y. Li, X. Yang, Y. Shang, Y. Wang, B. Gao, Z. Wang, Highly permeable and antifouling reverse osmosis membranes with acidified graphitic carbon nitride nanosheets as nanofillers, *J. Mater. Chem. A* 5 (2017) 19875–19883.
- [169] W.J. Lau, S. Gray, T. Matsuura, D. Emadzadeh, J.P. Chen, A.F. Ismail, A review on polyamide thin film nanocomposite (TFN) membranes: history, applications, challenges and approaches, *Water Res.* 80 (2015) 306–324.
- [170] S. Kim, X. Lin, R. Ou, H. Liu, X. Zhang, G.P. Simon, C.D. Easton, H. Wang, Highly crosslinked, chlorine tolerant polymer network entwined graphene oxide membrane for water desalination, *J. Mater. Chem. A* 5 (2017) 1533–1540.
- [171] V.N. Mochalin, O. Shenderova, D. Ho, Y. Gogotsi, The properties and applications of nanodiamonds, *Nat. Nanotechnol.* 7 (2012) 11.
- [172] P. Karami, S. Salkhi Khasraghi, M. Hashemi, S. Rabiei, A. Shojaei, Polymer/nanodiamond composites - a comprehensive review from synthesis and fabrication to properties and applications, *Adv. Colloid Interface Sci.* 269 (2019) 122–151. doi:10.1016/j.cis.2019.04.006.
- [173] V. Vatanpour, R.S.E. Naeni, A. Ghadimi, A. Karami, B. Sadatnia, Effect of detonation nanodiamond on the properties and performance of polyethersulfone nanocomposite membrane, *Diam. Relat. Mater.* 90 (2018) 244–255.

- [174] A. Tizchang, Y. Jafarzadeh, R. Yegani, S. Khakpour, The effects of pristine and silanized nanodiamond on the performance of polysulfone membranes for wastewater treatment by MBR system, *J. Environ. Chem. Eng.* 7 (2019) 103447.
- [175] S. Khakpour, Y. Jafarzadeh, R. Yegani, Incorporation of graphene oxide/nanodiamond nanocomposite into PVC ultrafiltration membranes, *Chem. Eng. Res. Des.* 152 (2019) 60–70.
- [176] M. Bhadra, S. Roy, S. Mitra, Nanodiamond immobilized membranes for enhanced desalination via membrane distillation, *Desalination*. 341 (2014) 115–119.
- [177] A. Bedar, P.K. Tewari, R.C. Bindal, S. Kar, Enhancing γ -radiation resistant property of polysulfone membranes with carboxylated nanodiamond: Impact and effect of surface tunability, *Appl. Surf. Sci.* 507 (2020) 144897.
- [178] H. Etemadi, R. Yegani, M. Seyfollahi, The effect of amino functionalized and polyethylene glycol grafted nanodiamond on anti-biofouling properties of cellulose acetate membrane in membrane bioreactor systems, *Sep. Purif. Technol.* 177 (2017) 350–362.
- [179] D. Qin, G. Huang, D. Terada, H. Jiang, M. Ito, A. Gibbons, R. Igarashi, D. Yamaguchi, M. Shirakawa, E. Sivaniah, others, Nanodiamond mediated interfacial polymerization for high performance nanofiltration membrane, *J. Memb. Sci.* (2020) 118003.
- [180] V.N. Mochalin, I. Neitzel, B.J.M. Etzold, A. Peterson, G. Palmese, Y. Gogotsi, Covalent incorporation of aminated nanodiamond into an epoxy polymer network, *ACS Nano*. 5 (2011) 7494–7502.
- [181] P. Karami, A. Shojaei, Morphological and mechanical properties of polyamide 6/nanodiamond composites prepared by melt mixing: effect of surface functionality of nanodiamond, *Polym. Int.* 66 (2017). doi:10.1002/pi.5289.
- [182] A. Rahimpour, M. Jahanshahi, S. Khalili, A. Mollahosseini, A. Zirepour, B. Rajaeian, Novel functionalized carbon nanotubes for improving the surface properties and performance of polyethersulfone (PES) membrane, *Desalination*. 286 (2012) 99–107.
- [183] A.K. Ghosh, B.-H. Jeong, X. Huang, E.M. V Hoek, Impacts of reaction and curing conditions on polyamide composite reverse osmosis membrane properties, *J. Memb. Sci.* 311 (2008) 34–45.
- [184] Y. Li, S. Huang, S. Zhou, A.G. Fane, Y. Zhang, S. Zhao, Enhancing water permeability and fouling resistance of polyvinylidene fluoride membranes with carboxylated nanodiamonds, *J. Memb. Sci.* 556 (2018) 154–163.
- [185] U. Roy, V. Drozd, A. Durygin, J. Rodriguez, P. Barber, V. Atluri, X. Liu, T.G. Voss, S. Saxena, M. Nair, Characterization of Nanodiamond-based anti-HIV drug Delivery to the Brain, *Sci. Rep.* 8 (2018) 1–12.
- [186] A.-Y. Jee, M. Lee, Surface functionalization and physicochemical characterization of diamond nanoparticles, *Curr. Appl. Phys.* 9 (2009) e144–e147.
- [187] M. Banisaid, A.N. Kharat, Synthesis and Characterizations of Nanodiamond and its Application as Anti-Polishing Agent on SiO₂ Substrate, *Int J Chem Sci.* 16 (2018) 262.
- [188] Y. Jin, W. Wang, Z. Su, Spectroscopic study on water diffusion in aromatic polyamide thin film, *J. Memb. Sci.* 379 (2011) 121–130.
- [189] A.P. Rao, S. V Joshi, J.J. Trivedi, C. V Devmurari, V.J. Shah, Structure-performance correlation of polyamide thin film composite membranes: effect of coating conditions on film formation, *J. Memb. Sci.* 211 (2003) 13–24.
- [190] M. Ionita, A.M. Pandeale, L.E. Crica, A.C. Obreja, Preparation and characterization of

- polysulfone/ammonia-functionalized graphene oxide composite membrane material, *High Perform. Polym.* 28 (2016) 181–188.
- [191] A. Zhou, C. Shi, X. He, Y. Fu, A.W. Anjum, J. Zhang, W. Li, Polyarylester nanofiltration membrane prepared from monomers of vanillic alcohol and trimesoyl chloride, *Sep. Purif. Technol.* 193 (2018) 58–68.
- [192] J. Zhang, Y. Hai, Y. Zuo, Q. Jiang, C. Shi, W. Li, Novel diamine-modified composite nanofiltration membranes with chlorine resistance using monomers of 1, 2, 4, 5-benzene tetracarbonyl chloride and m-phenylenediamine, *J. Mater. Chem. A* 3 (2015) 8816–8824.
- [193] Y. Hai, J. Zhang, C. Shi, A. Zhou, C. Bian, W. Li, Thin film composite nanofiltration membrane prepared by the interfacial polymerization of 1, 2, 4, 5-benzene tetracarbonyl chloride on the mixed amines cross-linked poly (ether imide) support, *J. Memb. Sci.* 520 (2016) 19–28.
- [194] C. Kong, T. Shintani, T. Kamada, V. Freger, T. Tsuru, Co-solvent-mediated synthesis of thin polyamide membranes, *J. Memb. Sci.* 384 (2011) 10–16.
- [195] J. Lee, R. Wang, T.-H. Bae, A comprehensive understanding of co-solvent effects on interfacial polymerization: Interaction with trimesoyl chloride, *J. Memb. Sci.* 583 (2019) 70–80.
- [196] T.D. Nguyen, K. Chan, T. Matsuura, S. Sourirajan, Viscoelastic and statistical thermodynamic approach to the study of the structure of polymer film casting solutions for making RO/UF membranes, *Ind. Eng. Chem. Prod. Res. Dev.* 24 (1985) 655–665.
- [197] T.D. Nguyen, T. Matsuura, S. Sourirajan, Effect of nonsolvent additives on the pore size and the pore size distribution of aromatic polyamide RO membranes, *Chem. Eng. Commun.* 54 (1987) 17–36. doi:10.1080/00986448708911895.
- [198] D. Dutta, A. Bhattacharyya, B.N. Ganguly, Microstructural study of aromatic polyamide membrane material, *J. Memb. Sci.* 224 (2003) 127–135. doi:10.1016/j.memsci.2003.08.001.
- [199] R.R. Sharma, S. Chellam, Temperature effects on the morphology of porous thin film composite nanofiltration membranes, *Environ. Sci. Technol.* 39 (2005) 5022–5030. doi:10.1021/es0501363.
- [200] E. Harder, D.E. Walters, Y.D. Bodnar, R.S. Faibish, B. Roux, Molecular dynamics study of a polymeric reverse osmosis membrane, *J. Phys. Chem. B* 113 (2009) 10177–10182. doi:10.1021/jp902715f.
- [201] Y. Zhang, J.R. Choi, S.-J. Park, Thermal conductivity and thermo-physical properties of nanodiamond-attached exfoliated hexagonal boron nitride/epoxy nanocomposites for microelectronics, *Compos. Part A Appl. Sci. Manuf.* 101 (2017) 227–236.
- [202] E. Roumeli, E. Pavlidou, A. Avgeropoulos, G. Vourlias, D.N. Bikiaris, K. Chrissafis, Factors controlling the enhanced mechanical and thermal properties of nanodiamond-reinforced cross-linked high density polyethylene, *J. Phys. Chem. B* 118 (2014) 11341–11352.
- [203] P. Karami, A. Shojaei, Improvement of dry sliding tribological properties of polyamide 6 using diamond nanoparticles, *Tribol. Int.* 115 (2017) 370–377.
- [204] P.J.J. Alvarez, C.K. Chan, M. Elimelech, N.J. Halas, D. Villagrán, Emerging opportunities for nanotechnology to enhance water security, *Nat. Nanotechnol.* 13 (2018) 634.
- [205] M.S. Mauter, I. Zucker, F. Perreault, J.R. Werber, J.-H. Kim, M. Elimelech, The role of nanotechnology in tackling global water challenges, *Nat. Sustain.* 1 (2018) 166–175.
- [206] The United Nations World Water Development Report 2020, (n.d.). <https://www.unwater.org/publications/world-water-development-report-2020/>.
- [207] A.K. Shukla, J. Alam, M. Alhoshan, L.A. Dass, M.R. Muthumareeswaran, Development of a

- nanocomposite ultrafiltration membrane based on polyphenylsulfone blended with graphene oxide, *Sci. Rep.* 7 (2017) 1–12.
- [208] A. Asad, D. Sameoto, M. Sadrzadeh, Overview of membrane technology, in: *Nanocomposite Membr. Water Gas Sep.*, Elsevier, 2020: pp. 1–28.
 - [209] S. Zhao, L. Zou, C.Y. Tang, D. Mulcahy, Recent developments in forward osmosis: opportunities and challenges, *J. Memb. Sci.* 396 (2012) 1–21.
 - [210] T.-S. Chung, S. Zhang, K.Y. Wang, J. Su, M.M. Ling, Forward osmosis processes: yesterday, today and tomorrow, *Desalination*. 287 (2012) 78–81.
 - [211] M.D. Firouzjaei, S.F. Seyedpour, S.A. Aktij, M. Giagnorio, N. Bazrafshan, A. Mollahosseini, F. Samadi, S. Ahmadalipour, F.D. Firouzjaei, M.R. Esfahani, others, Recent advances in functionalized polymer membranes for biofouling control and mitigation in forward osmosis, *J. Memb. Sci.* 596 (2020) 117604.
 - [212] M.D. Firouzjaei, A.A. Shamsabadi, S.A. Aktij, S.F. Seyedpour, M. Sharifian Gh, A. Rahimpour, M.R. Esfahani, M. Ulbricht, M. Soroush, Exploiting synergetic effects of graphene oxide and a silver-based metal–organic framework to enhance antifouling and anti-biofouling properties of thin-film nanocomposite membranes, *ACS Appl. Mater. Interfaces*. 10 (2018) 42967–42978.
 - [213] S. Yadav, H. Saleem, I. Ibrar, O. Naji, A.A. Hawari, A.A. Alanezi, S.J. Zaidi, A. Altaee, J. Zhou, Recent developments in forward osmosis membranes using carbon-based nanomaterials, *Desalination*. 482 (2020) 114375.
 - [214] B. Mi, M. Elimelech, Organic fouling of forward osmosis membranes: fouling reversibility and cleaning without chemical reagents, *J. Memb. Sci.* 348 (2010) 337–345.
 - [215] Y. Chun, D. Mulcahy, L. Zou, I.S. Kim, A short review of membrane fouling in forward osmosis processes, *Membranes (Basel)*. 7 (2017) 30.
 - [216] W.J. Lee, Z.C. Ng, S.K. Hubadillah, P.S. Goh, W.J. Lau, M.H.D. Othman, A.F. Ismail, N. Hilal, Fouling mitigation in forward osmosis and membrane distillation for desalination, *Desalination*. 480 (2020) 114338.
 - [217] Z. Liu, X. An, C. Dong, S. Zheng, B. Mi, Y. Hu, Modification of thin film composite polyamide membranes with 3D hyperbranched polyglycerol for simultaneous improvement in their filtration performance and antifouling properties, *J. Mater. Chem. A*. 5 (2017) 23190–23197.
 - [218] M.F. Ismail, M.A. Islam, B. Khorshidi, M. Sadrzadeh, Prediction of surface charge properties on the basis of contact angle titration models, *Mater. Chem. Phys.* 258 (2021) 123933.
 - [219] M.E. Xinglin Lu, Santiago Romero-Vargas Castrillón, Devin L. Shaffer, Jun Ma, In situ surface chemical modification of thin-film composite forward osmosis membranes for enhanced organic fouling resistance, *Environ. Sci. Technol.* 2013, 47 (2013) 12219–12228. doi:10.1021/es403179m.
 - [220] J. Yin, Y. Yang, Z. Hu, B. Deng, Attachment of silver nanoparticles (AgNPs) onto thin-film composite (TFC) membranes through covalent bonding to reduce membrane biofouling, *J. Memb. Sci.* 441 (2013) 73–82.
 - [221] S.-H. Park, S.O. Hwang, T.-S. Kim, A. Cho, S.J. Kwon, K.T. Kim, H.-D. Park, J.-H. Lee, Triclosan-immobilized polyamide thin film composite membranes with enhanced biofouling resistance, *Appl. Surf. Sci.* 443 (2018) 458–466.
 - [222] G.-R. Xu, J.-N. Wang, C.-J. Li, Strategies for improving the performance of the polyamide thin film composite (PA-TFC) reverse osmosis (RO) membranes: Surface modifications and nanoparticles incorporations, *Desalination*. 328 (2013) 83–100.

- [223] P. Karami, S. Salkhi Khasraghi, M. Hashemi, S. Rabiei, A. Shojaei, Polymer/nanodiamond composites - a comprehensive review from synthesis and fabrication to properties and applications, *Adv. Colloid Interface Sci.* 269 (2019) 122–151. doi:10.1016/J.CIS.2019.04.006.
- [224] V.N. Mochalin, Y. Gogotsi, Nanodiamond-polymer composites, *Diam. Relat. Mater.* 58 (2015) 161–171.
- [225] M. Raeiszadeh, A. Hakimian, A. Shojaei, H. Molavi, Nanodiamond-filled chitosan as an efficient adsorbent for anionic dye removal from aqueous solutions, *J. Environ. Chem. Eng.* 6 (2018) 3283–3294.
- [226] V. Turcheniuk, V. Raks, R. Issa, I.R. Cooper, P.J. Cragg, R. Jijie, N. Dumitrascu, L.I. Mikhalovska, A. Barras, V. Zaitsev, others, Antimicrobial activity of menthol modified nanodiamond particles, *Diam. Relat. Mater.* 57 (2015) 2–8.
- [227] E. Ferrero, S. Navea, C. Repolles, J. Bacardit, J. Malfeito, R.D.-A. Agua-Spain, Analytical methods for the characterization of Reverse Osmosis membrane fouling, in: *IDA World Congr. Proceedings*, Pap. IDAWC/PER11-240, 2011.
- [228] Z.F. Cui, Y. Jiang, R.W. Field, Fundamentals of pressure-driven membrane separation processes, in: *Membr. Technol.*, Elsevier, 2010: pp. 1–18.
- [229] Y. Qin, S. Yu, Q. Zhao, G. Kang, H. Yu, Y. Jin, Y. Cao, New insights into tailoring polyamide structure for fabricating highly permeable reverse osmosis membranes, *Desalination*. 499 (2021) 114840.
- [230] M. Rastgar, A. Karkooti, A. Sohrabi, P. Karami, N. Nazemifard, M. Sadrzadeh, Osmotic Dewatering Accelerates Inherent Sluggish Kinetics of Electro-Fenton Process: Toward Sustainable Removal of Organic Contaminants, *Chem. Eng. J.* (2020) 125043.
- [231] D. Chen, Q. Chen, T. Liu, J. Kang, R. Xu, Y. Cao, M. Xiang, Influence of l-arginine on performances of polyamide thin-film composite reverse osmosis membranes, *RSC Adv.* 9 (2019) 20149–20160.
- [232] S. Xu, F. Li, B. Su, M.Z. Hu, X. Gao, C. Gao, Novel graphene quantum dots (GQDs)-incorporated thin film composite (TFC) membranes for forward osmosis (FO) desalination, *Desalination*. 451 (2019) 219–230.
- [233] J.A. Idarraga-Mora, M.A. Lemelin, S.T. Weinman, S.M. Husson, Effect of short-term contact with C1–C4 monohydric alcohols on the water permeance of MPD-TMC thin-film composite reverse osmosis membranes, *Membranes (Basel)*. 9 (2019) 92.
- [234] L. Zheng, W.E. Price, L.D. Nghiem, Effects of fouling on separation performance by forward osmosis: the role of specific organic foulants, *Environ. Sci. Pollut. Res.* 26 (2019) 33758–33769.
- [235] X. Hao, S. Gao, J. Tian, S. Wang, H. Zhang, Y. Sun, W. Shi, F. Cui, New insights into the organic fouling mechanism of an in situ Ca²⁺ modified thin film composite forward osmosis membrane, *RSC Adv.* 9 (2019) 38227–38234.
- [236] H. Mahdavi, A. Rahimi, Zwitterion functionalized graphene oxide/polyamide thin film nanocomposite membrane: Towards improved anti-fouling performance for reverse osmosis, *Desalination*. 433 (2018) 94–107.
- [237] Z. Yang, Y. Wu, J. Wang, B. Cao, C.Y. Tang, In situ reduction of silver by polydopamine: A novel antimicrobial modification of a thin-film composite polyamide membrane, *Environ. Sci. Technol.* 50 (2016) 9543–9550.
- [238] M. Raeiszadeh, F. Taghipour, Inactivation of microorganisms by newly emerged microplasma UV lamps, *Chem. Eng. J.* 413 (2021) 127490.

- [239] J. Wehling, R. Dringen, R.N. Zare, M. Maas, K. Rezwani, Bactericidal Activity of Partially Oxidized Nanodiamonds, *ACS Nano*. 8 (2014) 6475–6483. doi:10.1021/nn502230m.
- [240] S. Szunerits, A. Barras, R. Boukherroub, Antibacterial applications of nanodiamonds, *Int. J. Environ. Res. Public Health*. 13 (2016) 413.
- [241] H. Etemadi, R. Yegani, V. Babaeipour, Study on the reinforcing effect of nanodiamond particles on the mechanical, thermal and antibacterial properties of cellulose acetate membranes, *Diam. Relat. Mater.* 69 (2016) 166–176.
- [242] A. Chatterjee, E. Perevedentseva, M. Jani, C.-Y. Cheng, Y.-S. Ye, P.-H. Chung, C.-L. Cheng, Antibacterial effect of ultrafine nanodiamond against gram-negative bacteria *Escherichia coli*, *J. Biomed. Opt.* 20 (2014) 51014.
- [243] S.F. Seyedpour, M. Dadashi Firouzjaei, A. Rahimpour, E. Zolghadr, A. Arabi Shamsabadi, P. Das, F. Akbari Afkhami, M. Sadrzadeh, A. Tiraferri, M.A. Elliott, Toward Sustainable Tackling of Biofouling Implications and Improved Performance of TFC FO Membranes Modified by Ag-MOFs Nanorods, *ACS Appl. Mater. Interfaces*. (2020).
- [244] M. Pejman, M. Dadashi Firouzjaei, S. Aghapour Aktij, P. Das, E. Zolghadr, H. Jafarian, A. Arabi Shamsabadi, M. Elliott, M. Sadrzadeh, M. Sangermano, In Situ Ag-MOF Growth on Pre-Grafted Zwitterions Imparts Outstanding Antifouling Properties to Forward Osmosis Membranes, *ACS Appl. Mater. Interfaces*. 12 (2020) 36287–36300.
- [245] M. Pejman, M.D. Firouzjaei, S.A. Aktij, E. Zolghadr, P. Das, M. Elliott, M. Sadrzadeh, M. Sangermano, A. Rahimpour, A. Tiraferri, Effective strategy for UV-mediated grafting of biocidal Ag-MOFs on polymeric membranes aimed at enhanced water ultrafiltration, *Chem. Eng. J.* (2021) 130704.
- [246] A. Mollahosseini, A. Rahimpour, M. Jahamshahi, M. Peyravi, M. Khavarpour, The effect of silver nanoparticle size on performance and antibacterality of polysulfone ultrafiltration membrane, *Desalination*. 306 (2012) 41–50.
- [247] J. Shen, B.S. Richards, A.I. Schäfer, Renewable energy powered membrane technology: Case study of St. Dorcas borehole in Tanzania demonstrating fluoride removal via nanofiltration/reverse osmosis, *Sep. Purif. Technol.* 170 (2016) 445–452.
- [248] C. Atallah, A.Y. Tremblay, S. Mortazavi, Silane surface modified ceramic membranes for the treatment and recycling of SAGD produced water, *J. Pet. Sci. Eng.* 157 (2017) 349–358.
- [249] X. Jian, Y. Dai, G. He, G. Chen, Preparation of UF and NF poly (phthalazine ether sulfone ketone) membranes for high temperature application, *J. Memb. Sci.* 161 (1999) 185–191. doi:10.1016/S0376-7388(99)00112-X.
- [250] H.C. Chu, J.S. Campbell, W.G. Light, High-temperature reverse osmosis membrane element, *Desalination*. 70 (1988) 65–76. doi:10.1016/0011-9164(88)85044-6.
- [251] D.L. Shaffer, M.E. Tousley, M. Elimelech, Influence of polyamide membrane surface chemistry on gypsum scaling behavior, *J. Memb. Sci.* 525 (2017) 249–256. doi:10.1016/j.memsci.2016.11.003.
- [252] M. Mänttari, A. Pihlajamäki, E. Kaipainen, M. Nyström, Effect of temperature and membrane pre-treatment by pressure on the filtration properties of nanofiltration membranes, *Desalination*. 145 (2002) 81–86. doi:http://dx.doi.org/10.1016/S0011-9164(02)00390-9.
- [253] Y. Roy, D.M. Warsinger, others, Effect of temperature on ion transport in nanofiltration membranes: Diffusion, convection and electromigration, *Desalination*. 420 (2017) 241–257.
- [254] Y. Roy, others, Factors contributing to the change in permeate quality upon temperature variation in nanofiltration, *Desalination*. 455 (2019) 58–70.

- [255] P. Karami, B. Khorshidi, J.B.P. Soares, M. Sadrzadeh, Fabrication of Highly Permeable and Thermally-Stable Reverse Osmosis Thin Film Composite Polyamide Membranes, *ACS Appl. Mater. Interfaces*. 12 (2019) 2916–2925.
- [256] I.S. Al-Mutaz, M.A. Al-Ghunaimi, Performance of reverse osmosis units at high temperatures, in: *IDA World Congr. Desalin. Water Reuse*, Bahrain, 2001: pp. 26–31.
- [257] L. Shamaei, P. Karami, B. Khorshidi, R. Farnood, M. Sadrzadeh, Novel Lignin-Modified Forward Osmosis Membranes: Waste Materials for Wastewater Treatment, *ACS Sustain. Chem. Eng.* 9 (2021) 15768–15779.
- [258] M. Esmacili, T. Virtanen, J. Lahti, M. Mänttari, M. Kallioinen, Vanillin as an antifouling and hydrophilicity promoter agent in surface modification of polyethersulfone membrane, *Membranes (Basel)*. 9 (2019) 56.
- [259] M. Yavari, S. Maruf, Y. Ding, H. Lin, Physical aging of glassy perfluoropolymers in thin film composite membranes . Part II . Glass transition temperature and the free volume model, *J. Memb. Sci.* (2016). doi:10.1016/j.memsci.2016.08.033.
- [260] J.W. Krumpfer, T. Schuster, M. Klapper, K. Müllen, Make it nano-Keep it nano, *Nano Today*. 8 (2013) 417–438. doi:10.1016/j.nantod.2013.07.006.
- [261] M.M. Pendergast, E.M.V. Hoek, A review of water treatment membrane nanotechnologies, *Energy Environ. Sci.* 4 (2011) 1946. doi:10.1039/c0ee00541j.
- [262] M. Shi, Z. Wang, S. Zhao, J. Wang, S. Wang, A support surface pore structure re-construction method to enhance the flux of TFC RO membrane, *J. Memb. Sci.* 541 (2017) 39–52.
- [263] I.M.A. ElSherbiny, A.S.G. Khalil, M. Ulbricht, Tailoring Surface Characteristics of Polyamide Thin-Film Composite Membranes toward Pronounced Switchable Wettability, *Adv. Mater. Interfaces*. 6 (2019) 1801408.

Appendix A

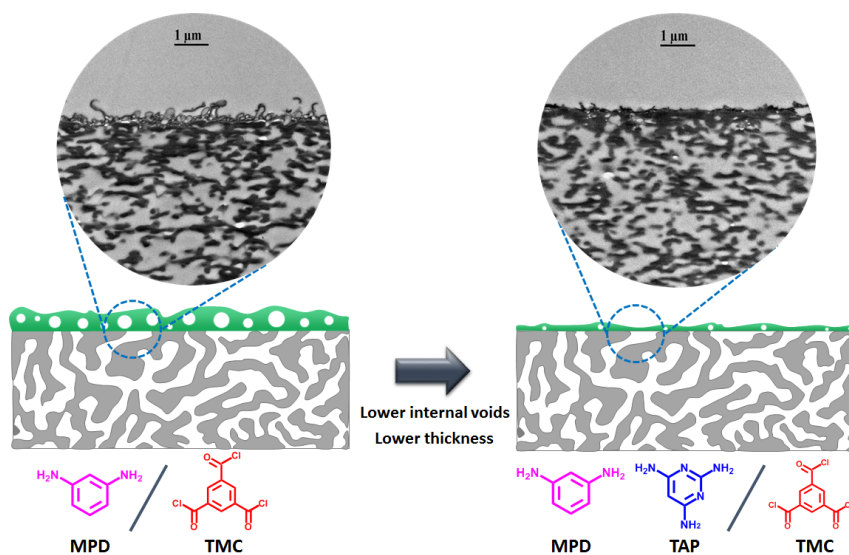


Figure A1: Schematic representation of polyamide structure for M0 and M4, along with their respective FESEM images.

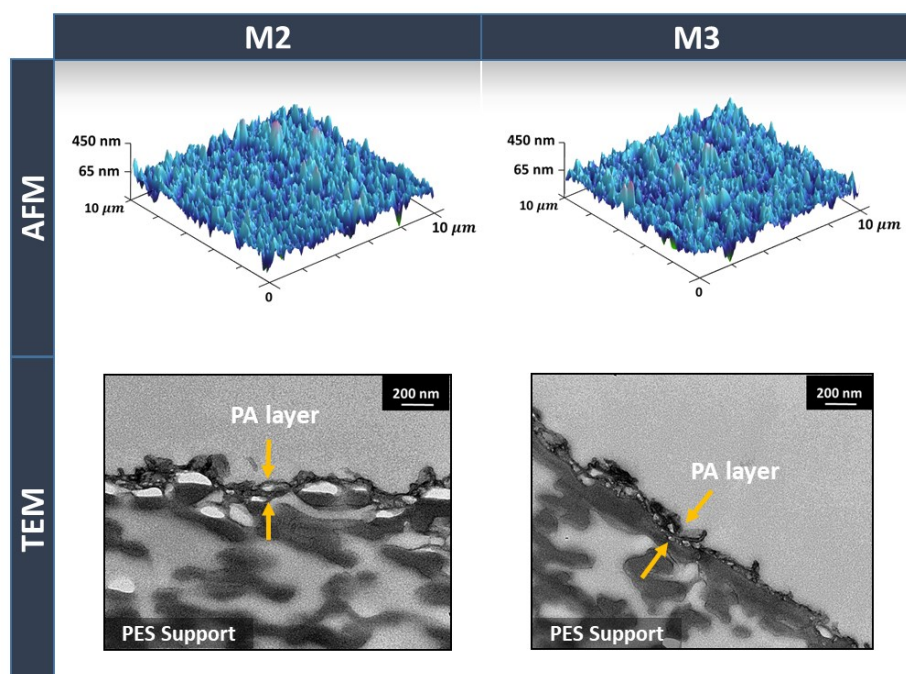


Figure A2. 3D AFM images and cross-section TEM images of TFC samples (M2 and M3).

Table A1. Average roughness (R_a), root mean square roughness (R_q), and surface area difference (SAD) of synthesized TFC membranes (M2 and M3)

Sample	Roughness		
	R_a (nm)	R_q (nm)	SAD (%)
M2	58.8 ± 0.5	76.1 ± 1.7	40.9 ± 0.4
M3	56.9 ± 0.5	75.3 ± 2.6	43.6 ± 1.3

Appendix B

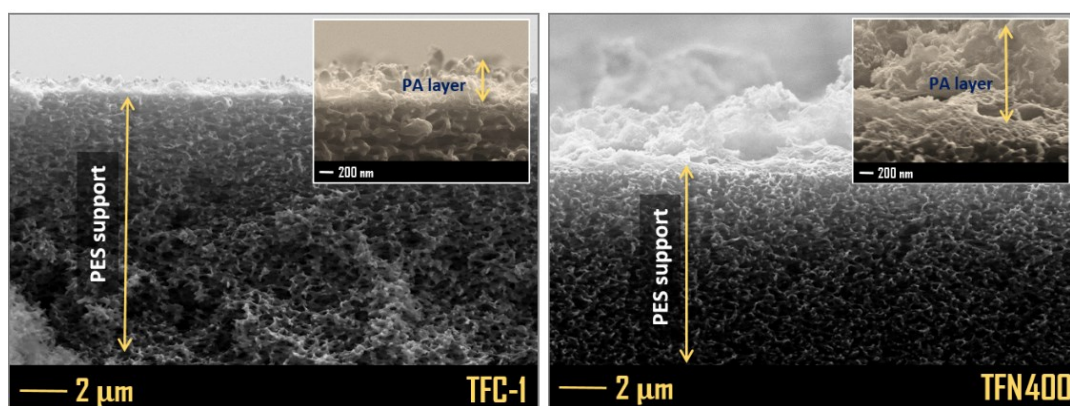


Figure B1: Cross-section FESEM images of TFC-1 and TFN400.



Figure B2: Water contact angle of synthesized TFC/TFN membranes

Figure B2 illustrates the water contact angle of synthesized membranes. The water contact angle was decreased from 88.4° to 58.3° for TFC-1 and TFN400, respectively, showing 34% reduction. Improvement of the wettability of TFN membranes can be attributed to the presence of more hydrophilic ND particles in the polyamide layer. Furthermore, for a wettable surface (contact angle $< 90^\circ$), the contact angle is smaller for a rougher surface (based on the Wenzel model) [131,263]. Therefore, higher roughness for TFN membranes can further contribute to reduction of the apparent contact angle.